1968

Analytical and experimental methods for determining the properties of materials at very high rates of loading

A. G. Behring

ANALYTICAL AND EXPERIMENTAL METHODS FOR DETERMINING THE PROPERTIES OF MATERIALS AT VERY HIGH RATES OF LOADING

BY

ALLEN GLENN BEHRING, 1943

A

THESIS

submitted to the faculty of

THE UNIVERSITY OF MISSOURI - ROLLA

in partial fulfillment of the requirements for the

Degree of

MASTER OF SCIENCE IN MECHANICAL ENGINEERING

Rolla, Missouri

1968

Approved by

R. B. Detting (advisor) Paul Detting

C E Antle

ABSTRACT

In the following report, some of the properties of ALCOA 7075 T651 aluminum, when subjected to high rates of loading, are experimentally investigated by impacting two rods of the material longitudinally.

One rod is accelerated to a uniform velocity with an air gun launcher. The stationary second rod is instrumented with strain gages on its lateral surface in order to determine the strain-time history following impact. A detailed description of the experimental equipment is included.

Simple, one-dimensional theory is used to determine the dynamic, elastic modulus of the test material under the impact condition. Several observations regarding the behavior of the material under dynamic, plastic loading conditions are made.

The importance of equipment frequency response is noted and a method is suggested for estimating the experimental error in strain measurement resulting from equipment frequency response limitations. Several other possibilities of experimental error are noted and suggestions for improvement of the experimental apparatus are given.

A theoretical development for the case of the longitudinal impact of two viscoelastic rods is presented and the numerical results are summarized for the impact of two rods of a Maxwell material.

Computer programs to facilitate the determination of air gun parameters and to evaluate the solutions for the viscoelastic case are included.

ACKNOWLEDGEMENTS

I am appreciative of the assistance rendered by several persons who have contributed significantly toward the completion of this investigation. I am especially grateful to Dr. R. B. Oetting for suggesting the thesis topic and for acting as my advisor. Drs. W. S. Gatley and E. E. Hornsey have contributed significantly to the theoretical portion of this thesis and have my sincere thanks.

Messrs. Dick Smith and Lee Anderson have provided valuable technical assistance throughout both the construction and experimental phases of this investigation.

I am certainly grateful to the Department of Mechanical and Aerospace Engineering for financing the experimentation and for providing me with a graduate assistantship during its conduct.

My deepest thanks to my wife, Elizabeth, for her encouragement and for typing the manuscript.

TABLE OF CONTENTS

LIST OF ILLUSTRATIONS

Figures

LIST OF TABLES

I. INTRODUCTION

Man has long recognized the need for adequate description of the behavior of materials in various environments. In many cases, the construction and application of devices has been made economically and physically possible only through extensive theoretical analysis and testing.

In the design of structures, it has been found necessary to possess knowledge of the behavior of materials under various loading conditions. Because of the variety of loading that is possible and the endless spectrum of structural shapes, simple one-dimensional tests have been devised to yield basic design information which, hopefully, can be applied to more complex conditions. Although the use of results obtained by one-dimensional tests is restricted, their popularity has been enhanced by the simplicity with which they can be conducted and analyzed. It has also been found that one-dimensional tests generally yield results that are valuable in the analysis of multi-dimensional problems. One such example, the static tension test, has virtually become a standard test for materials.

Most students of the subject agree that the science of wave propagation in solids first began to flourish during the nineteenth century. It is thought that much of the progress in this area followed as a result of the observations that the "rigid body treatment" was inadequate to describe some problems where large amplitude stresses were produced from very high rates of loading (as in impact).

As is the case with many problems in science and engineering, analysis of the general case of wave propagation in solids involves the solution of very complicated equations. It has been observed that under certain conditions,

simplifications of the general case can be made. One such simplification of the general case of wave propagation involves the analysis of wave propagation in uniform rods.

It is known that Pochammer (1876) and Chree (1889) were independent authors of the classic theory of multi-dimensional wave propagation in round, uniform rods of semi-infinite length. It is generally accepted, however, that Saint-Venant (1883) was the first to intensively examine the case of one-dimensional wave propagation in rods due to impact loading. Since the time of Saint-Venant, an enormous amount of literature has been produced with regard to rod problems alone.

Analyses have been presented for rods whose circular cross-section varies as a function of a spatial coordinate (both continuously and discontinuously) for rods of non-circular cross-section and for curved rods. A wide variety of boundary conditions have been considered, including the interaction of the lateral surface of a rod with a surrounding medium, and various end conditions. Among the initial value problems that have been considered are those which involve: the longitudinal impact of rods (of equal or unequal diameter and material); the non-longitudinal impact of rods; the application of pressure pulses, velocities, or heat sources to the ends of both infinite and semi-infinite rods; and the collision of rods with rigid, finite or semi-infinite masses. The effects of magnetic fields and high or low temperatures on wave propagation in rods have also been examined.

These primary investigations have given rise to the analysis of wave propagation in rods of materials which are not ideally elastic, but which can be described as being aleotropic or inhomogeneous. Some problems have been solved for rods which are of anelastic materials, among them being those that can be described as viscoelastic, elastoplastic, or elasto-viscoplastic.

Recently, the study of "hypervelocity impact" has been intensively pursued. This phenomenon involves impact velocities that approach or exceed the velocity of wave propagation in the material, leading to the production of stresses which are of the same order of magnitude as the elastic modulus. Solutions to these problems have involved the treatment of materials as compressible fluids.

Some of these problems have been solved for the two and three-dimensional cases. The large majority of investigators have, however, considered only one-dimensional effects. Certainly, the examination of one-dimensional problems in wave propagation has led to valuable information regarding the effects of wave propagation on the material in which the waves are propagated and has provided valuable information for use with multi-dimensional problems.

II. LITERATURE REVIEW

A. Elastic and Plastic Waves

The behavior of most metals, when subjected to rapid loading conditions, can normally be described in terms of some type of elastoplastic or elasto-viscoplastic analysis.

1. Elastoplastic Theory

Karman [1] and Taylor [2] were among the first proponents of the elastoplastic (strain-rate independent) theory. The distinction of this method of analysis is that it involves the use of the statically-determined stress-strain curve to predict the propagation of waves in materials which have received loading in the plastic range. Basically, the theory states that each level of stress included by the elastic limit of the material is propagated with the elastic wave velocity while each level of stress in the plastic range of loading is propagated with a velocity which depends upon the slope of the static stress-strain curve at that level of stress. Due to the fact that most stress-strain curves are observed to be "concave downward" in the plastic region, this theory suggests that the elastic levels of stress will be propagated with a velocity that exceeds those velocities associated with the plastic levels of stress.

2. Elasto-viscoplastic Theory

It has been found that the response of some materials to rapid plastic loading is distinctly different than that predicted by the strain-rate independent theory. This phenomenon is normally characterized by an "upward shift" of the static stress-strain curve in the plastic range of loading and may be accompanied by an increase in the ultimate strength of the material. Malvern [3] suggested

that these characteristics could be predicted by a strain-rate dependent constitutive equation in the plastic range of loading. Analysis of the Malvern equation shows that if the material is subjected to "step" straining above the elastic limit, its stress-strain relation will instantaneously reduce to an extension of the elastic curve into the plastic range. The equation also predicts that the dynamic stress-strain curve will approach that of the static case if the strain level is sustained for long periods of time.

3. Experimental Methods

Some interesting experiments, investigating the effect of strain-rate on various materials, have been conducted using the "split Hopkinson pressure bar." A thin wafer of material is sandwiched between two rods which have been aligned longitudinally. A compressive pulse is applied to one of the rods and passes through the rod-wafer-rod interface and into the second rod. Through post facto analysis of the strain-time and/or displacement-time histories of the rods (which are assumed to remain elastic during the test), it is possible to deduce the stress-strain history of the specimen. A more detailed description of the apparatus that is used can be found in publications by Davies [4] and Lindholm [5] with criticism by Bell [6]. Although there has been a substantial amount of testing by this method, conclusions regarding the strain-rate dependence of materials are many times obviated by published results which do not agree qualitatively much less quantitatively.

Perhaps the most utilitarian test of strain-rate dependence is that which involves the longitudinal collision of two rods of equal diameter. For rods which are of sufficiently small diameter, simple one-dimensional considerations are normally adequate to describe the resultant wave phenomena. One-dimensional theory predicts the production of infinite strain-rate as a result of the collision of the rods. Thus, for this limiting condition, it can be determined if the

material shows strain-rate dependency. If the material is not observed to show strain-rate characteristics under these conditions, it is very likely that it will not demonstrate strain-rate dependence at reduced rates of loading. Experiments using this method have been conducted for the elastic case by Krafft [7] and Ripperger [8] and for the elastic-plastic case by Bell [9,10] . Oetting [11] has used this method for studies in the plastic range and at low temperature. The case of a rod, remaining elastic, and impacting a second rod (of a different material) at such a velocity that a plastic level of stress is produced in the second rod has been experimentally examined by Waser, Rand, and Marshall [12].

4. Spallation

Spallation, or scabbing, is another phenomenon commonly associated with the propagation of elastic-plastic waves. It may be described briefly as a fracturing of material which is located at some distance from the immediate area of impact or load application. It is generally considered that the mechanism primarily responsible for this phenomenon is the reflection of compressive stress waves as waves of tension at the "free boundaries" of the material, and is a direct result of the fact that most materials can sustain higher stress levels in compression than in tension. The level of the reflected tensile pulse must necessarily exceed the ultimate stress of the material, but this is not a sufficient condition for spallation to occur. Some of the phenomena which are known to effect the spallation process are: (a) duration of tensile load; (b) strain-rate dependence; (c) crack propagation speed; (d) ductility; and (e) magnitude of the tensile load. In the case of the impact of two rods of different lengths and of equal strain-rate dependent materials, spallation manifests itself as the fracturing of a section of the longest rod which is equal to the length of the shortest rod. This effect was observed by Oetting [11] in an examination of the impact of lucite rods.

A more detailed description of the spallation phenomenon can be found in a publication by Broberg [13].

B. Viscoelastic Waves

1. Introduction

It has been observed that some materials exhibit (to varying degrees) properties such that they respond both viscously and elastically to applied loads. Such materials have been called "viscoelastic" materials. Among the materials that have been observed to exhibit these characteristics are: concrete; metals at elevated temperature; lead; and certain of the newly-developed synthetic materials.

The elementary method of analysis of viscoelastic materials considers that their constitutive equations can be represented by series and parallel combinations of linear springs and viscous dashpots (viscoelastic models). A good discussion of the macroscopic and microscopic implications of this analogy is given by Bland [14] and by Flügge [15].

The behavior of these materials under quasi-static loading conditions is ordinarily reported in terms of their "creep" or "relaxation" characteristics, which is respectively constituted by their observed response to constantly-applied stress or constantly-applied strain. The response of these materials in problems involving wave propagation can generally be termed as "frequency dependent," and it is common that their properties, under these conditions, are reported in terms of "complex modulii."

Unfortunately, the problems in viscoelastic wave propagation become very complicated and are generally soluble in closed form only for the simplest of problems with the most elementary models. Solutions to more complex problems are usually obtained via numerical approximations.

2. One-Dimensional Viscoelastic Wave Propagation

Because of the complexity of problems in viscoelastic wave propagation, the one-dimensional approximation has proven to be a valuable method of analysis.

Lee and Kanter [16] have considered the effect of a step velocity applied at the ends of both finite and semi-infinite rods of a Maxwell material.[1] Morrison [17] has considered the effect of a step velocity applied at the ends of semi-infinite rods of both Voigt and three-parameter materials.[2] The method of characteristics has been used by Glauz and Lee [18] to examine the case of a step velocity applied to the end of a semi-infinite rod of a four-parameter material.[3] Lee and Morrison [19] compare the results obtained for the case of the semi-infinite rod and the various models considered by Lee and Kanter, Lee and Morrison, and Glauz and Lee with observations regarding simplifications that can be made in material modeling. The effects of stress, strain, and sinusoidal motion applied at the ends of semi-infinite and finite rods were examined (with the "hereditary integral") by Berry and Hunter [20] for materials which obey Boltzmann's principle of superposition. The propagation of a strain pulse in a rod of polyethelene (assumed to be semi-infinite) was experimentally examined by Norris [21] using the Hopkinson pressure bar.

---

[1] The Maxwell model consists of a spring and a dashpot arranged in a series combination.

[2] The Voigt model consists of a spring and a dashpot in parallel arrangement. An example of a three-parameter model is a Voigt model combined in series with a spring or dashpot.

[3] A four-parameter model is a series combination of two Voigt models or a series combination of a Voigt model with a Maxwell model.

III. THEORETICAL CONSIDERATIONS

A. Introduction

In the developments that are presented herein, it will be assumed that the elementary one-dimensional theory as applied to the longitudinal propagation of waves in rods is valid. It will be assumed that the rods are of circular cross-section, of constant area in the unstrained state, and are composed of an isotropic, homogeneous material. Further assumptions are that "small" strains (such that the equations of linear elasticity apply) are exclusively present, body forces and temperature variations are negligible, plane cross-sections remain plane, and that the stress present at any section of a rod acts uniformly over that section. Additionally, it will be assumed that the duration of a disturbance that traverses a rod is large compared to the quantity (rod diameter/wave propagation velocity). The validity of the one-dimensional treatment under these conditions has been demonstrated by Kolsky [23].

A rod, conforming to the above restrictions, is shown in Figure 1. With reference to Figure 1: L represents the length of the rod in the unstrained state; x is the unstrained (lagrangean) coordinate; t is time; U(x,t) is the displacement of a layer of rod material with respect to its corresponding unstrained coordinate, x, at time, t; and a is a constant. It is considered that A_o and ρ_o are the unstrained area and mass density of the rod, respectively. The

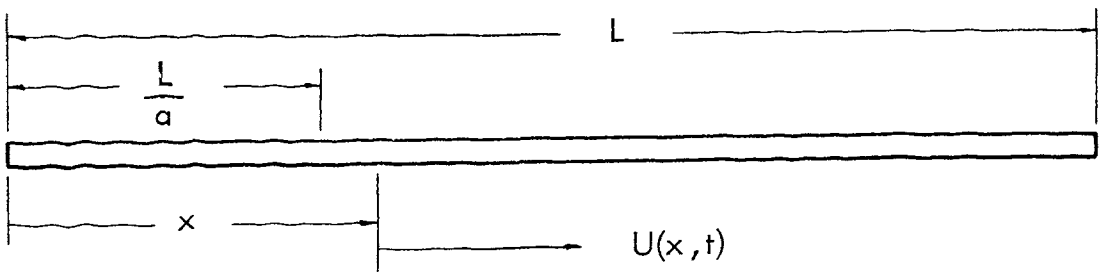

Figure 1. Uniform rod

uniaxial stress in the rod will be denoted as σ and the uniaxial strain as ε . Stress is defined as the force acting on a section of the rod per unit of the unstrained area and strain as the change in length of an infinitessimal section of the rod at x divided by its unstrained length. For small strains

$$\varepsilon = \frac{\partial U}{\partial x} = U_x \quad . \tag{1}$$

B. Method of Characteristics Solution: The impact of two elastic rods

It is thought that this approximate method for describing the longitudinal propagation of waves in a rod was first used by Karman [1] and Taylor [2] in their studies of elastic-plastic wave propagation in rods and wires. Recently, this theory (adapted to the longitudinal collision of two rods) was used by Waser, Rand, and Marshall [12] in their study of a strain-rate independent material and by Oetting [11] in his study of two highly strain-rate dependent materials.

Application of the continuity and momentum equations to an infinitessimal section of the rod of Figure 1 yields the equations

$$\varepsilon_t = U_{xt} = V_x \tag{2}$$

and

$$U_{tt} = \frac{1}{\rho_o} \sigma_x = V_t \quad . \tag{3}$$

where V is the velocity of particles relative to the Lagrangean reference frame and the subscripts x and t denote partial differentiation with respect to the spatial coordinate and time, respectively.

For small strains, the velocity of propagation of a disturbance with respect

to an undisturbed portion of the rod, C, is given by

$$C = \sqrt{\frac{1}{\rho_o}\frac{d\sigma}{d\varepsilon}} \quad . \tag{4}$$

Let the variable, $\emptyset$ be defined by the equation

$$d\emptyset = Cd\varepsilon \quad . \tag{5}$$

In the elastic range of the material

$$\frac{d\sigma}{d\varepsilon} = E = \frac{\sigma}{\varepsilon} \tag{6}$$

where E is the elastic modulus. For strain-rate independent materials that have been loaded plastically, $\frac{d\sigma}{d\varepsilon}$ normally has a distinct value for each level of plastic stress. If it is assumed that the concern is only with materials that are loaded in the elastic range, or with materials that are highly strain-rate dependent,[1] then equation (4) becomes

$$C = \sqrt{\frac{E}{\rho_o}} \quad . \tag{7}$$

It can then be seen from equation (7) that C is not dependent on ε and equation (5) becomes

$$\emptyset = C\varepsilon \quad . \tag{8}$$

Combining equation (8) with equation (2) yields the equation

$$\emptyset_t - CV_x = 0 \quad . \tag{9}$$

---

[1] For materials that obey the flow law of Malvern [3] , equation 6 applies in the plastic range as well as in the elastic range of loading if the loading rate is very high and the loading time is small. These characteristics of the Malvern equation are discussed briefly in Appendix 3.

Combining equation (8) with equation (3), using equations (6) and (7), gives a second equation

$$V_t - C\emptyset_x = O \quad . \tag{10}$$

Alternately adding and subtracting equations (9) and (10) results in

$$(V \pm \emptyset)_t \quad \mp \quad C(V \pm \emptyset)_x = O \quad . \tag{11}$$

Equation (11) is the set of "characteristics equations" describing particle motion in a rod of a material which displays an invariant propagation velocity.

Equation (11) is also, by definition, the total derivative[1] (D) of the quantity $(V + \emptyset)$ or the quantity $(V - \emptyset)$, where

$$D = \frac{\partial}{\partial t} + \frac{dx}{dt}\frac{\partial}{\partial x} \quad . \tag{12}$$

Thus, for an observer moving along the rod with velocity $\frac{dx}{dt} = \mp C$, the quantity $(V \pm \emptyset)$ appears as a constant. This is equivalent to saying that along lines of constant slope $\frac{dx}{dt} = \mp C$ in the x-t plane, $(V \pm \emptyset)$ is a constant. In equation form, this is

$$(V + \emptyset)\Big|_{\text{slope} = -C} = \text{Constant} \tag{13}$$

$$(V - \emptyset)\Big|_{\text{slope} = +C} = \text{Constant} \quad . \tag{14}$$

In general, there is a distinct constant associated with each line.

---

[1] The total derivative is also known as the "comoving" or "substantial" derivative. A description of its properties is given by Frederick and Chang [22].

A disturbance can be induced within a rod by impacting it longitudinally with a second rod of equal cross-sectional area. One rod is initially at rest and will be designated the "test rod" (subscript, T). The second rod has an initial, uniform velocity, V_o, with respect to the test rod and will be identified as the "impacter" (subscript, I). At time $t = O$, the impacter has just reached a face of the test rod such that the rods are not, as yet, strained due to impact. The origin of the Lagrangean coordinate, x, is defined to be at the "free end" of the impacter. Then, at $t = O$, the impacter and projectile constitute a total length, L. Let the length of the impacter be designated by L/a where a is a constant greater than two. With the stipulation that the interface of the rods exists at $x = L/a$, the system is arranged as that shown in Figure 1 for the uniform rod.

In this analysis, it will be considered that both rods are of identical material, such that a "matched impedance" condition $(\rho_o A_o C)_I = (\rho_o A_o C)_T$ exists at the interface of the rods. A compressive load will thus be transmitted undiminished at the interface.[1] As long as the rods remain in contact, the following conditions must be met at the interface:

$$\begin{aligned} \sigma_I &= \sigma_T \\ U_I &= U_T \\ V_I &= V_T \quad . \end{aligned} \tag{15}$$

In view of the specified initial conditions,

$$\begin{aligned} V_I &= V_o \\ U_I &= O \\ V_T &= U_T = O \quad . \end{aligned} \tag{16}$$

---

[1] It was shown by Waser, Rand and Marshall [12] that reflections will not occur at the interface of two equal-diameter rods if the impedance of the impacter is equal to, or less than, the impedance of the test rod. The condition of free transmission at the interface (for matched impedance) has also been described by Kolsky [23].

Using equations (13), (14), (15), and (16) it is possible to construct a "characteristics net." The significant characteristics of this net are shown in Figure 2.

Equation (8) can now be used to calculate the strain present at any point in the characteristics diagram and equation (6) yields the corresponding stress. It can thus be seen that the maximum magnitude of the stress, σ_E, and the maximum magnitude of the strain, ε_E, are respectively given by

$$\sigma_E = \frac{EV_o}{2C} \tag{17}$$

$$\varepsilon_E = \frac{V_o}{2C} \cdot \tag{18}$$

Vertical lines drawn between the characteristics of Figure 2 (e.g., line D-E) indicate the length of the non-zero stress or strain distribution at the value of time indicated by the intersection of an extension of the line with the t-axis. Horizontal lines drawn between the characteristics of Figure 2 (e.g., line F-G) for a particular value of x indicate the duration of the pulse at that value of x. It should be noted that the latter procedure can, in general, yield multi-valued results for the duration as a function of time.

Through further analysis of Figure 2 it can be determined that a compressive wave of magnitude σ_E is initiated at the interface of the bars and propagates into the test rod with velocity C and into the projectile with velocity -C until it has reached the free face of the projectile ($t = L/aC$). At $t = (L/aC)^+$, the wave begins to move through the interface of the rods in the +x direction and subsequently propagates completely into the test rod. Due to reflection effects at the free end of the test rod, the wave vanishes about point A at $t = L/C$. At $t = (L/C)^+$, a wave of tension appears at point A and subsequently propagates toward the interface of the rods. When the wave of tension reaches the interface of the rods, the rods must separate (tension cannot exist at the

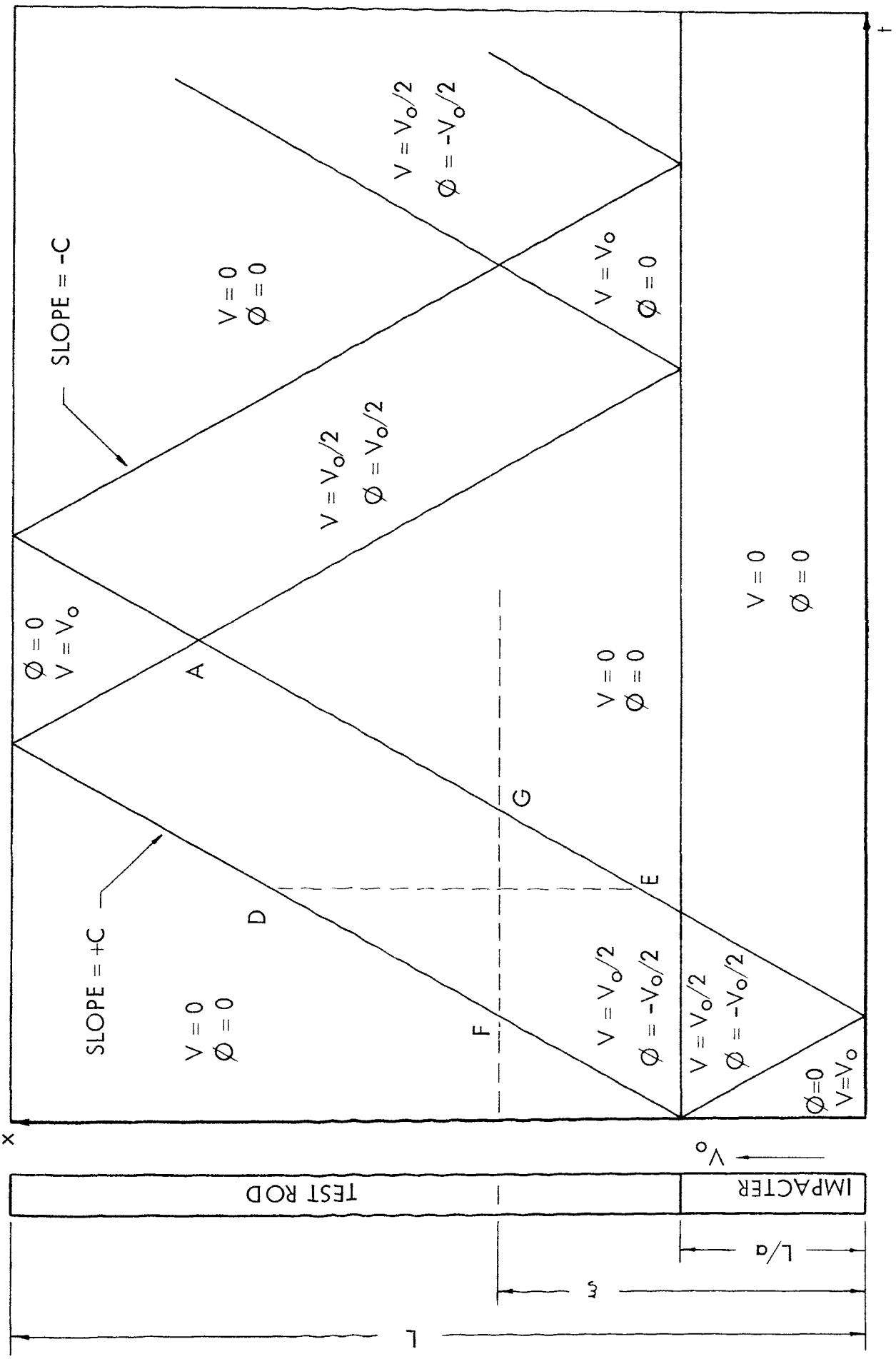

Figure 2. Characteristics diagram

interface). After separation, the wave is reflected at $x = L/a$ and continues to propagate within the test rod as a wave of alternating sign.

Since the pulse first appears as a wave of tension at $x = L - L/a$, this is where spallation or scabbing will first occur, if it occurs at all. Also, it may be seen from Figure 2 that if the impacter and test rod are of equal lengths the impact will produce only a single compressive pulse.

C. Traveling Wave Solution: The impact of two elastic rods

It can be shown that displacements, U, of the rod of Figure 1 with respect to the spatial coordinate, x, satisfy the wave equation

$$U_{tt} = C^2 U_{xx} \tag{19}$$

where

$$U = f(x-Ct) + g(x+Ct) \quad . \tag{20}$$

In the method of characteristics solution it has effectively been stated that the colliding rods can be considered as one continuous rod as long as tension is not present at the interface.[1] Proceeding with this assumption, the rod of Figure 1 exists with the following initial conditions:

$$\begin{aligned} U(x,o) &= 0 = U_x(x,o) \qquad (0 \leq x \leq L) \\ U_t(x,o) &= V_o\left[1 - H(x-L/a)\right], \quad (0 \leq x \leq L) \end{aligned} \tag{21}$$

and the boundary conditions:

$$U_x(0,t) = U_x(L,t) = 0 \tag{22}$$

where H(x) is Heaviside's step function.

---

[1] This condition has been implied by Goldsmith [24], p. 38, in his solution of a similar problem by the traveling wave method.

Equation (20) represents the sum of two traveling waves; $f(x - Ct)$ is a wave traveling in the $+x$ direction and $g(x + Ct)$ is a wave traveling in the $-x$ direction. For the elastic case, the waves retain their shape and propagate with a velocity of magnitude C. By suitable partial differentiation, it can be shown that

$$\sigma = E\left[\frac{\partial f}{\partial v} + \frac{\partial g}{\partial w}\right] \tag{23}$$

where $v = x - Ct$, $w = x + Ct$; and that

$$\frac{\partial f}{\partial v} = \frac{1}{2}\left[\frac{\partial U}{\partial x} - \frac{1}{C}\frac{\partial U}{\partial t}\right], \quad \frac{\partial g}{\partial w} = \frac{1}{2}\left[\frac{\partial U}{\partial x} + \frac{1}{C}\frac{\partial U}{\partial t}\right] . \tag{24}$$

Using equations (24) and (21), evaluation of equation (23) at $t = 0$ yields

$$\sigma(x,o) = -\frac{EV_o}{2C}\left[1-H\left(x-\frac{L}{a}\right)\right] + \frac{EV_o}{2C}\left[1-H\left(x-\frac{L}{a}\right)\right] . \tag{25}$$

Let time be defined by the non-dimensional variable $T = Ct/L$, $\sigma_E = \frac{EV_o}{2C}$, and $a = 5$; then, using equation (25), the waves ($T = O$) are as depicted in Figure 3.

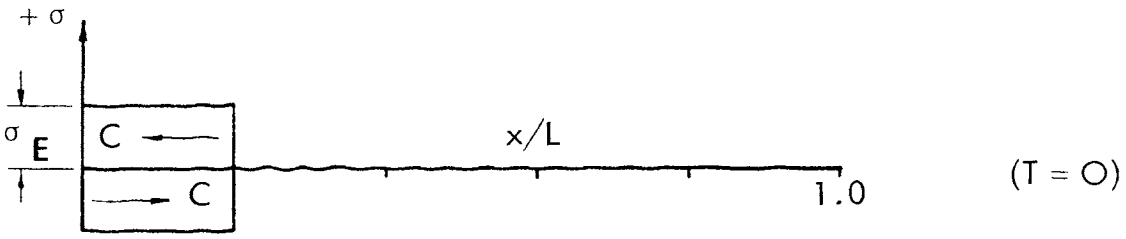

Figure 3. Traveling waves ($T = O$)

It should be noted that since both ends of the rod are free, the traveling stress waves will be reflected as waves of opposite sign at these boundaries. Summation of the two waves at increasing values of T reveals that a compressive

stress wave of magnitude σ_E is generated at the interface and propagates with velocity C into both the impacter and test rod (see Figs. 4-A to 4-C). At T = 0.2, the length of the pulse is 0.4L. At $T = 0.2^+$, the wave begins to move through the interface and is subsequently reflected at the free end of the test rod as a wave of tension. At T = 1.6, the tension wave has just reached the interface and the rods separate (tension cannot exist at the interface). The wave is now reflected as a wave of compression at x = 0.2L and continues to propagate back and forth in the test rod with alternating sign. A sequence of stress distributions within the rods for the first traverse of the stress wave is shown in Figures 4-A to 4-G.

By comparison of Figure 4 with Figure 2 it can be seen that the assumption of a continuous rod and subsequent use of the traveling wave method has yielded results which are equivalent to those obtained by the method of characteristics (with a = 5).

D. Fourier Series Solution: The impact of two elastic rods

With the assumption of a continuous rod, yet another equivalent solution can be obtained through separation of variables and Fourier series. Application of the boundary conditions (22) and the initial conditions (21) for a = 5 yields

$$\sigma = -\frac{2EV_o}{C\pi}\sum_{n=1}^{\infty}\frac{1}{n}\cdot\sin(n\pi/5)\cdot\sin(n\pi x/L)\cdot\sin(n\pi Ct/L) \qquad (26)$$

$$\varepsilon = -\frac{2V_o}{C\pi}\sum_{n=1}^{\infty}\frac{1}{n}\cdot\sin(n\pi/5)\cdot\sin(n\pi x/L)\cdot\sin(n\pi Ct/L)\ . \qquad (27)$$

Equations (26) and (27) apply only until a state of tension exists at the interface of the rods (T = 1.6). A solution for time $T \geq 1.6$ can be obtained by using the series evaluated at T = 1.6 to provide initial conditions for a second boundary value problem. The solution for $T \geq 1.6$ involves, however, a transformation of coordinates and a consequent doubly infinite series and will not be presented here.

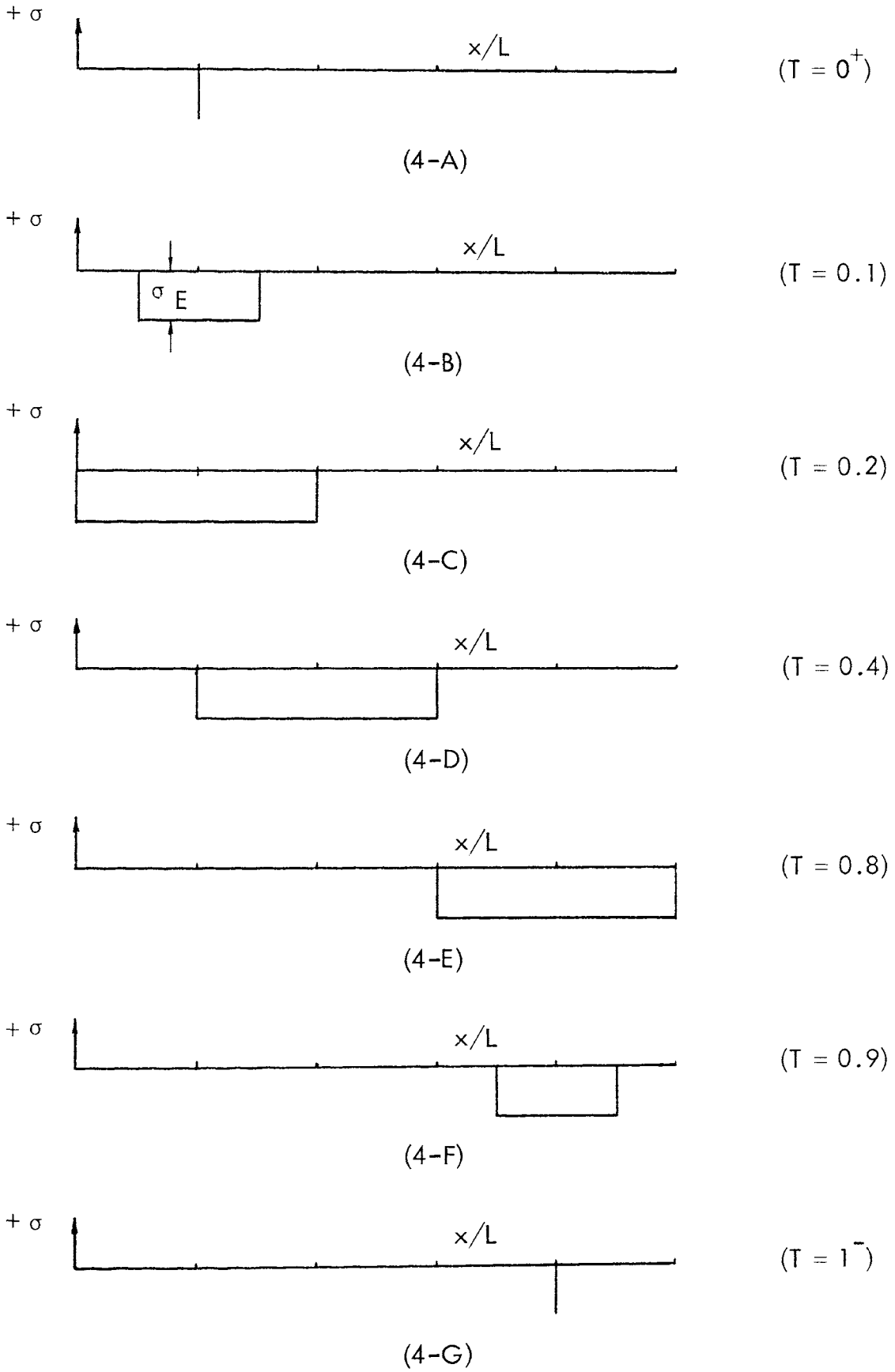

Figure 4. Elastic stress distributions at (T)

E. Viscoelastic Solution: The impact of two viscoelastic rods

A Maxwell material is one for which the stress-strain relation can be described by a linear spring and a viscous dashpot arranged in series. If E is the spring constant and η is the coefficient of viscous damping, the Maxwell model is as shown in Figure 5.

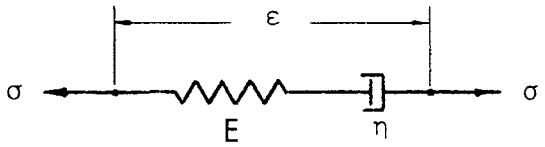

Figure 5. Maxwell model

The equation which describes the stress-strain relation of a material has been called its "constitutive equation." The constitutive equation of the Maxwell model is

$$\frac{1}{E}\frac{d\sigma}{dt} + \frac{1}{\eta}\sigma = \frac{d\varepsilon}{dt}$$

or, after substitution of $W_o = E/\eta$

$$W_o\sigma + \frac{d\sigma}{dt} = E\frac{d\varepsilon}{dt} \quad . \tag{28}$$

The Maxwell model is ultimately viscous, i.e., it will strain indefinitely upon the application of a constant load and it will act instantaneously as a simple spring upon the application of step loading. If the coefficient of the dashpot assumes a value of infinity, the model becomes a simple spring. If the coefficient of the spring becomes infinite, the model becomes a simple dashpot.

1. The Correspondence Principle

A form of the correspondence principle was used to obtain solutions for the stress and strain resulting from the collision of two rods of a Maxwell material.

The general procedure for applying this form of the correspondence principle to a one-dimensional problem is as follows:

1. The solution of a problem in elasticity is obtained as a function of the spatial coordinate, elastic modulus and time.
2. The "elastic solution" of Step 1 is found in a suitable transform plane.
3. The constitutive equation of the viscoelastic model under consideration is transformed and solved for the stress-strain relation (corresponding transform - varying modulus).
4. The corresponding transform - varying modulus of Step 3 is substituted for the elastic modulus in Step 2.
5. The inverse of the transformed solution (resulting from Step 4) is found to obtain the viscoelastic solution in the t-plane.

The Laplace transform will be used in the application of Steps 2 through 5. Its use with the correspondence principle when applied to problems of dynamic elasticity is subject to the restrictions discussed in the following paragraphs.

It was stated by Bland [14] that the constitutive equation of the general, linear viscoelastic model is of the form

$$P(d)\,\sigma = Q(d)\,\varepsilon \tag{29}$$

where (if p_n and q_n are constants)

$$P(d) = \sum_{n=0}^{k} p_n \frac{d^n}{dt^n} \quad \text{and} \quad Q(d) = \sum_{n=0}^{j} q_n \frac{d^n}{dt^n} \ .$$

For any viscoelastic model considered by Bland, the highest order of the operators, Q(d) is equal to or greater than the highest order of the operators, P(d). Consider

the limiting condition where the highest order of P(d) is equal to the highest order of Q(d). Substitution of equation (29) into the elementary form of the wave equation

$$\frac{\partial \sigma}{\partial x} = \rho_o \frac{\partial^2 U}{\partial t^2} \tag{30}$$

yields

$$\frac{\partial}{\partial x}\left[\sum_{n=o}^{k} q_n \frac{\partial^n}{\partial t^n}\right]\varepsilon = \rho_o\left[\sum_{n=o}^{k} p_n \frac{\partial^{n+2}}{\partial t^{n+2}}\right] U \quad . \tag{31}$$

Taking the Laplace transform of equation (31), assuming that the initial conditions involving stress and strain vanish, and noting that $\overline{\varepsilon} = \overline{U}_x$ results in

$$\left[\sum_{n=o}^{k} q_n s^n\right] \frac{\partial^2 \overline{U}}{\partial x^2} = \rho_o\left[\sum_{n=o}^{k} p_n s^{n+2}\right] \overline{U}$$

$$- \rho_o p_k\left[s^{k+1}U(x,o) + s^k \dot{U}(x,o) + s^{k-1}\ddot{U}(x,o) + \ldots\right] - \ldots \tag{31a}$$

where the bar notation indicates a transformed variable. Taking the Laplace transform of equation (29) and assuming the same initial conditions, the result is

$$\left[\sum_{n=o}^{k} p_n s^n\right] \overline{\sigma} = \left[\sum_{n=o}^{k} q_n s^n\right] \overline{\varepsilon} \quad . \tag{32}$$

Thus, the corresponding s-varying modulus is

$$\frac{Q(s)}{P(s)} = \frac{\overline{\sigma}}{\overline{\varepsilon}} = \left[\sum_{n=o}^{k} q_n s^n\right] \Big/ \left[\sum_{n=o}^{k} p_n s^n\right] \quad . \tag{33}$$

Transforming equation (30), the result is

$$\frac{\partial \overline{\sigma}}{\partial x} = \rho_o\left[s^2 \overline{U} - sU(x,0) - \dot{U}(x,o)\right] \quad . \tag{34}$$

Using equation (33) with equation (34) and noting that $\bar{\varepsilon} = \bar{U}_x$, the result is

$$\left[\sum_{n=o}^{k} q_n s^n\right] \frac{\partial^2 \bar{U}}{\partial x^2} = \rho_o \left[\sum_{n=o}^{k} p_n s^n\right] \left[s^2 \bar{U} - sU(x,o) - \dot{U}(x,o)\right] . \qquad (34a)$$

Equation (34a) is equal to equation (31a) only if the second order (and higher) partials of displacement with respect to time evaluated at (x,o) vanish.

Thus, it has been shown that this form of the correspondence principle (using Laplace transforms) can be applied to the wave equation if the following conditions prevail:

$$\frac{\partial^n \varepsilon}{\partial t^n}(x,o) = \frac{\partial^n \sigma}{\partial t^n}(x,o) = 0, \quad (n=o,1,2,3\ldots)$$

$$\frac{\partial^n U}{\partial t^n}(x,o) = 0, \quad (n=2,3,4\ldots) \qquad (35)$$

Equations of the form of (31a) have been solved by Lee and Kanter [16], Lee and Morrison [19], and Morrison [17]. However, since their concern was exclusively with linear operators, these solutions could have been obtained by using the correspondence principle with the elastic solution, equations (35) satisfied. This form of the correspondence principle (using the one-sided Fourier transform) has been applied by Bland [14] to solve a problem of viscoelastic wave propagation in a semi-infinite rod.

2. Application of the Correspondence Principle

The problem of the longitudinal impact of two rods satisfies equations (35).

Transforming equation (28), $(W_o + s)\bar{\sigma} = Es\,\bar{\varepsilon}$

thus, $\frac{\bar{\sigma}}{\bar{\varepsilon}} = \frac{Q(s)}{P(s)} = \frac{Es}{W_o + s}$.

Let E assume some finite value, say E_o. Now, noting that $E = \rho_o C^2$ (see equation 7), C^2 in a transformed elastic solution will be replaced by

$$\frac{E_o}{\rho_o}\left[\frac{s}{s + W_o}\right] = C_o^2\left[\frac{s}{s + W_o}\right] \quad . \tag{36}$$

Taking the Laplace transform of equations (26) and (27), replacing C^2 with equation (36) and performing the inverse transformation, the result is

$$\sigma = -\frac{2E_oV_o}{C_o\pi}\exp(-\frac{W_o}{2}t)\sum_{n=1}^{\infty}\frac{1}{n\sqrt{1-\Delta^2}}\cdot\sin(n\pi/5)\cdot\sin(bx)$$
$$\cdot\sin(bC_o\sqrt{1-\Delta^2}t) \tag{37}$$

and,

$$\varepsilon = -\frac{2V_o}{C_o\pi}\left\{\exp(-\frac{W_o}{2}t)\sum_{n=1}^{\infty}\frac{1}{n}\cdot\sin(n\pi/5)\cdot\sin(bx)\left[\frac{(1-2\Delta^2)}{\sqrt{1-\Delta^2}}\right.\right.$$
$$\left.\cdot\sin(bC_o\sqrt{1-\Delta^2}t) - 2\Delta\cos(bC_o\sqrt{1-\Delta^2}t)\right]$$
$$\left. + \frac{W_oL}{C_o\pi}\sum_{n=1}^{\infty}\frac{1}{n^2}\cdot\sin(n\pi/5)\cdot\sin(bx)\right\} \tag{38}$$

where

$$W_o = \frac{E}{\eta}, \quad b = \frac{n\pi}{L}, \quad C_o^2 = \frac{E_o}{\rho_o}, \quad \text{and} \quad \Delta = \frac{W_o}{2bC_o} \quad .$$

It has been verified that equations (37) and (38) satisfy initial conditions (21), boundary conditions (22), the constitutive equation of the Maxwell model (28), and the wave equation (19) (after substitution of the appropriate operators for C^2). The series are convergent and real-valued for all values of W_o and t and reduce to the elastic solutions (26) and (27) when $\eta = \infty$.

3. Numerical Evaluation

Equations (37) and (38) were evaluated numerically by choosing the non-dimensional parameters, $W_o L/C_o$ (called the damping paramter, τ_o), the characteristic time, $T = C_o t/L$, and the normalized reference coordinate, x/L. Stress and strain distributions within the rods for various values of τ_o and for times, T, varying from 0 to 1 were obtained using an IBM model 360 digital computer. Results were displayed graphically with the aid of a Calcomp 566 incremental plotter. The computer program that was used to evaluate equations (37) and (38) is listed in Appendix 2.

Composites of the stress and strain distributions obtained from an evaluation of the first 150 terms of equations (37) and (38) with $\tau_o = 1.00$ and for various values of T are shown in Figures 6 and 7, respectively. The values of stress and strain for the viscoelastic case are reported as multipliers of the magnitudes of the respective stress and strain that would be realized for the elastic case ($n = \infty$). The corresponding magnitudes of the elastic stress and strain are:

$$\sigma_E = \frac{E_o V_o}{2C_o} \qquad \varepsilon_E = \frac{V_o}{2C_o} \quad .$$

As an example, the value of stress for the viscoelastic case is equal to the product of a "stress multiplier" and the corresponding value of the elastic stress magnitude, σ_E . In viewing the results, it is important to remember that the interface of the rods exists at $x/L = 0.2$. Reference to the results of the traveling wave solution for the elastic case (Figs. 4-A through 4-G) will serve to clarify the results of the viscoelastic case.

The small oscillations indicated in Figures 6 and 7 are the result of the non-infinite evaluation of equations (37) and (38). The parts of the distributions which are nearly vertical are thought to be so; however, they do not appear vertical because of finite increments in x/L.

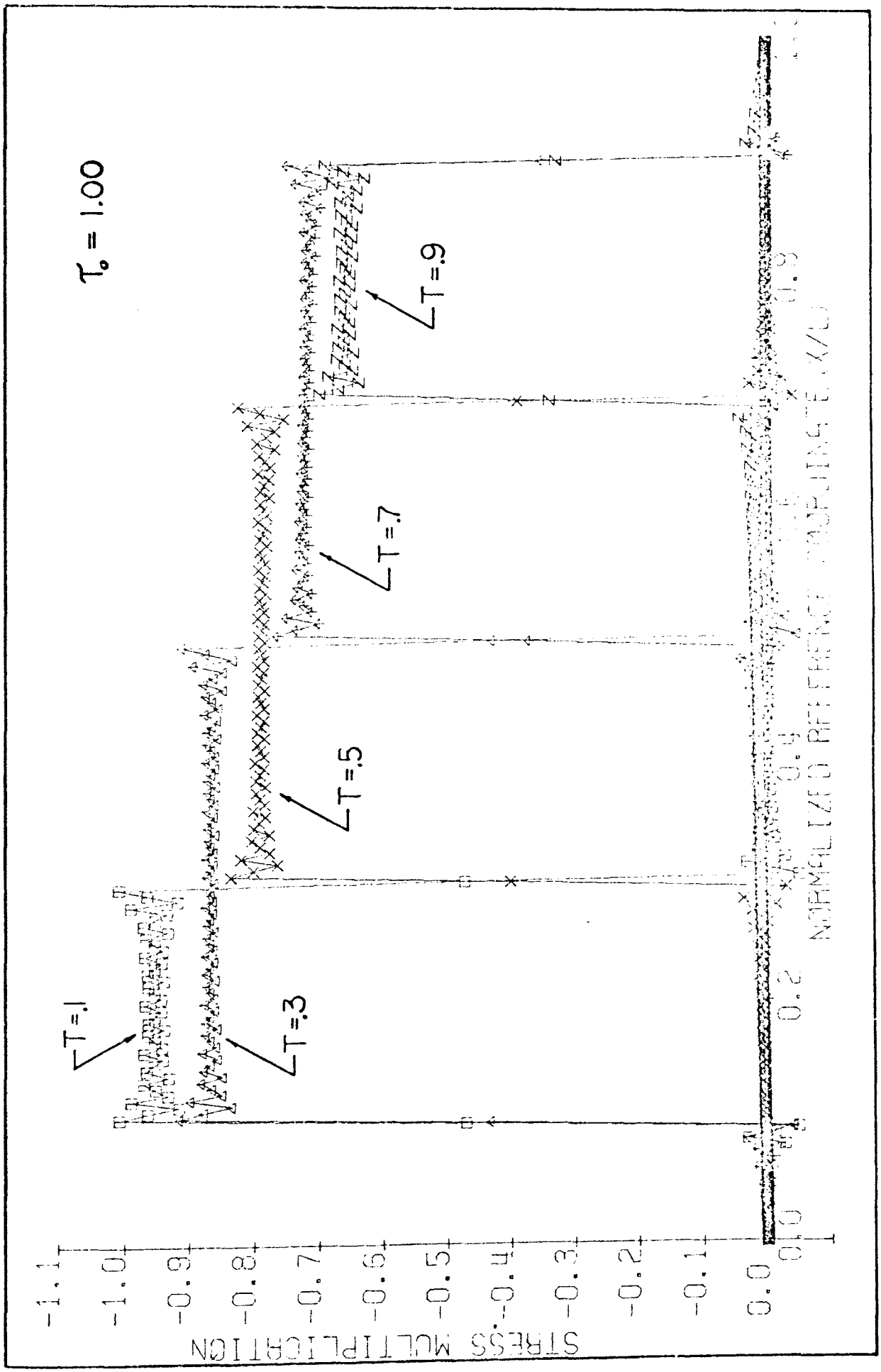

Figure 6. Maxwell stress distributions at (T)

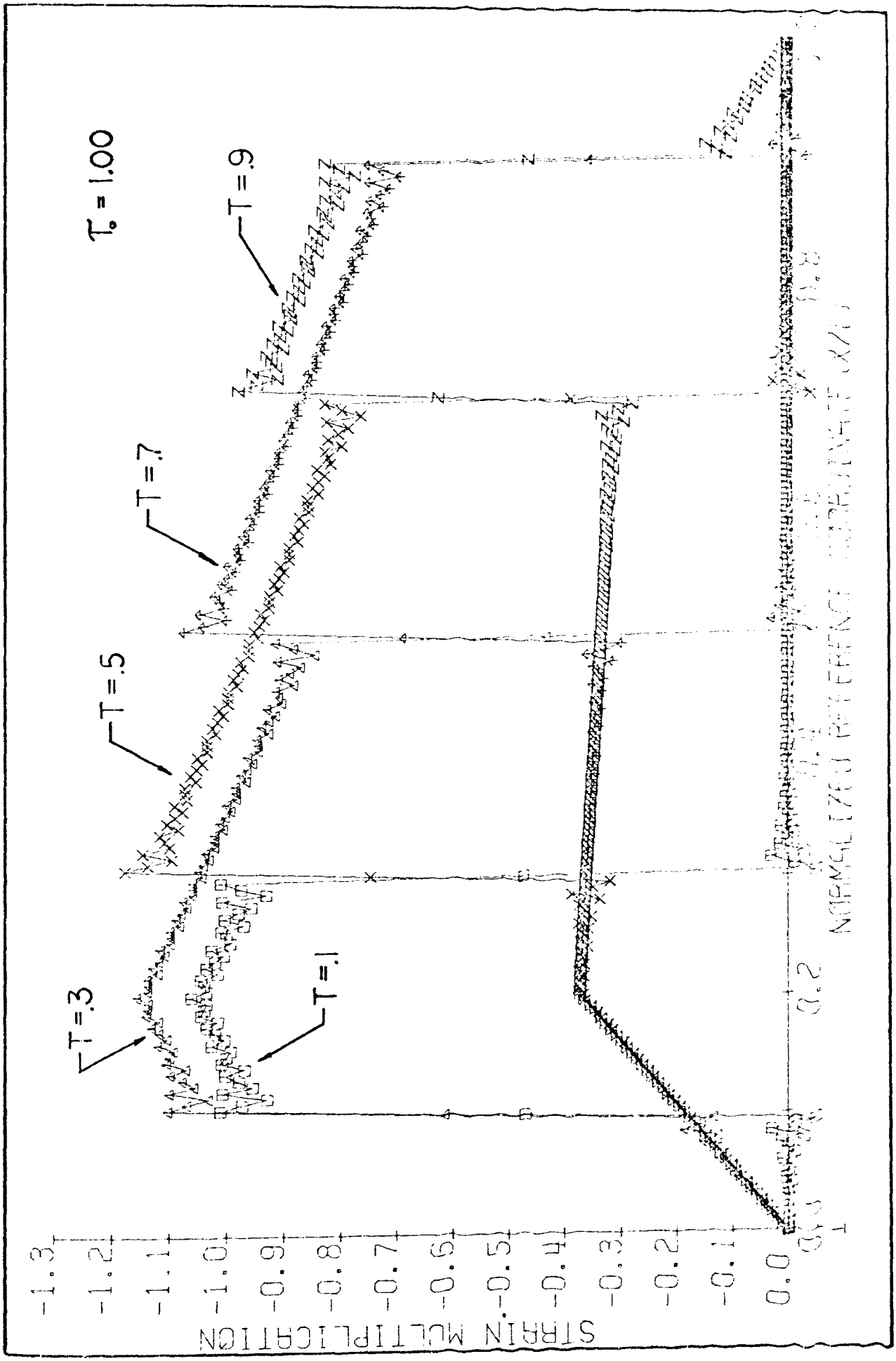

Figure 7. Maxwell strain distributions at (T)

4. Summary of Numerical Results

The solutions, evaluated at various values of $\tau_o > 0$, indicate:

1. The pulse front is propagated with the velocity C_o.
2. The stress and strain, evaluated at the interface and at $T = 0^+$, are equal to the corresponding elastic values.
3. The stress, evaluated at the interface and for $(0^+ < T \leq 0.4)$, is less than the corresponding elastic value (the difference varying directly with the magnitude of τ_o).
4. The strain, evaluated at the interface and for $(0^+ < T \leq 1)$ is greater than the corresponding elastic value (the difference varying directly with the magnitude of τ_o).
5. A "residual stress" condition exists in the rods following the passage of the main pulse. The magnitude of this stress phenomenon is a direct function of the mangitude of τ_o and decays with time.
6. A "residual strain" condition exists in the rods following the passage of the main pulse. The magnitude of this residual strain is a direct function of the mangitude of τ_o and increases with time as long as the residual stress is present.
7. The strain in the rods varies with the magnitude of the stress and the time during which the stress is present.
8. The magnitude of the stress distribution appears to decay exponentially, the rate of decay being a function of the magnitude of τ_o.
9. The "crests" of resultant pulses become increasingly distorted as τ_o is increased.
10. It appears that a reflected tensile pulse will not occur for $\tau_o \gtrsim 2\pi$.
11. The maximum strain occurs at the interface of the rods.

Apparently, the problem of the longitudinal impact of two finite viscoelastic rods has not previously been solved. Hence, a direct comparison of results is not possible. Lee and Kanter [16] have, however, considered the problem of a step velocity applied to an end of a finite rod of a Maxwell material. The aspects of the solutions that can be compared are observed to agree qualitatively. For example, Lee and Kanter have shown that the stress wave is propagated with the elastic wave velocity (C_o) and that the initial stress amplitude $(T = O^+)$ is equal to the elastic stress amplitude. These investigators have not published a solution for the corresponding strain distributions.

IV. MEASUREMENT SYSTEM

The elastic properties of 7075 T651 aluminum at very high rates of loading were determined by subjecting two one-half inch diameter rods of the material to longitudinal impact.

A. Preparation of Test Material

Experimental work was conducted using impacter rods which varied from 2 to 12 inches in length and test rods which varied from 8 to 60 inches in length. In all experiments, the length of the test rod was equal to or greater than the length of the impacter. The test material, as obtained from the supplier, was in the form of one-half inch diameter rods of 12 foot lengths. The test rods and impacters were cut to prescribed length on a flat-bed lathe to insure that the end faces of the rods were perpendicular to their axes of revolution. It was observed that this method also produced very smooth, uniform end faces. No machine work was performed on the lateral surfaces of the rods. It was determined that the maximum variation in the diameter of the rod material at a given section was $\pm$ 0.001 inch.

B. Strain Gages

The test rods were instrumented with Budd metalfilm strain gages (type C12-121-A) in order to determine their response to the impact condition. The characteristics of these gages are as follows: effective gage length = 0.125 inch; gage width = 0.085 inch; gage factor = 2.08 $\pm$0.5%; resistance = 120 $\pm$ 0.2 ohms; epoxy-backed; and temperature and aluminum compensated.

Two strain gages were attached to each test rod such that they were diametrically opposed and so that their strain axes were parallel with the axis

of the rod. Also, the gages were placed such that their tabs were away from the impact end of the test rod. To insure proper positioning of the strain gages on the test rods, longitudinal alignment lines and circumferential location lines were lightly scribed on the rods with a vernier height gage. Eastman 910 adhesive was used to attach the strain gages to the test rods.

C. Wheatstone Bridge

The strain gages were electrically connected so that they became opposite arms of the Wheatstone bridge shown in Figure 8. In view of the geometrical location of the gages, this arrangement negates the presence of any bending strain and doubles the output with respect to axial strain. Initial balancing of the bridge is accomplished with the 25 k ohm resistor in series with the galvanometer (for protection of the galvanometer). Final balancing is accomplished with the 25 k ohm resistor short circuited. Calibration and strain determination are done with the 25 k ohm resistor in series with the galvanometer. (This provides an effectively open circuit between points C and D.)

D. Oscilloscope and Camera

A Tektronix model 564 storage oscilloscope (with 3A3 differential amplifier and 3B3 time base plug-in units) was used to read the output of the Wheatstone bridge. This scope and plug-in unit arrangement provides an upper frequency response limit of 500 k Hz (high bandwidth) and an upper frequency response limit of 5 kHz (low bandwidth) with display voltage variable from 0.1 mv/cm to 10 mv/cm, sweep time capability from 10 sec/cm to 0.1 micro sec/cm, and corresponding delayed sweep capability.

Photographs of the stored display were taken with a Tektronix oscilloscope camera.

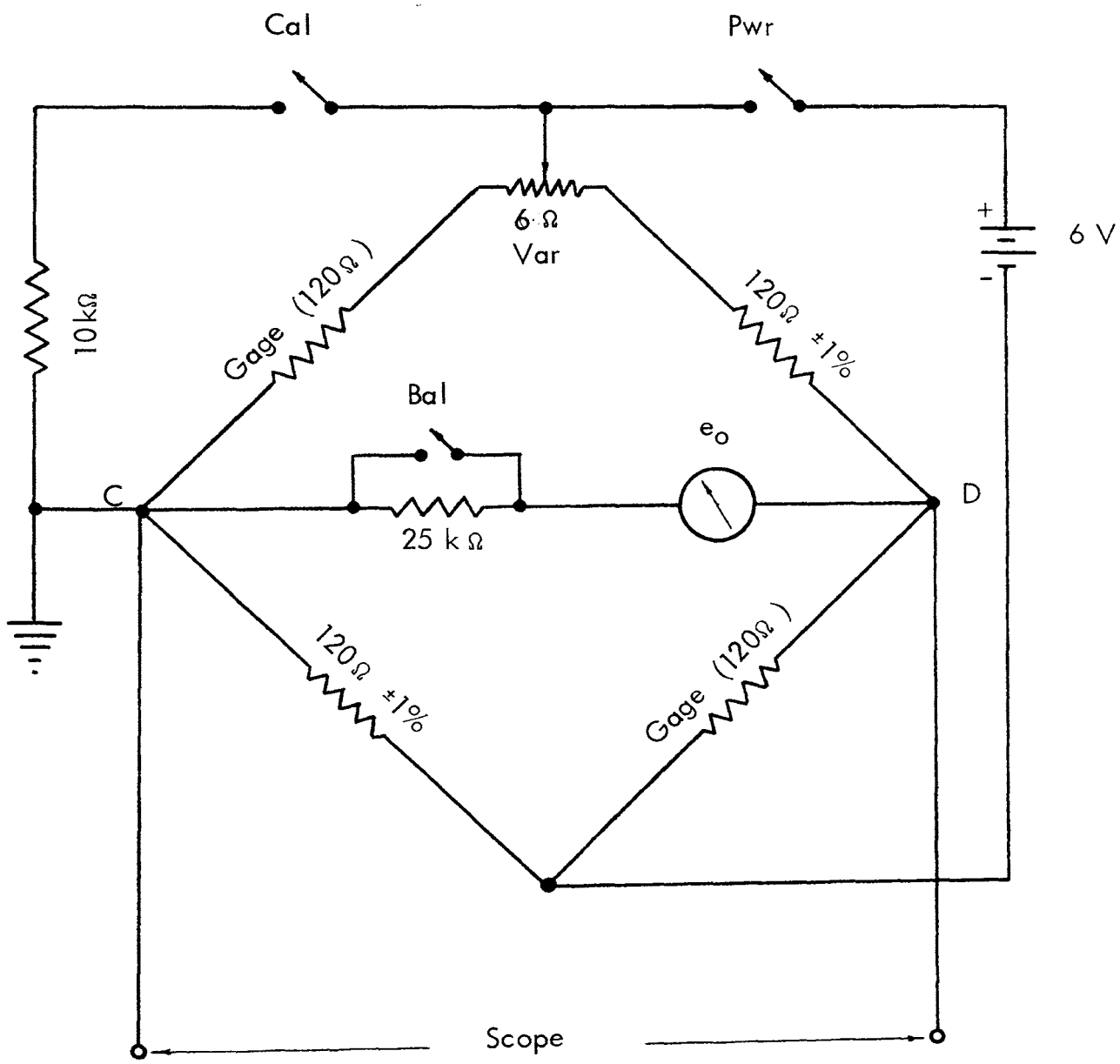

Figure 8. Wheatstone bridge

E. Air Gun Launcher

The impacting rod was accelerated to a uniform velocity using the air gun launcher shown in Figures 9 and 10. The air gun consists basically of a pressure chamber section and a barrel-silencer section. The barrel-silencer was sized so that it permitted unrestricted passage of the impacter. Prior to firing, the impacter was normally placed at the breech end of the barrel and the barrel was isolated from the pressure chamber with a diaphragm (aluminum foil). One type of the foil ruptured consistently at a chamber pressure near 32 psig and the other type at chamber pressures near 55 psig.

Air pressure was slowly admitted to the chamber until the bursting pressure (prescribed by the number and combination of foil thicknesses) was achieved. The pressure differential across the impacter then permitted it to be accelerated toward the muzzle end of the barrel-silencer. The silencer served to bleed-off the pressure differential across the impacter, thereby producing a nearly uniform impacter velocity at the muzzle. The original gun geometry was determined using a form of the Pidduck-Kent limiting solution. A description of this method and a listing of the computer program that was used are given in Appendix 1.

F. Velocity Measurement

The velocity of the impacter was measured over a one-foot section of the silencer using the output of a photo-electric triggering device to start and stop an electronic counter. The photo-trigger device consisted of two separate channels, one of which is shown in Figure 11. A light beam (produced by a D.C., high-intensity lamp) was shown through a pair of silencer holes at each of the designated velocity-measurement points. These light beams then fell on the corresponding photo-tubes associated with each channel of the photo-trigger device. The circuitry and light source associated with the velocity measurement station nearest the pressure chamber of the air gun has been designated as photo-station 1.

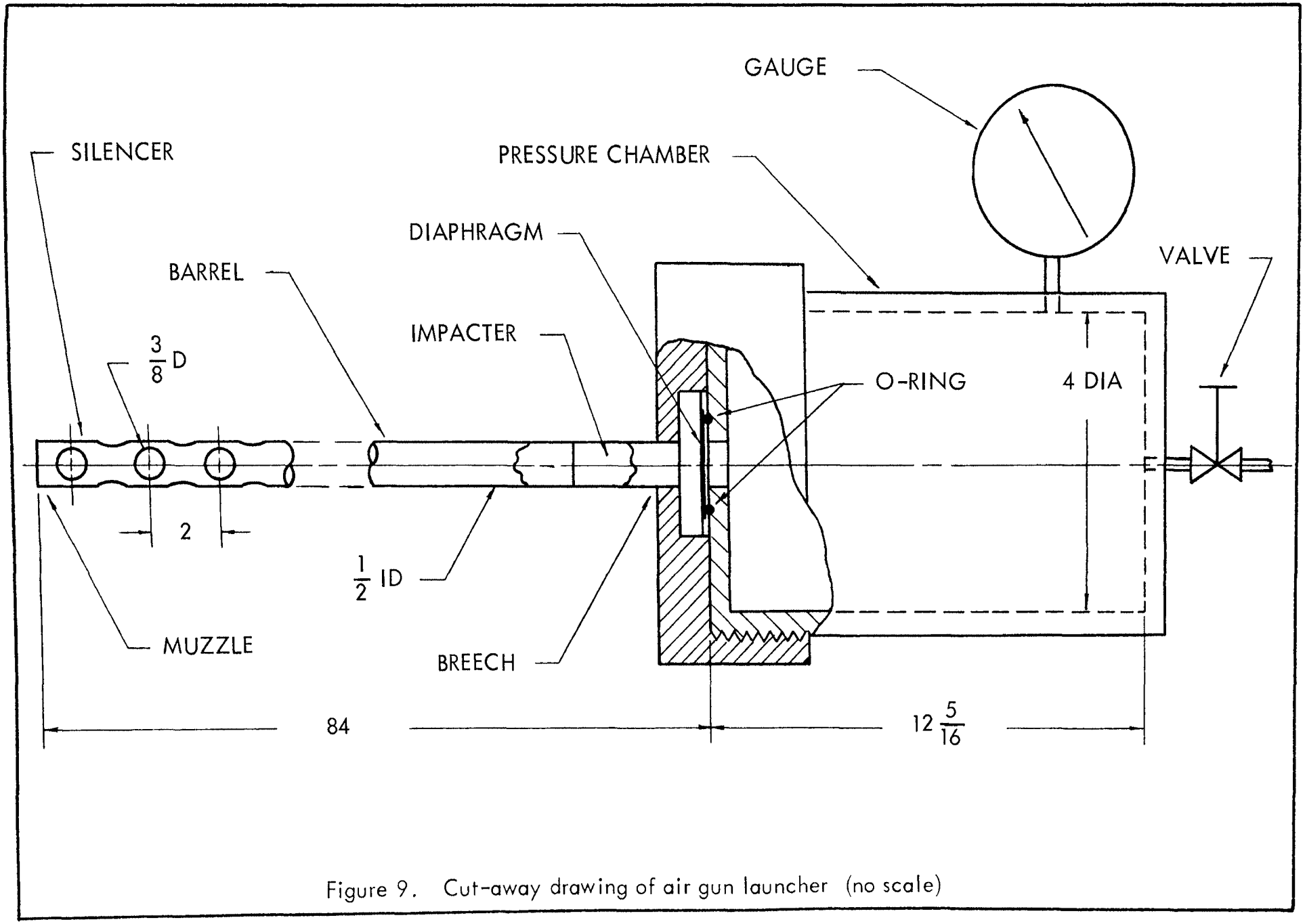

Figure 9. Cut-away drawing of air gun launcher (no scale)

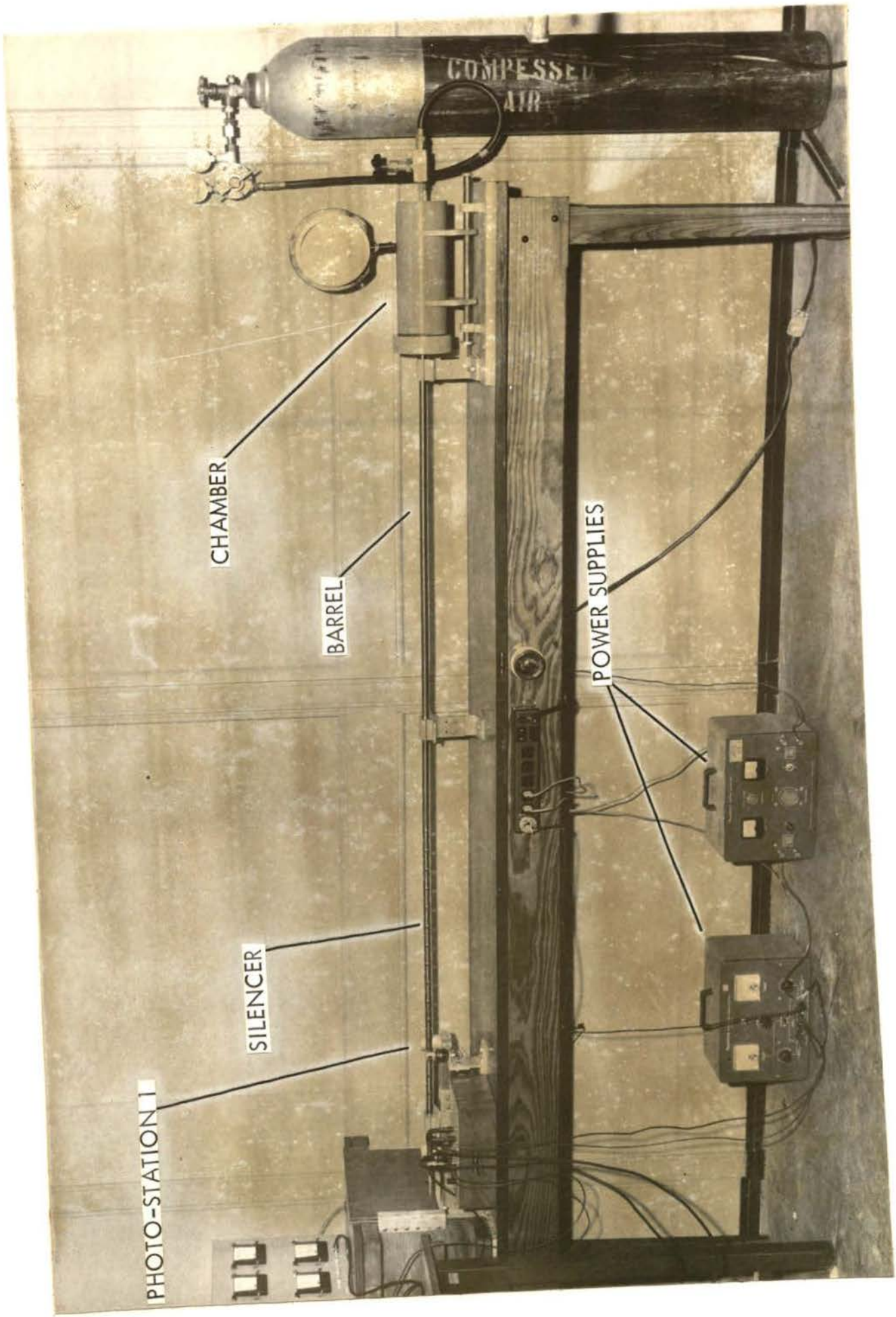

Figure 10. Air gun launcher

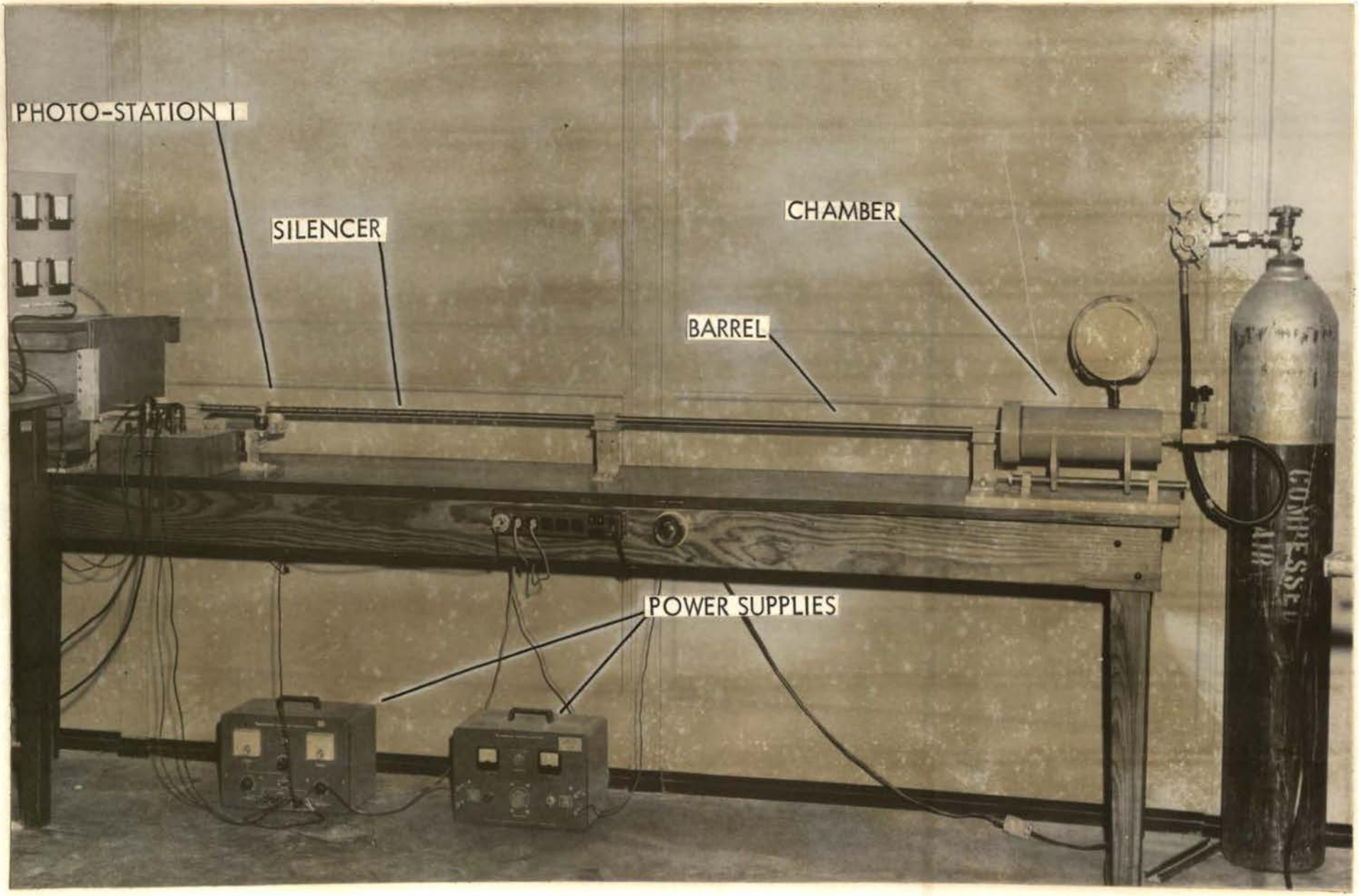

Figure 10. Air gun launcher

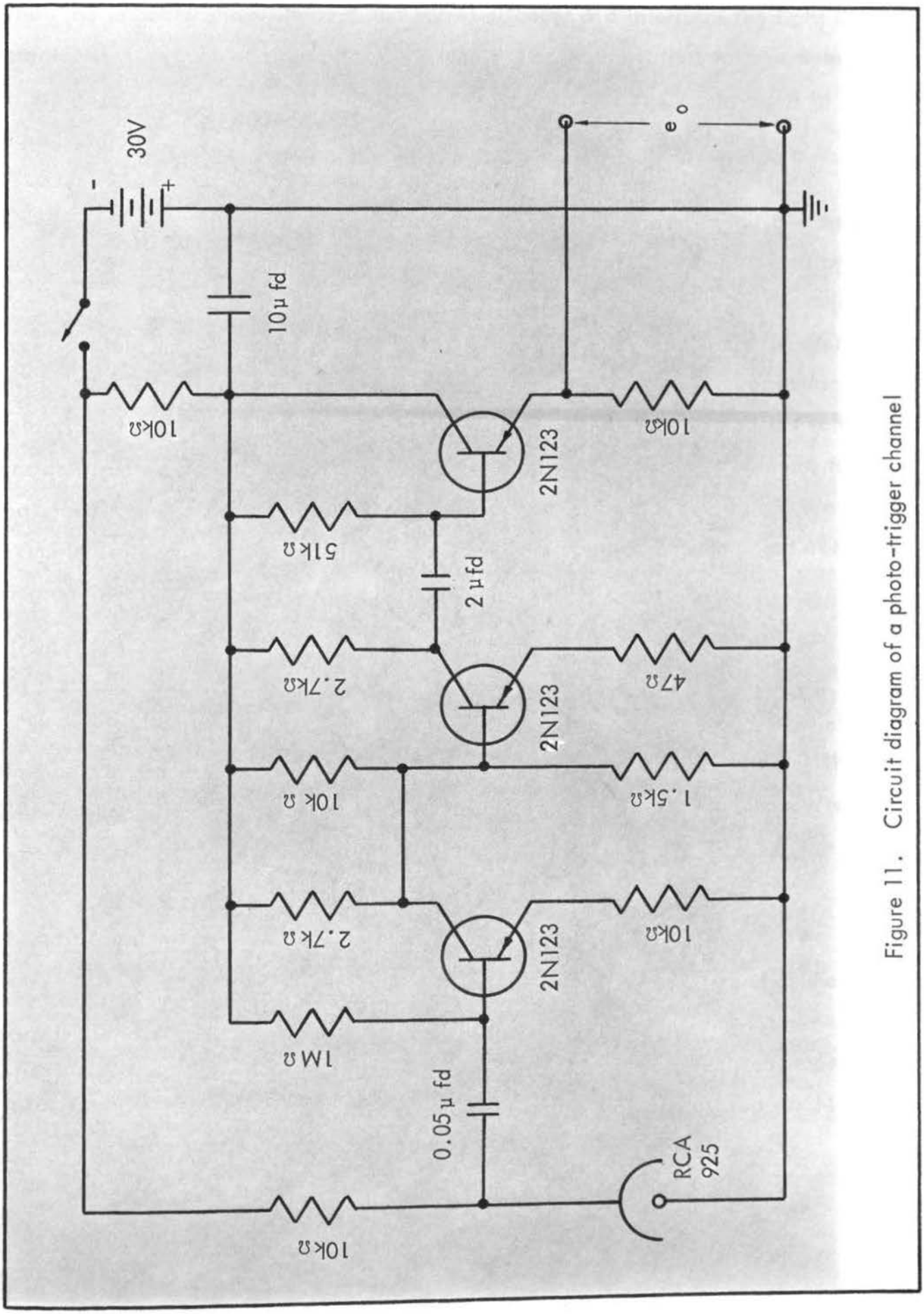

Figure 11. Circuit diagram of a photo-trigger channel

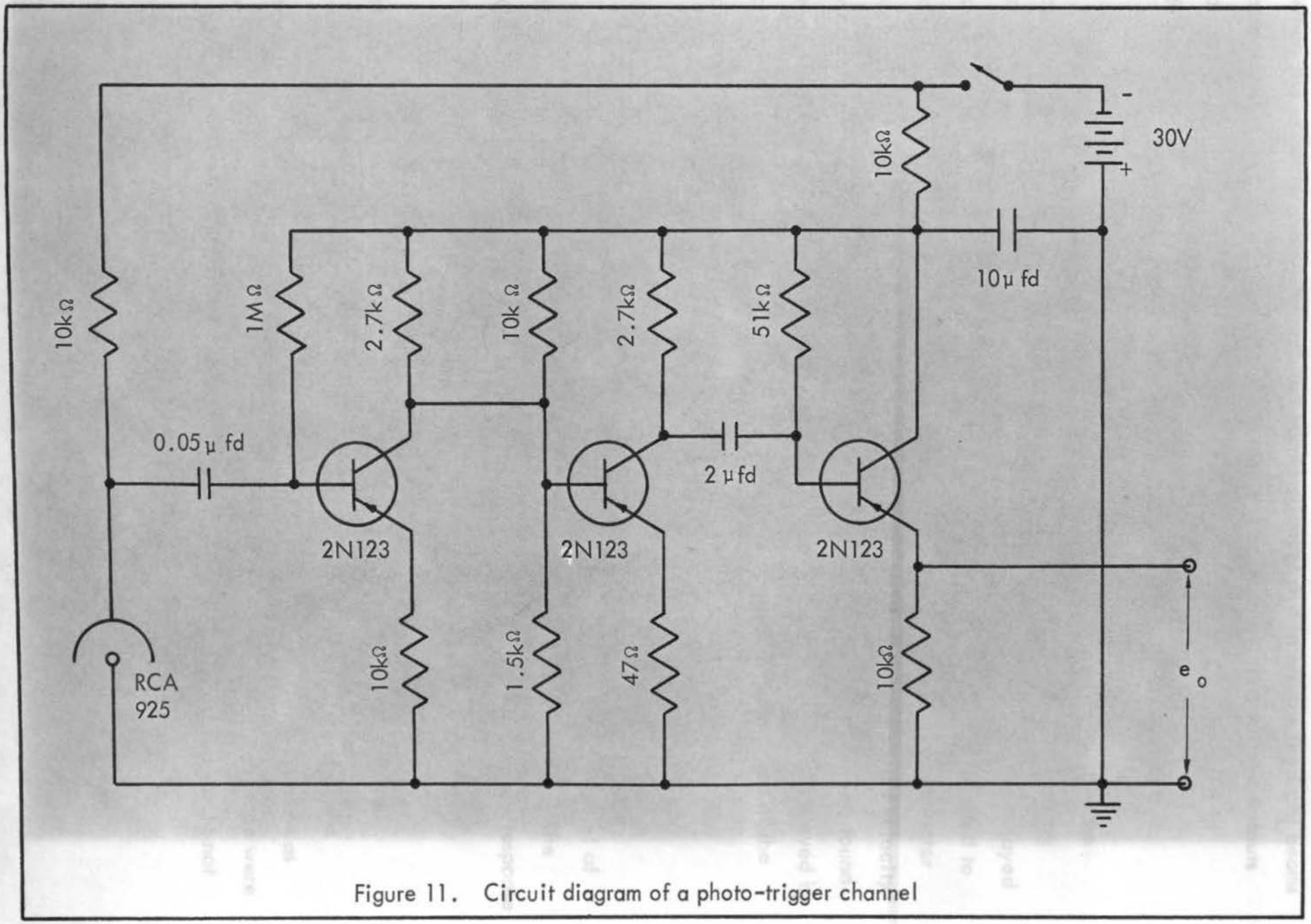

Figure 11. Circuit diagram of a photo-trigger channel

When the impacter passes through the barrel-silencer and interrupts the light beams associated with each photo-station, the result is two consecutive voltage outputs on separate channels. Sample outputs of photo-stations 1 and 2 are shown in Figures 12 and 13, respectively.

The voltage output of the second photo-station was used to initiate the oscilloscope trace. In order to insure that the first compressive pulse resulting from the impact would be displayed, it was found necessary to employ the delayed sweep feature of the oscilloscope. It was learned that the delay time required to display the first pulse near the beginning of the trace was a function of impacter velocity. Hence, a calibration curve of required delay time-vs-impacter velocity was constructed from test results as impacter velocity was increased. It was found that good trace location (for an expected impacter velocity) could be achieved by a simple projection of the existing curve as it developed during the phase of the program involving gradual increases in impacter velocity.

G. Electronic Counter

A General Radio type 1191 counter was used to determine the interval of time between the consecutive voltage pulse outputs of the photo-stations. The General Radio has a time base of 10 M Hz, dual channel inputs, frequency response from D.C. to 20 M Hz, and a threshold level of ± 100 mv.

H. Test Rod Position

The test rod was placed upon a support table at the muzzle end of the barrel-silencer, as shown in Figure 14, such that 13/16 inch of the test rod was within the silencer at the time of impact. Five thicknesses of electrical tape were wrapped around the test rod at two locations to insure that the test rod would not come in contact with the support table following impact.

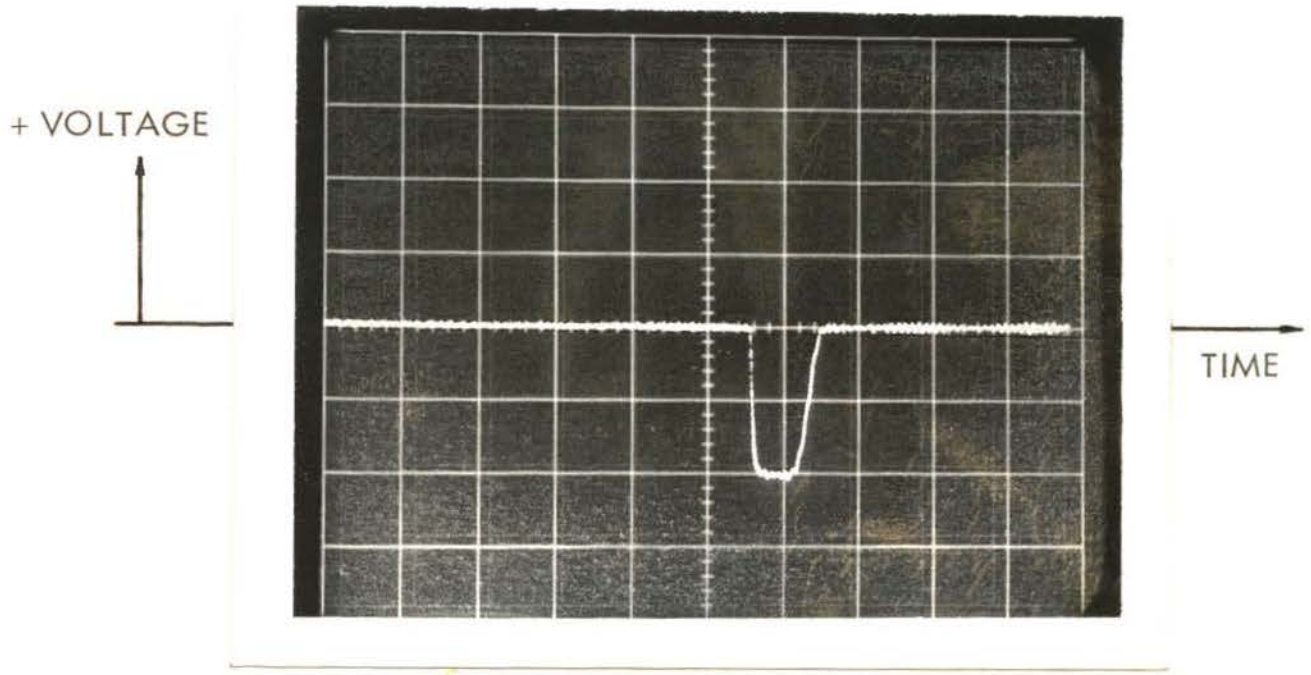

Figure 12. Sample output of photo-station 1. $V_o \approx 140$ fps, impacter length = 3 in, sweep time = 1 msec/div, amplification = 2 v/div, and bandwidth = 5 kHz.

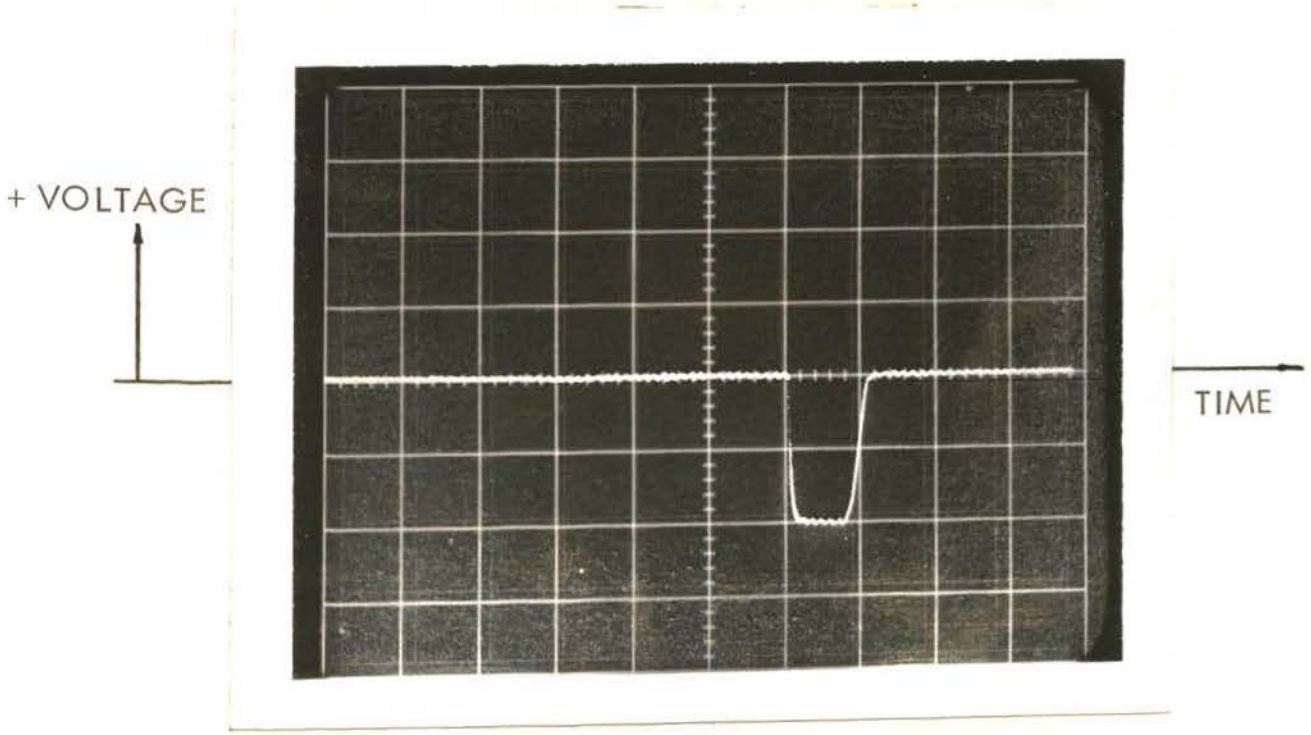

Figure 13. Sample output of photo-station 2. $V_o \approx 140$ fps, impacter length = 3 in, sweep time = 1 msec/div, amplification = 2 v/div, and bandwidth = 5 kHz.

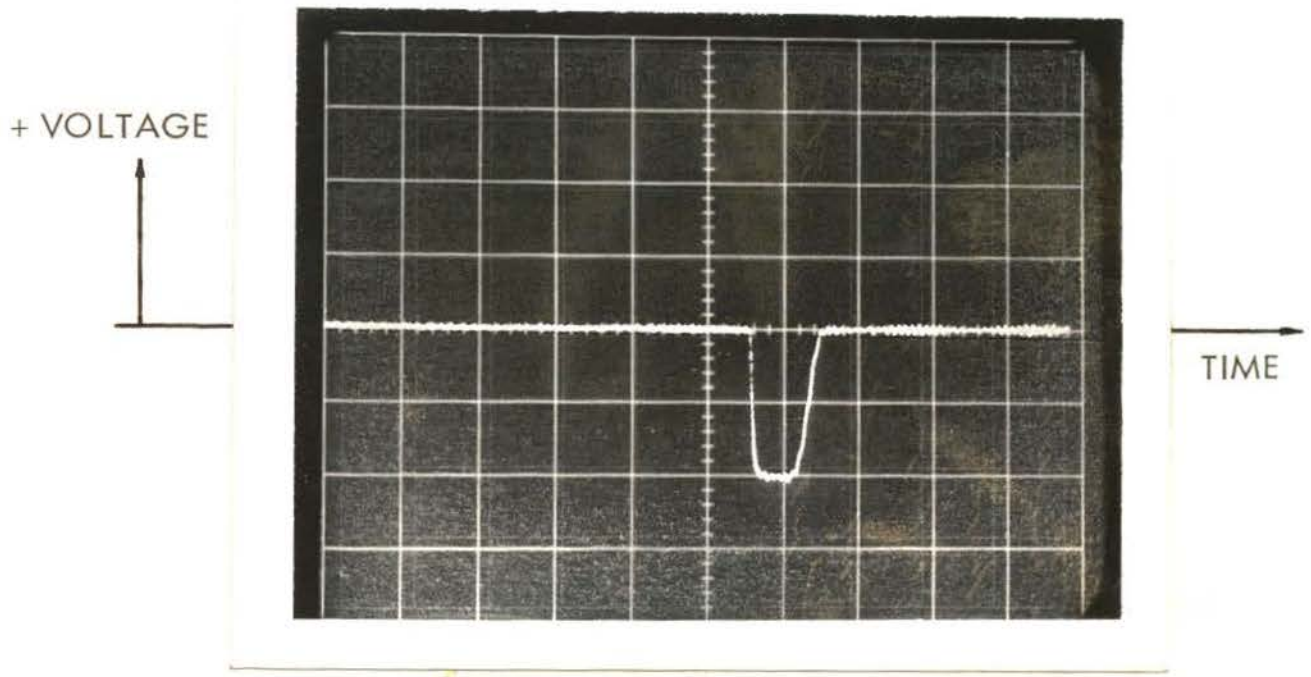

Figure 12. Sample output of photo-station 1. $V_o \approx 140$ fps, impacter length = 3 in, sweep time = 1 msec/div, amplification = 2 v/div, and bandwidth = 5 kHz.

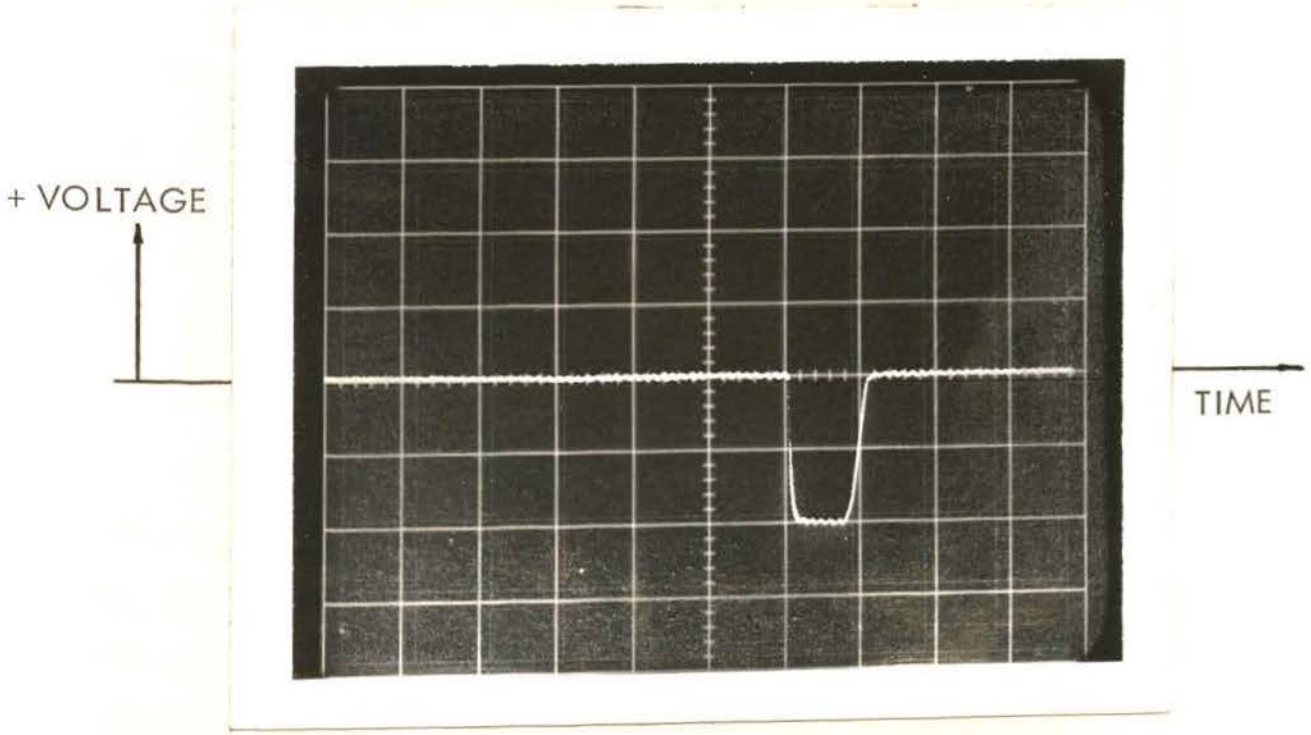

Figure 13. Sample output of photo-station 2. $V_o \approx 140$ fps, impacter length = 3 in, sweep time = 1 msec/div, amplification = 2 v/div, and bandwidth = 5 kHz.

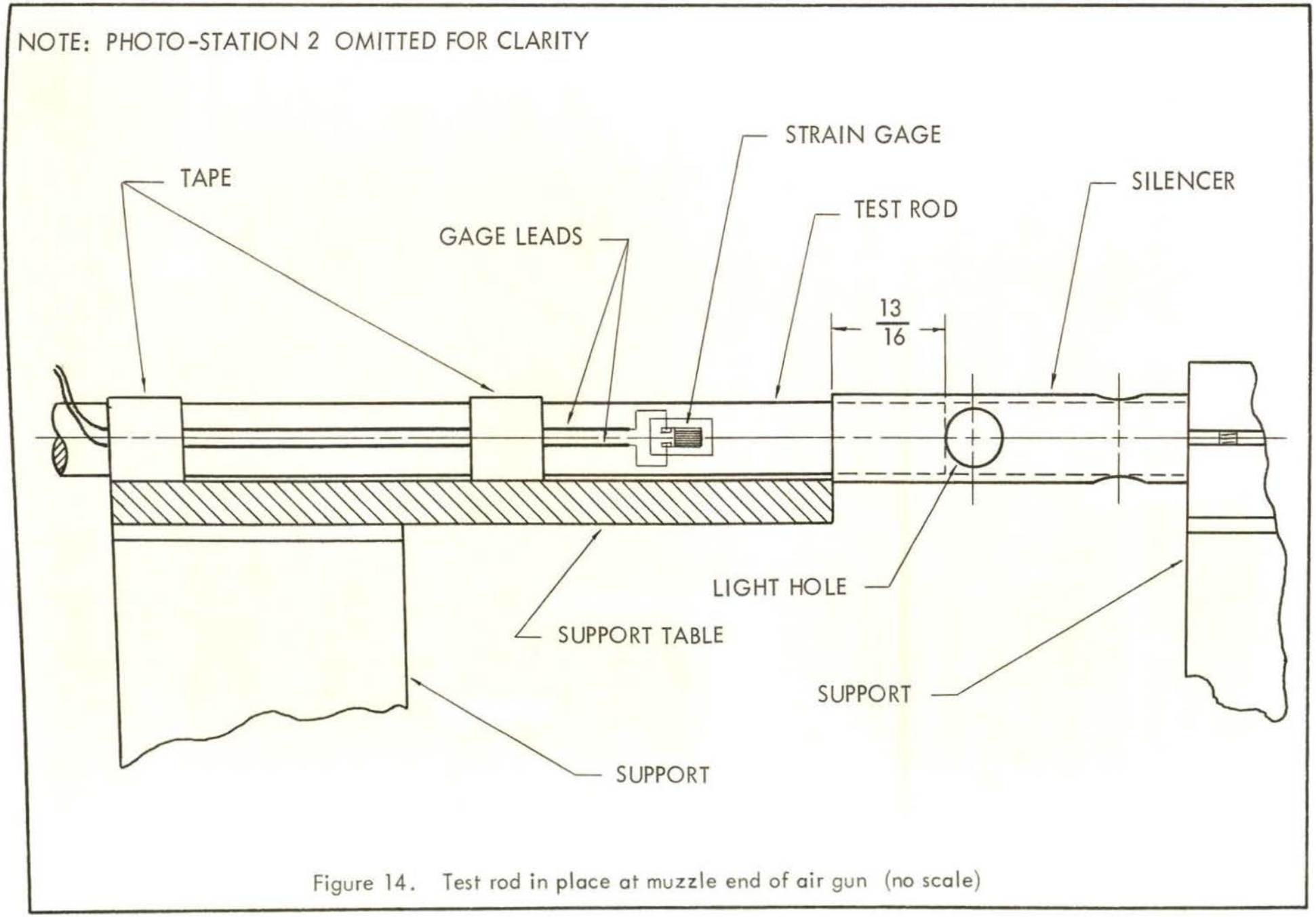

Figure 14. Test rod in place at muzzle end of air gun (no scale)

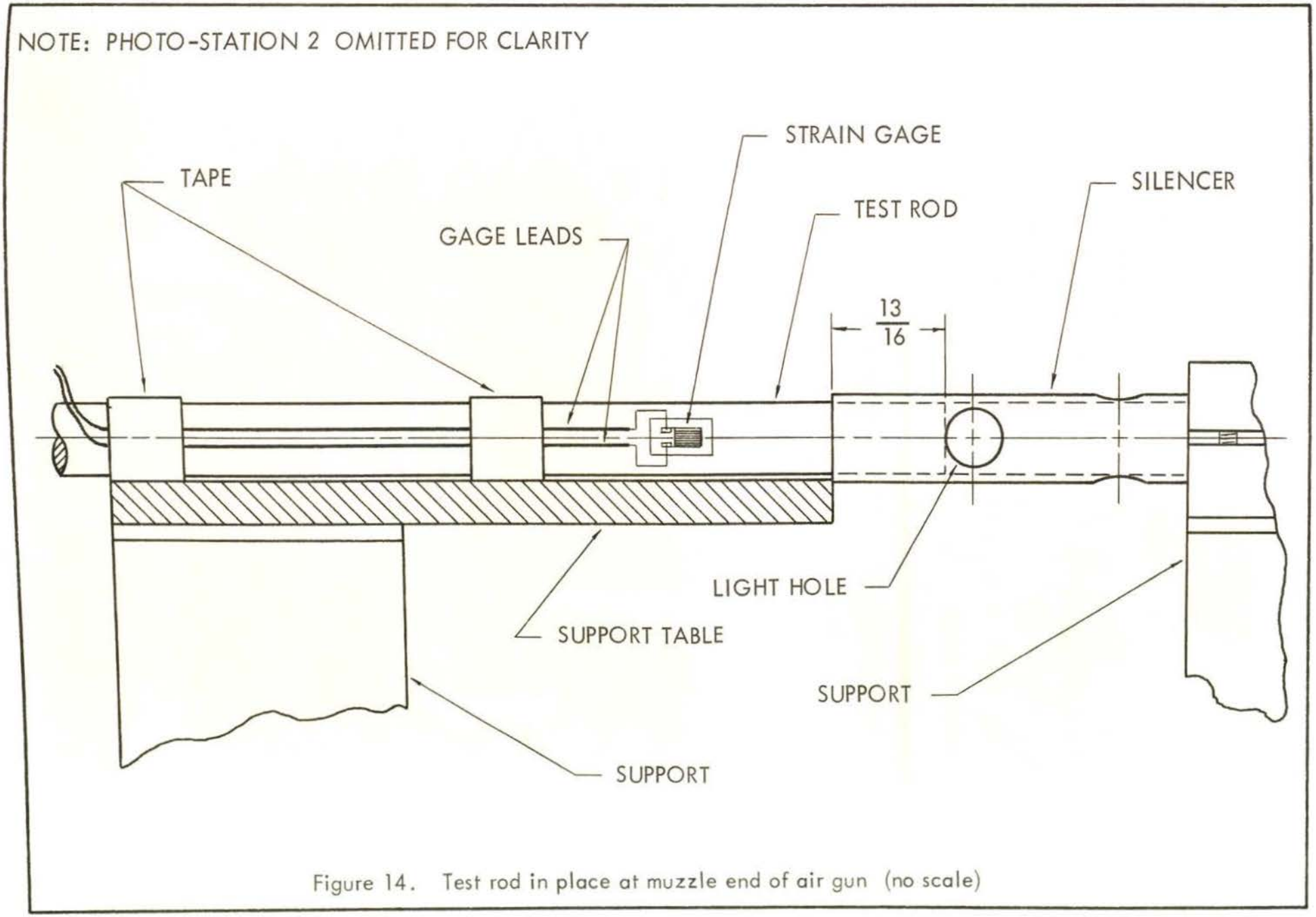

Figure 14. Test rod in place at muzzle end of air gun (no scale)

The original alignment of the support table was accomplished using a dummy rod which was identical to the test rod in that it was of the same material and that it was also wrapped with five thicknesses of electrical type. The tape was placed on the dummy rod such that it entered the silencer three inches when placed in position on the support table. The height and inclination of the support table were then adjusted so that the dummy rod slid freely in the silencer with both wrappings of tape in contact with the polished support table. At this point, alignment lines (parallel to the longitudinal axis of the dummy rod) were placed on the support table. This procedure was used as an additional assurance that the test rod would be properly aligned when placed in position prior to the test. It was generally observed, however, that accurate alignment of the test rod could be achieved merely by placing it at its test position.

A photograph of the muzzle end of the air gun with the test rod in place, and of the velocity and strain measuring equipment, is shown in Figure 15.

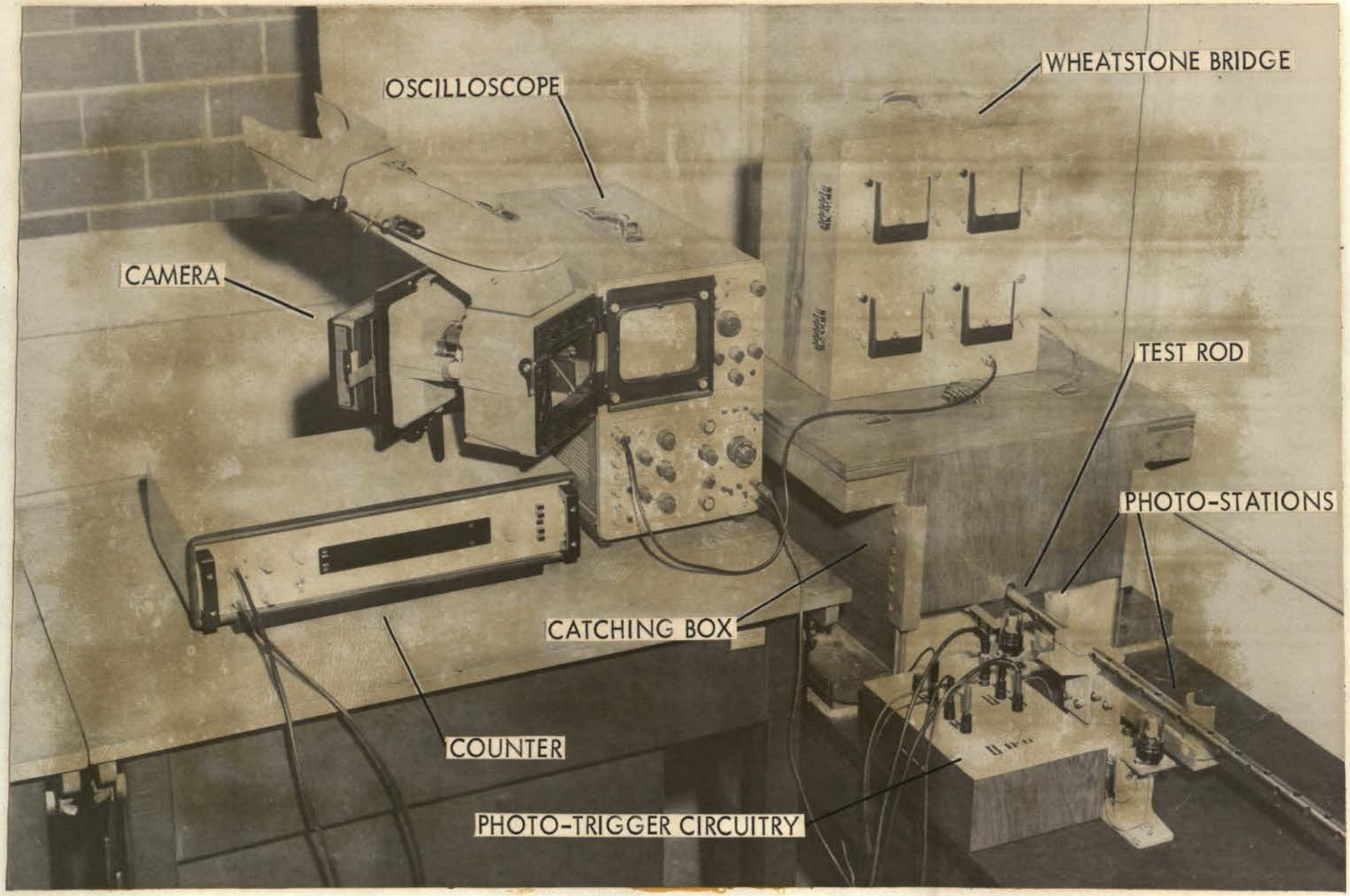

Figure 15. Velocity and strain measuring equipment

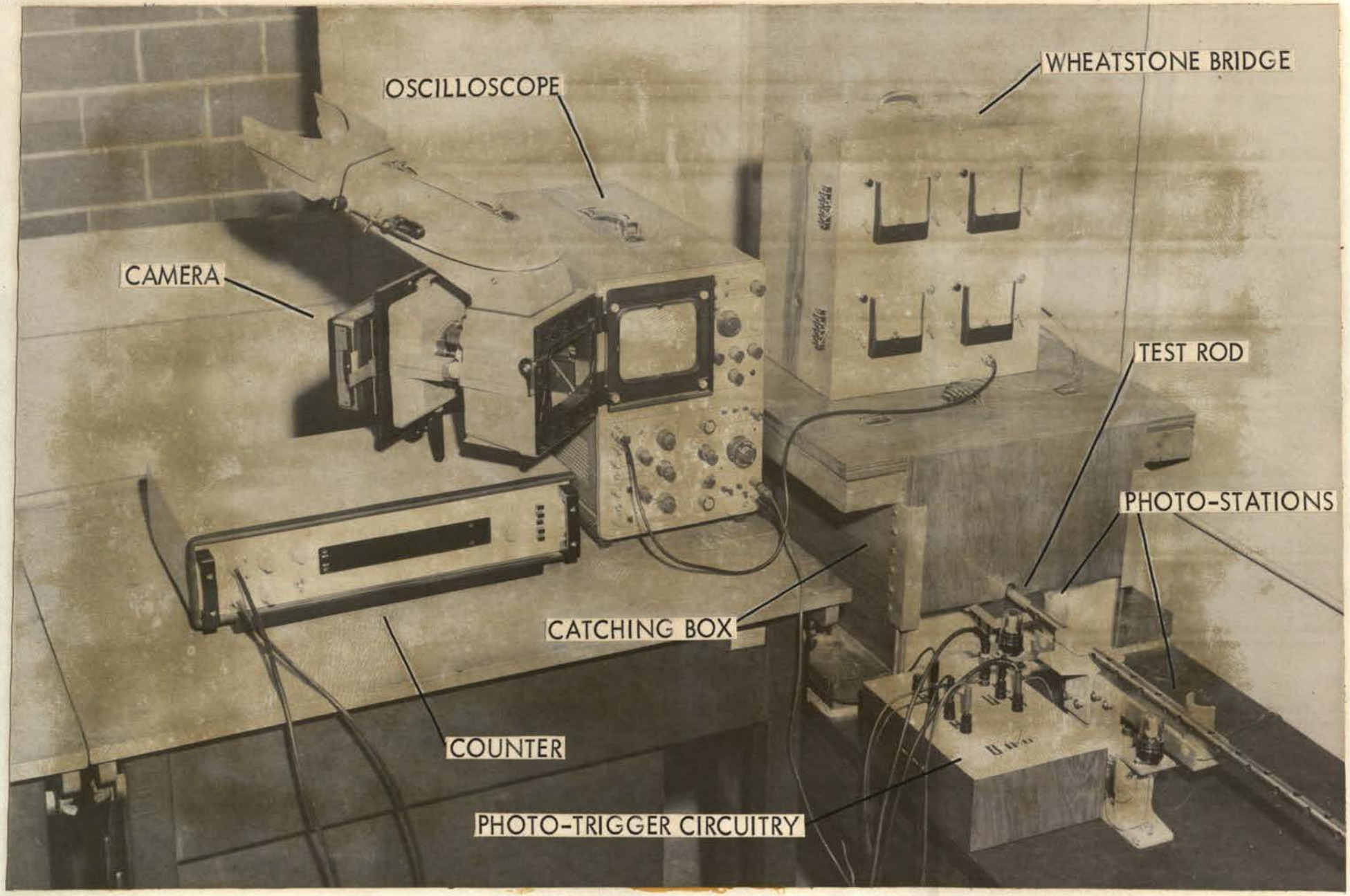

Figure 15. Velocity and strain measuring equipment

V. EXPERIMENTAL PROGRAM

During all phases of the experimental program, electrical equipment was allowed at least one-half hour to attain operating temperature.

A. Air Gun Evaluation

The initial phase of the experimental program consisted of the testing and evaluation of the air gun launcher. Calibration curves of impacter velocity-vs-chamber pressure were constructed from experimental data and compared to theoretical predictions.

It was observed that a 2.5 volt threshold level for the electronic counter provided consistent results and triggering that was not influenced by electrical noise.

The initial length of the barrel-silencer of the air gun was chosen to be 84 inches. The barrel was originally 60 inches long with the silencer constituting the remaining 24 inches. It was initially observed that the shape of the experimental velocity-pressure curve for a two-inch projectile did not compare well with theoretical predictions for an air gun with a 60 inch barrel length. It was ascertained that the number and size of the pressure-relief holes in the silencer did not allow sufficient pressure-relief to insure that the impacter was not accelerating within the velocity-measurement portion of the silencer. The number and size of the pressure-relief holes were then empirically increased. This procedure was repeated several times until the slopes of experimental and theoretical impacter velocity-chamber pressure curves were observed to compare favorably (see Appendix 1). A final determination of the magnitude of the acceleration was made by changing the location of the photo-stations such that the average velocity of the impacter was measured at a location six inches nearer the pressure chamber.

The results yielded by this method showed a negligible difference in average impacter velocity between the photo-stations for chamber loading pressures on the order of 200 psig. At this point, the length of the silencer had been increased to 36 inches and 68 pressure-bleed holes of 3/8 inch in diameter had been produced in the silencer.

B. Test Procedure

The second phase of the experimental program consisted of the determination of the strain-vs-time relation at a location on the test rod resulting from its collision with the impacting rod.

Initial tests were made at low impacter velocities in order to determine that all associated equipment was operating properly. The following procedure was consistently observed in the conduct of tests: (a) the air gun barrel-silencer was cleaned to insure that no pieces of aluminum foil diaphragm were present as a result of previous testing; (b) the magnitude of the expected strain was determined from elementary considerations using the expected impacter velocity and the oscilloscope amplifier gain correspondingly set; (c) the delay time for the oscilloscope sweep was set, corresponding to the expected impacter velocity; (d) the test rod was placed at its proper position on the support table and the leads of the strain gages were connected to the Wheatstone bridge; (e) a light oil was applied to the lateral surface of the impacter and the excess removed with a clean cloth; (f) the impacter was placed within the barrel; (g) the proper combination of foils was placed at the chamber-breech interface and the chamber was closed; (h) the lights of the photo-stations were turned on and the photo-stations were triggered by a manual interruption of the light sources in order to determine if the counter and scope were being triggered properly; (j) air was slowly admitted to the chamber until the diaphragm burst and its bursting pressure was noted; and (k) a photograph of the stored display was taken with the oscilloscope camera.

VI. EXPERIMENTAL RESULTS

A. Determination of Results

When strain gages are mounted at a location $x = \xi$ on the test rod of Figure 2, the strain-time history indicated by the gages can be determined by following a line drawn through $x = \xi$ and parallel to the t-axis in the direction of increasing t. The validity of this theoretical consideration for the case of rods made from 7075 T651 aluminum was the chief concern of the experimental program.

The Aluminum Company of America [25] lists the properties of cold finished 7075 T651 aluminum rod as follows: (a) modulus of elasticity - 10.4×10^6 psi; (b) yield strength - 66,000 psi; (c) ultimate strength - 77,000 psi; and (d) density - 0.101 lb_m/cu in. The 7075 prefix indicates that this material contains the following percentages of alloying elements: (a) 1.6% copper; (b) 2.5% magnesium; (c) 0.3% chromium; and (d) 5.6% zinc. The T651 suffix indicates that the material has been solution heat-treated and subsequently stress-relieved by stretching to a permanent strain of 1.5 to 3.0%.

Experimental results were obtained by interpreting photographs of oscilloscope traces that resulted from tests at various impacter velocities. A graphical representation of a typical oscilloscope trace is shown in Figure 16.

It was determined during the course of the experimentation that direct viewing of the stored display yielded results that differed slightly from those obtained from the photographed trace. Calibration of this error revealed that the photographed results showed magnitudes that were smaller by a factor of approximately 0.025 division/division, the error being zero at the center of the

graticule and increasing almost linearly in both the voltage and time directions. It was observed that a small distance existed between the graticule face and the face of the cathode-ray tube of the oscilloscope and this condition caused the observed parallax error. All distances measured from photographed oscilloscope traces were appropriately corrected to insure accurate representation of the results.

A calibration check prior to each shot showed a consistent calibration voltage of -18 mv. With reference to the Wheatstone bridge of Figure 8, the calibration strain is

$$\varepsilon_{cal}(\%) = \frac{-120\,\Omega}{(2)(2.08)(10120\,\Omega)} \times 100\% = -0.2851\%\ \text{strain}$$

where 2.08 is the gage factor as provided by the strain gage manufacturer. Dividing the equivalent strain by the calibration voltage results in a strain-voltage calibration of 0.01584% strain/mv.

Once the corrected magnitude of the first voltage pulse was determined, it was then possible to calculate the corresponding magnitude of the strain pulse by using the strain-voltage calibration of 0.01584% strain/mv.

Three methods were used to determined the velocity of wave propagation in the test material. The first method (t_1 method) involved determination of the duration of the first compressive pulse (see Fig. 16) and dividing this time into the theoretical pulse length (2L/a). In the second method (t_2 method) the elapsed time between the beginning of the first compressive pulse and the beginning of the first tensile pulse was determined (see Fig. 16) and divided into the distance traveled by the wave front during this time, $2(L - \xi)$. In the third method (t_3 method), the elapsed time between the beginning of the first compressive pulse and the beginning of the last determinable tensile pulse was measured and divided into the corresponding distance traveled by the wave front. In Figure 16, the last determinable tensile pulse corresponds to the second tensile pulse.

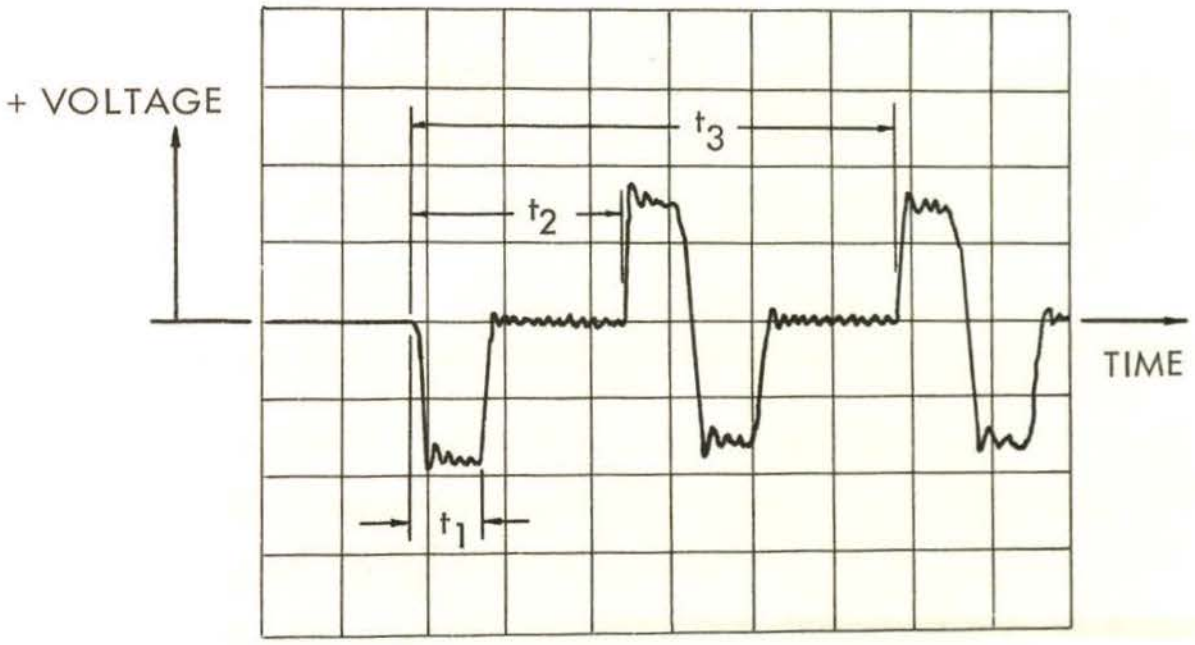

Figure 16. Graphical reproduction of a typical oscilloscope trace. Graticule divisions (div) shown.

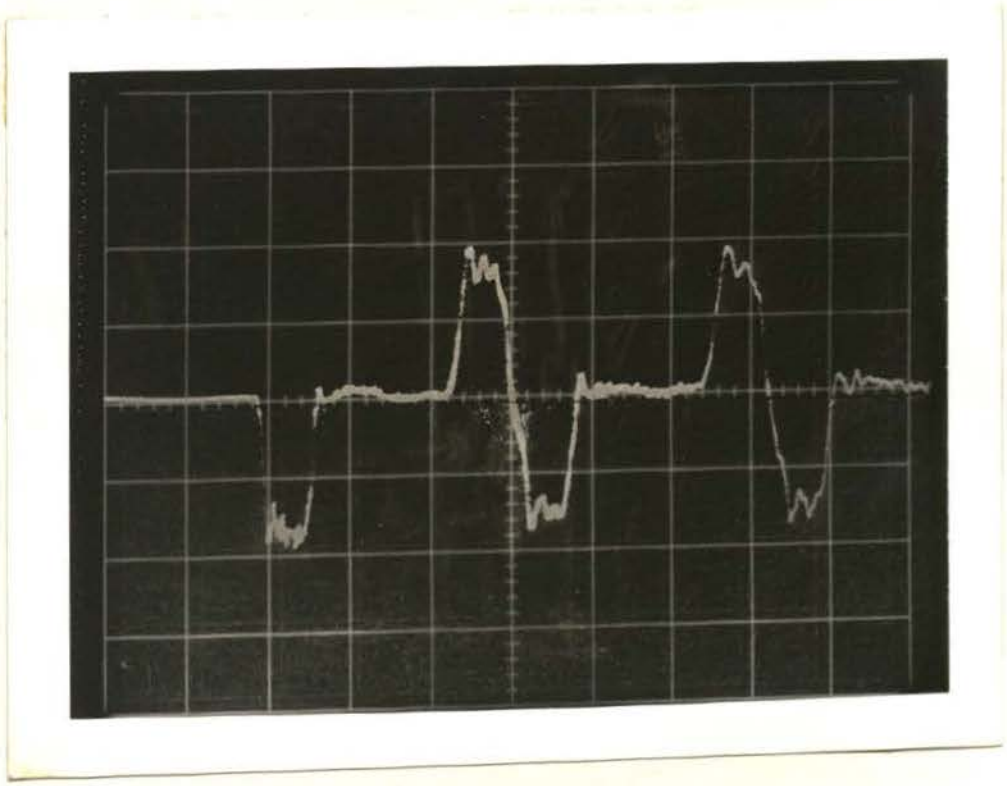

Figure 17. Photograph of stored oscilloscope trace for Shot Number 6. V_o = 95.3 fps, sweep time = 50 μ sec/div, amplification = 10 mv/div, bandwidth = 500 kHz, cal = 0.01584% strain/mv, L = 19 in, L/a = 3 in, and ξ = 7 in.

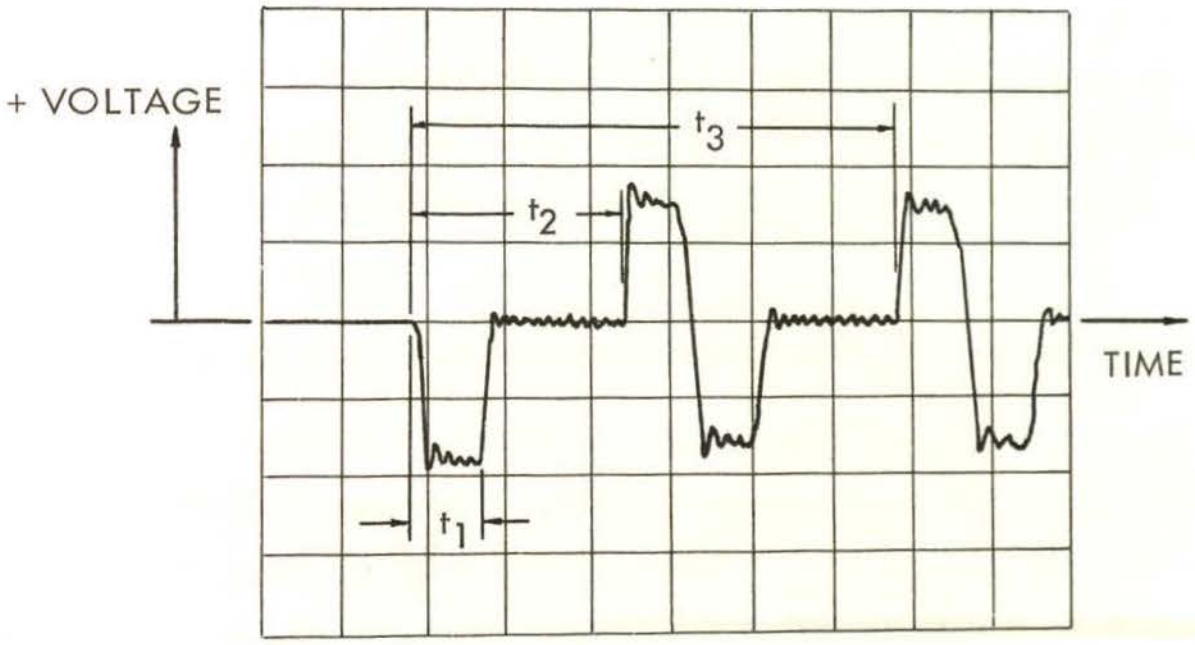

Figure 16. Graphical reproduction of a typical oscilloscope trace. Graticule divisions (div) shown.

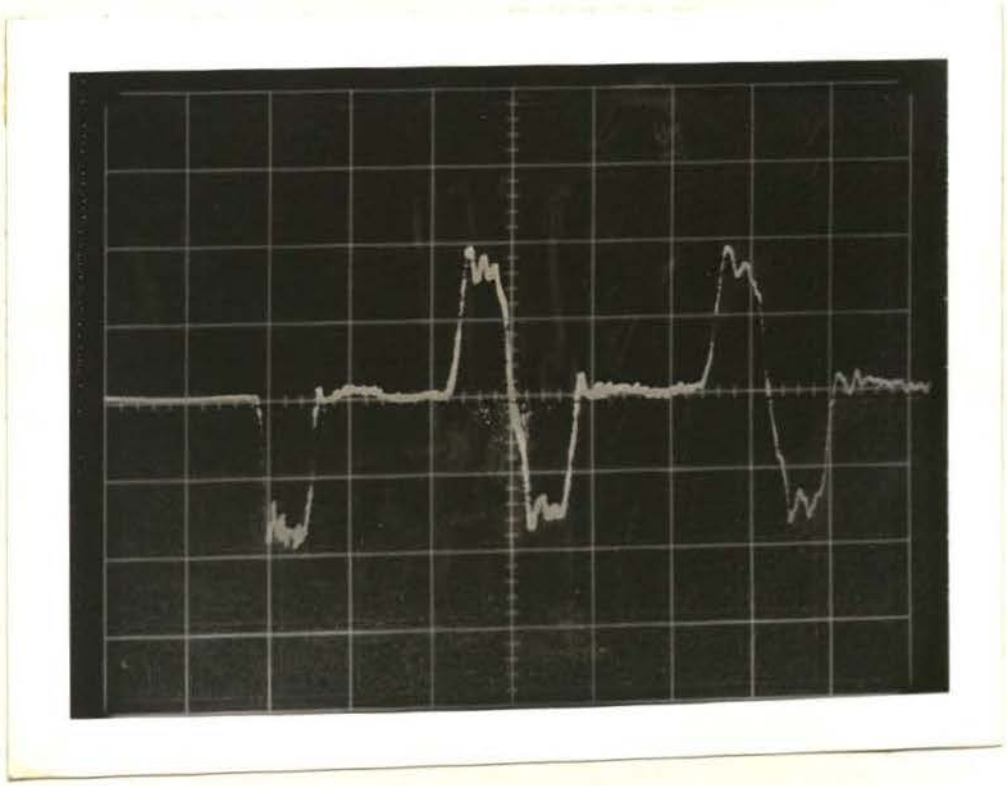

Figure 17. Photograph of stored oscilloscope trace for Shot Number 6. V_o = 95.3 fps, sweep time = 50 μ sec/div, amplification = 10 mv/div, bandwidth = 500 kHz, cal = 0.01584% strain/mv, L = 19 in, L/a = 3 in, and ξ = 7 in.

A photograph of the stored trace that was obtained as a result of Shot Number 6 is shown in Figure 17. From Figure 17 it is determined that the maximum magnitude of the first compressive pulse is 1.80 div (averaging small oscillations) with a corrected magnitude of 1.025 div (1.80) = 1.84 div. The resultant maximum strain is

$$\varepsilon = -(1.84 \text{ div})(10 \text{ mv/div})(0.01584\% \text{ strain/mv}) = -0.292\% \text{ strain}.$$

Applying the t_3 method to Figure 17, it is determined that the distance from the beginning of the first compressive pulse to the beginning of the second tensile pulse is 5.58 div with the corrected magnitude of 5.58 div (1.025) = 5.72 div. From the characteristics diagram of Figure 2 it is determined that the distance traveled by the wave front during this time is $4(L - \xi) + 2(\xi - L/a)$ or, from Figure 17, 4(19 - 7 in) + 2(7 -3 in) = 56 in. Thus, the propagation velocity (by the t_3 method) is determined to be

$$C = \frac{56 \text{ in}}{(12 \text{ in/ft})(5.72 \text{ div})(50 \times 10^{-6} \text{ sec/div})} = 16{,}320 \text{ fps}.$$

The results obtained by using the above methods with photographed traces for various impacter velocities are shown in Table I. Due to the characteristics of the photograph obtained as a result of Shot Number 9, it was not possible to determine the propagation velocity by the t_2 or t_3 methods. Strain gage failures after the passage of the first compressive pulse did not allow determination of the propagation velocity by the t_2 or t_3 methods for Shots 10, 11, and 12.

The plotted results of maximum compressive strain-vs-impacter velocity (from Table I) are shown in Figure 18. These variables show a nearly linear relationship at impacter velocities up to 237.0 feet/second. The maximum deviation from the observed linearity occured at the highest value of impacter velocity (389 feet/second).

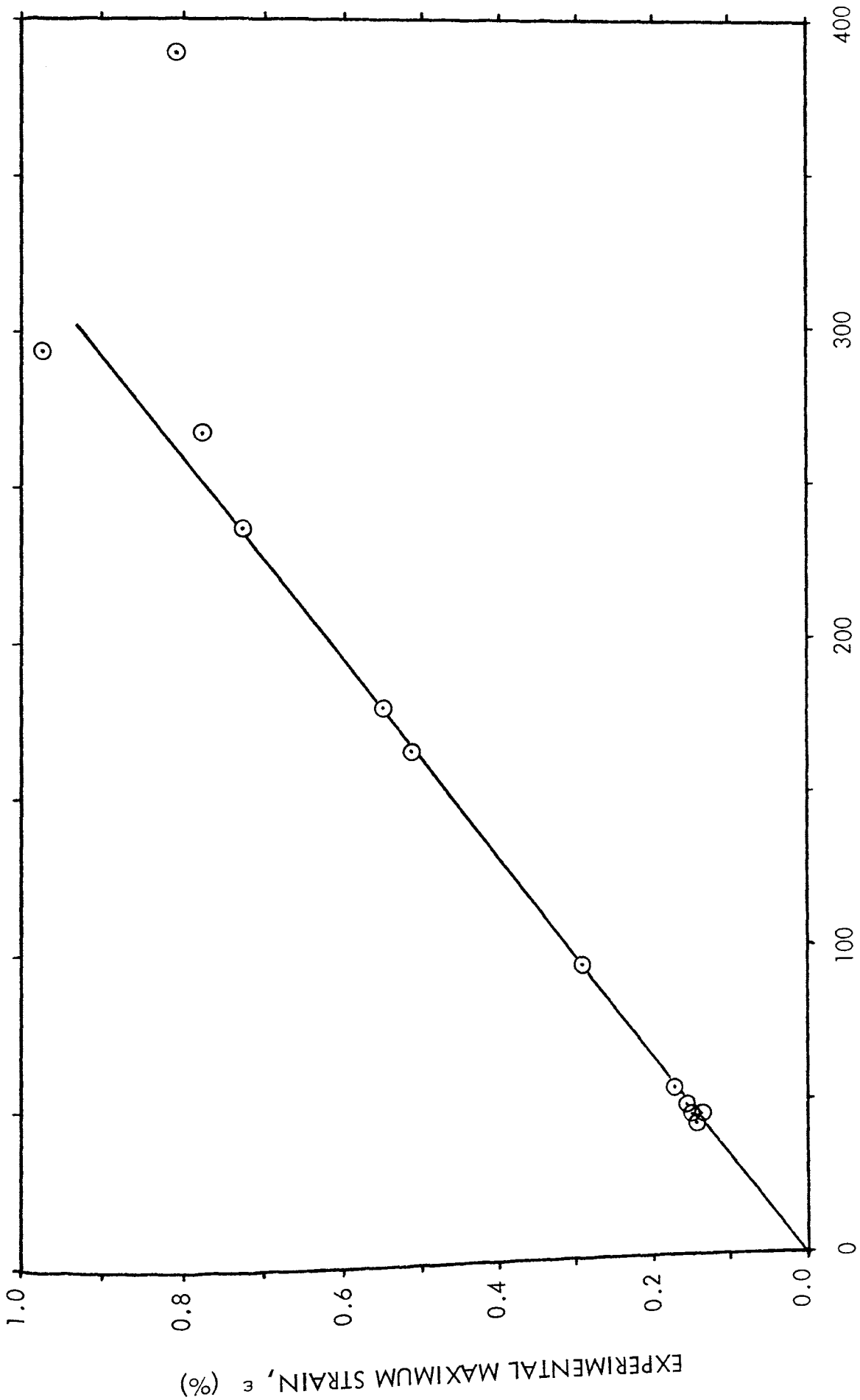

Figure 18. Experimental maximum strain-vs-impacter velocity

If only the linear portion of the strain-impacter velocity curve is considered, it is possible to determine an "impact modulus" relating theoretical stress to measured strain using the equations

$$\varepsilon = \frac{V_o}{2C}$$

and

$$E = \rho_o C^2 \tag{39}$$

resulting in

$$E = \frac{\rho_o}{4}\left[\frac{V}{\varepsilon}\right]^2 . \tag{40}$$

From the linear portion of the plot shown in Figure 18, $V_o/\varepsilon = 32{,}500$ ft/sec. Using this with equation (40), the result is

$$E_1 = \frac{(0.101\ lb_m/cu\ in)(12\ in/ft)(32{,}500\ fps)^2}{4(32.2\ ft-lb_m/lb_f-sec^2)} = 9.94 \times 10^6\ psi$$

where E_1 is the impact modulus of elasticity.

Figure 19 shows a plot of propagation velocity as a function of impacter velocity. It appears from an analysis of Figure 19 that the velocity of wave propagation is not a function of impacter velocity over the range of impacter velocities employed. It was also observed that the average propagation velocities resulting from each of the three measurement methods (t_1, t_2, and t_3) did not differ appreciably (16,310, 16,500, and 16,270 ft/sec, respectively). The average propagation velocity (all results weighed equally) was determined to be 16,350 ft/sec. Using this average result with equation (39), the result is

$$E_2 = \frac{(0.101\ lb_m/in^3)(16{,}350\ fps)^2(12\ in/ft)}{(32.2\ ft-lb_m/lb_f-sec^2)} = 10.1 \times 10^6\ psi$$

where E_2 is the impact modulus of elasticity.

In view of the two independently-determined values of the impact

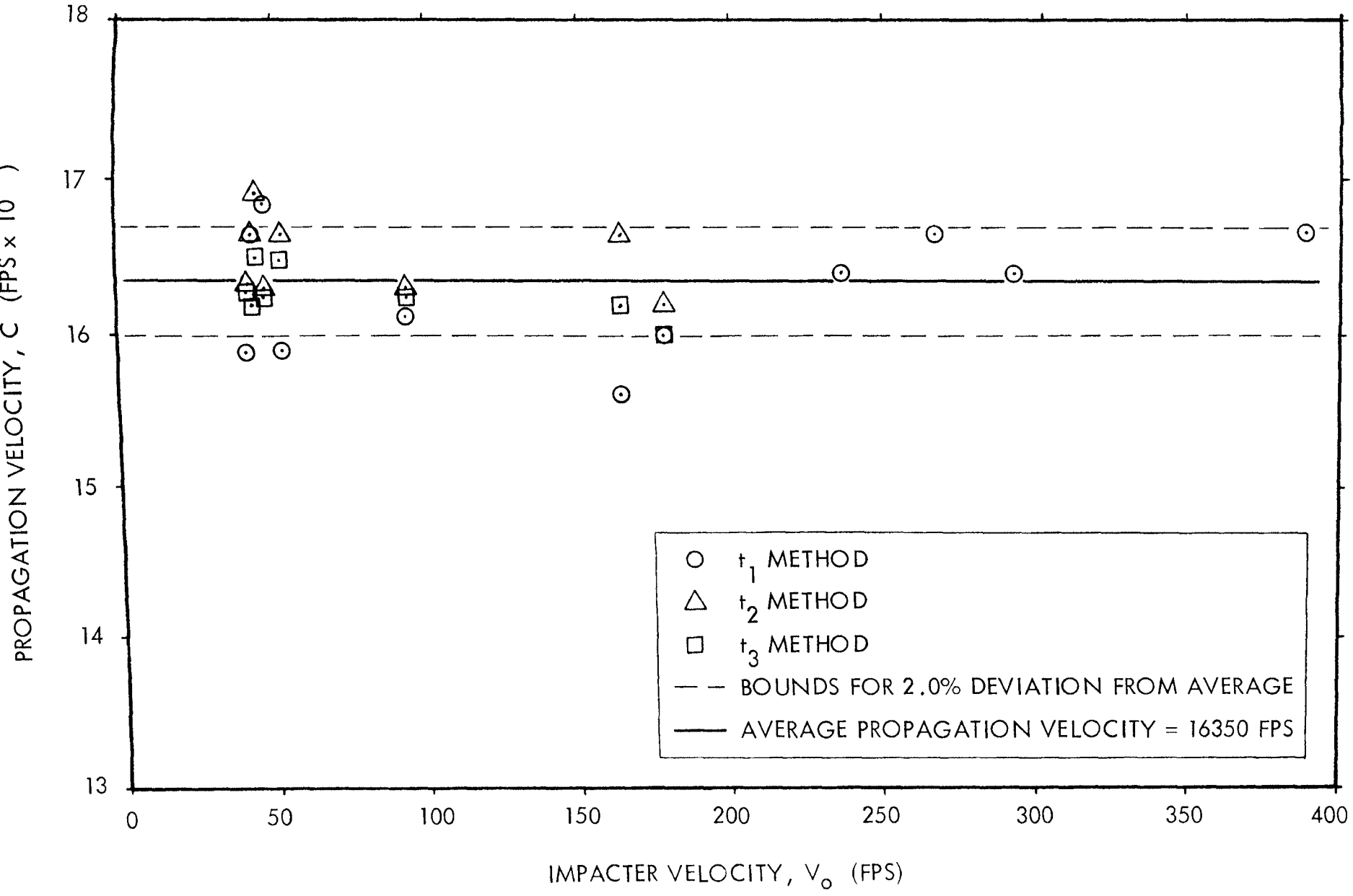

Figure 19. Propagation velocity-vs-impacter velocity

modulus (E_1 and E_2) it was considered that the value of $E = 10.0 \times 10^6$ psi would adequately describe the dynamic stress-strain relationship. Using $E = 10.0 \times 10^6$ psi with the equation

$$\sigma = -\frac{EV_o}{2C} = -\frac{EV_o}{2\sqrt{E/\rho_o}} = -\frac{\sqrt{E\rho_o}}{2} V_o$$

results in

$$\sigma\,(\text{psi}) = -\left[\frac{(10.0 \times 10^6\ \text{psi})(0.101\ \text{lb}_m/\text{in}^3)(12\ \text{in/ft})}{(32.2\ \text{lb}_m - \text{ft/lb}_f - \text{sec}^2)}\right]^{\frac{1}{2}} \frac{V_o}{2}\left[\text{ft/sec}\right] = -307.0\ V_o \qquad (41)$$

also, $\varepsilon = \frac{\sigma}{E}$, or

$$\varepsilon\,(\text{in/in}) = \frac{\sigma\,(\text{psi})}{(10.0 \times 10^6\ \text{psi})} = -3.07 \times 10^{-5}\ V_o \qquad (42)$$

Equations (41) and (42) were evaluated at the experimental values of impacter velocity and the results are indicated in Table I. A graph of theoretical stress-vs-experimental strain was constructed using the results listed in Table I and is shown in Figure 20. The manufacturer-specified properties of the aluminum (under static loading conditions) are also indicated by Figure 20.

B. Analysis of Experimental Results

Analysis of Figure 20 reveals that a linear relationship between theoretical stress and experimental maximum strain exists up to stresses which are greater than the statically-determined ultimate stress. The slope of this curve is approximately 4% less than the static modulus of elasticity. This fact implies that the use of the static modulus of elasticity of this material to predict dynamic strains at stress levels up to the yield stress will generally be acceptable in design problems.

For those shots where the magnitude of the stress pulse (via elastic theory) was less than the static elastic limit (see Fig. 20) it was observed that for each

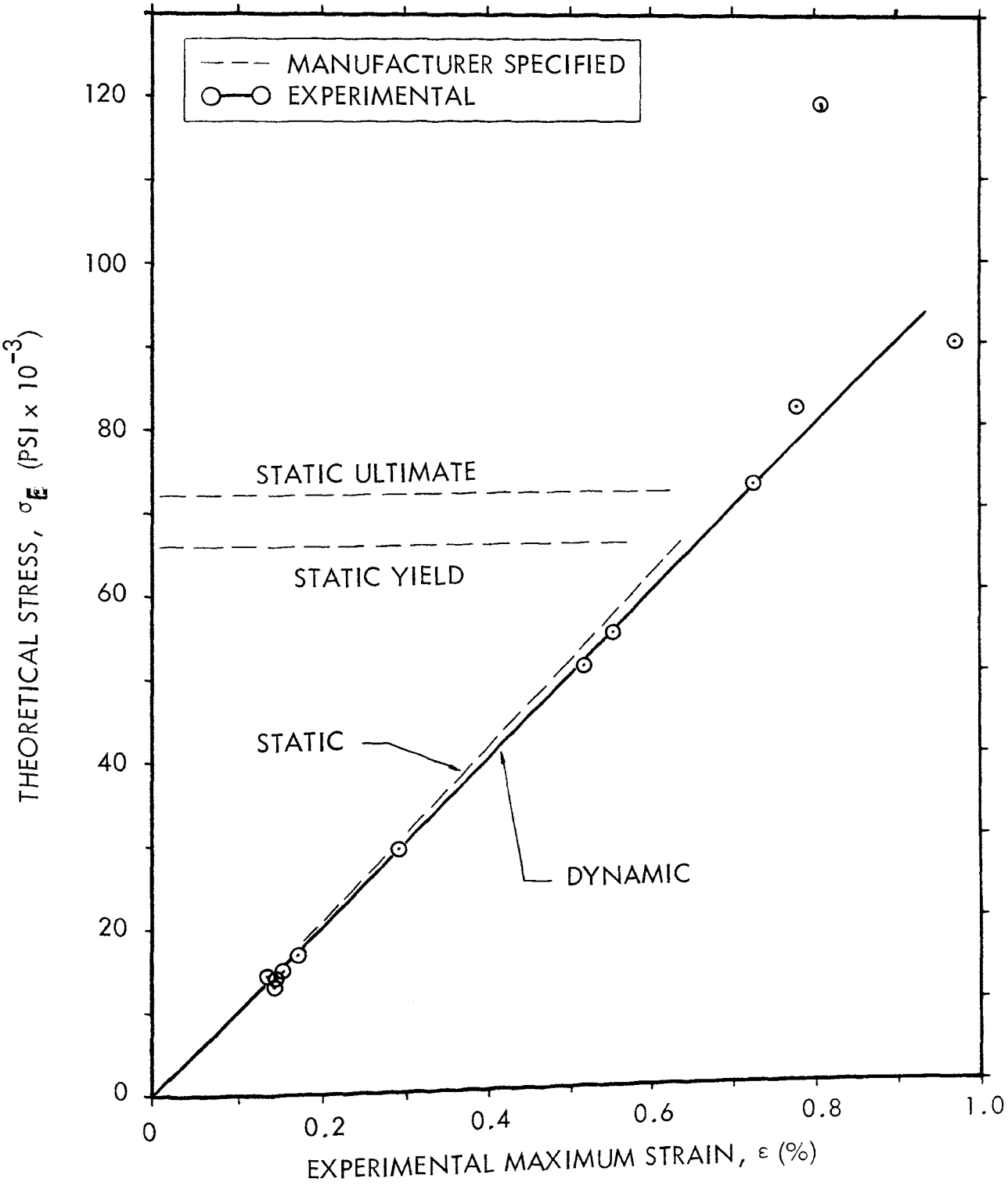

Figure 20. Theoretical stress-vs-experimental maximum strain

shot the crest of the first strain pulse was nearly flat, e.g., Figure 17. It was noted, however, that for shots where the elastically-predicted maximum stress exceeded the statically-determined yield stress, an apparent discontinuity developed in the strain pulse rise time. An example of this phenomenon is shown in Figure 21.

With reference to Figure 21, it is determined that the strain at the gage location first rises very sharply and then abruptly changes slope at $\varepsilon \approx -0.65\%$ strain. The strain continues to increase at a reduced rate to a magnitude approximately predicted by elastic theory (see Fig. 20). The shots (9 through 12) that resulted in elastically-predicted stress levels exceeding the static yield stress of 66,000 psi showed a similar discontinuity in rise time at $\varepsilon \approx -0.65\%$ strain. From Figure 20 it can be seen that $\varepsilon = 0.65\%$

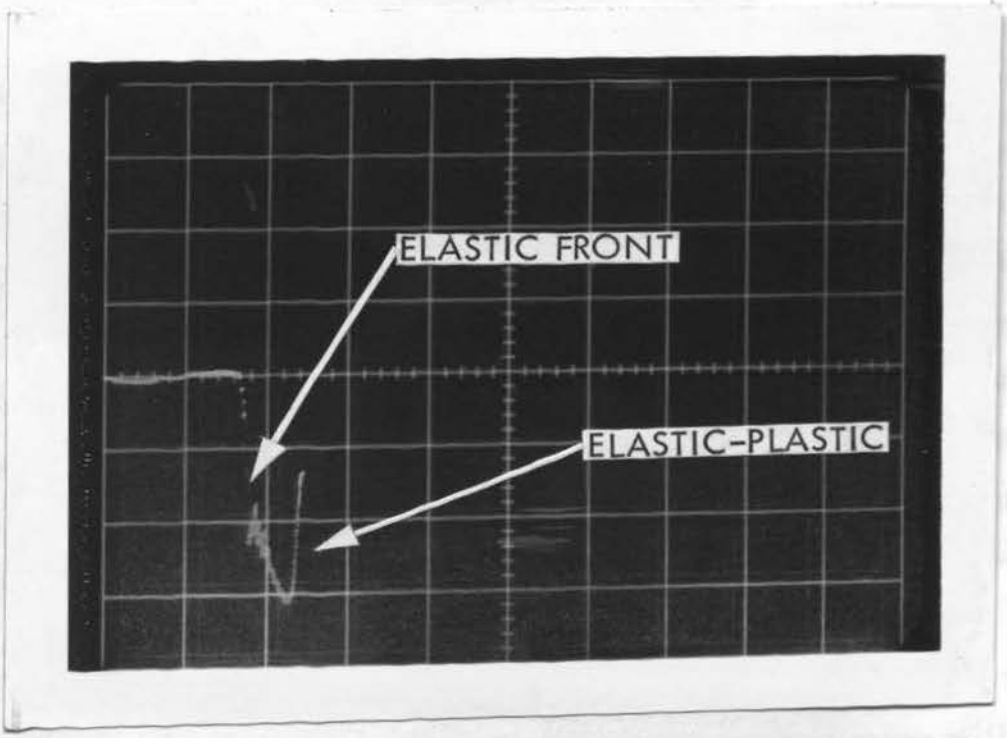

Figure 21. Photograph of stored oscilloscope trace for Shot Number 11. $V_o = 294$ fps, sweep time = 50 μ sec/div, amplification = 20 mv/div, bandwidth = 500 kHz, cal = 0.01584% strain/mv, L = 11 in, L/a = 3 in, and $\xi = 5.5$ in. Gage failed after first pulse.

shot the crest of the first strain pulse was nearly flat, e.g., Figure 17. It was noted, however, that for shots where the elastically-predicted maximum stress exceeded the statically-determined yield stress, an apparent discontinuity developed in the strain pulse rise time. An example of this phenomenon is shown in Figure 21.

With reference to Figure 21, it is determined that the strain at the gage location first rises very sharply and then abruptly changes slope at $\varepsilon \approx -0.65\%$ strain. The strain continues to increase at a reduced rate to a magnitude approximately predicted by elastic theory (see Fig. 20). The shots (9 through 12) that resulted in elastically-predicted stress levels exceeding the static yield stress of 66,000 psi showed a similar discontinuity in rise time at $\varepsilon \approx -0.65\%$ strain. From Figure 20 it can be seen that $\varepsilon = 0.65\%$

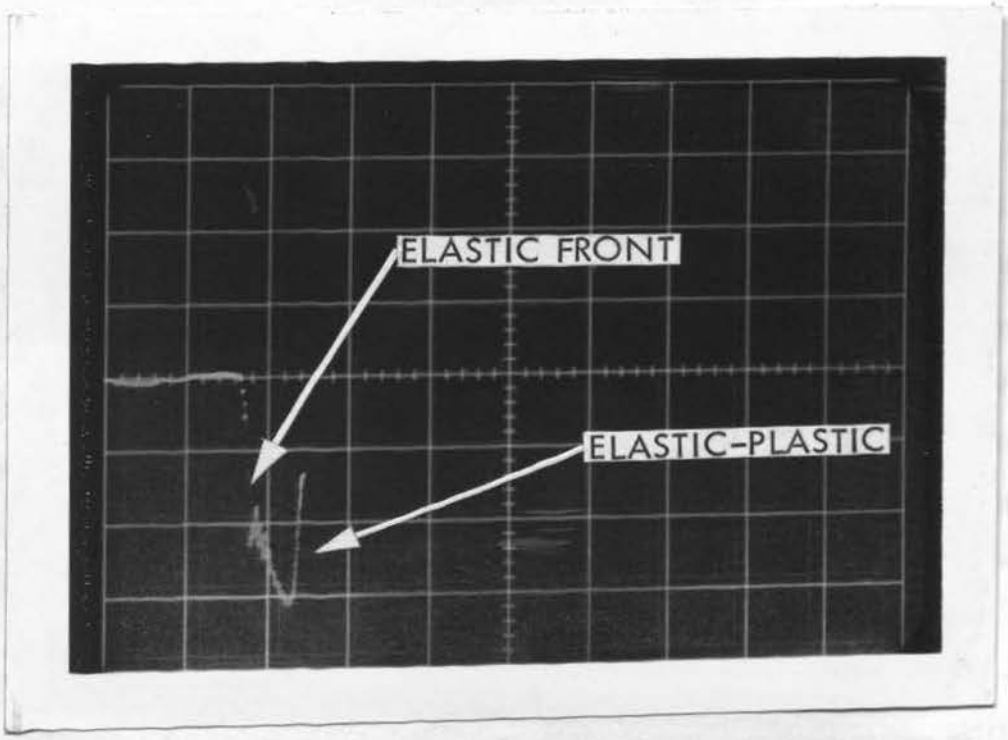

Figure 21. Photograph of stored oscilloscope trace for Shot Number 11. $V_o = 294$ fps, sweep time = 50 μ sec/div, amplification = 20 mv/div, bandwidth = 500 kHz, cal = 0.01584% strain/mv, L = 11 in, L/a = 3 in, and $\xi = 5.5$ in. Gage failed after first pulse.

strain corresponds to an elastic stress level of 65,000 psi (approximately equal to the statically-determined yield stress of 66,000 psi). This phenomenon would seem to indicate that the pulse consists of an elastic front followed by a region of elastic strain superimposed upon plastic strain. Unfortunately, due to strain gage failures (e.g., Fig. 21), it was not possible to determine if plastic strain existed following passage of the main pulse. It is the opinion of this investigator that residual plastic strain did exist following the passage of the first elastic-plastic pulse.

It appears that the above described phenomena correspond well with results predicted by the strain-rate independent theory as proposed by Karman [1] and Taylor [2]. This theory predicts the existence of a distinct wave velocity for each level of plastic stress given by the equation

$$C = \sqrt{\frac{1}{\rho_o} \frac{d\sigma}{d\varepsilon}}$$

where $\frac{d\sigma}{d\varepsilon} = E$ in the elastic region and is a single-valued function of strain in the plastic region of the static stress-strain curve. Due to the nature of most experimentally-determined static stress-strain curves (e.g., aluminum), the elastic stresses will be propagated at a velocity which exceeds those wave velocities associated with each stress level in the plastic region. It is to be observed, however, that since the level of elastic stress constitutes a large portion of the total elastically-predicted stress level (for the range of impacter velocities considered experimentally) the primary indication of pulse length should correspond to that predicted by the elastic theory. This was approximately verified by the experimental results (see Table I - Propagation velocity).

The strain-rate dependent theory, after Malvern [3], predicts that for the impact case (instantaneously applied load) the initial stress will rise to a value predicted by an extension of the elastic curve into the plastic region.

The stress is then predicted to decrease with time, becoming the value predicted by the static stress-strain curve for large values of time. It can be seen that the constitutive equation proposed by Malvern [3] bears a distinct similarity to the constitutive equation of the Maxwell model for short times. It was also noticed that the results of experimentation in the plastic range of loading (e.g., Fig. 21) bear a distinct similarity to the strain distributions predicted for the collision of two Maxwellian rods (Fig. 7). A brief discussion of the implications of the Malvern equation is given in Appendix 3.

In view of the above theoretical considerations, it was concluded that the material could not be judged as being either strain-rate independent or strain-rate dependent[1] and that further extensive experimentation would be required for this determination to be made. As a result of this fact, the stress strain curve of Figure 20 only indicates the elastically-determined theoretical stress versus the experimentally-determined maximum strain and does not imply that the stresses indicated above the elastic limit are actually present during impact. If the material is strain-rate dependent, after Malvern [3] , these stress levels correspond to the stress present at the instant of impact. If the material is strain-rate independent, after Karman [1] and Taylor [2], the true stress is smaller than that indicated by Figure 20 for those shots made above the observed elastic limit stress.

With these considerations in mind, it was concluded that the results served to demonstrate that the maximum strain could be satisfactorily predicted (within 6%) by a simple extension of the elastic curve for impacter velocities up to approximately 300 fps. This statement must be tempered by the fact that

---

[1] 7075 T6 aluminum was found to be insensitive to strain rates up to $(10^3$ in/in)/sec by Maiden and Green [26] who employed the split-Hopkinson pressure bar.

the projectiles used in the plastic range were 3 inches in length (corresponding to an elastic pulse length of approximately 30 micro-seconds). It is very likely that the duration of the elastic pulse will, in part, determine the level of the plastic strain. The strain pulses were measured at a point 2.5 inches from the location of the interface of the rods in Shots 9 and 12, and 4 inches from the interface in Shots 10 and 11. The point of measurement has possible significance with regard to the level of maximum strain in the plastic region of loading due to the absorbtion of energy in the process of plastic straining.

Small-amplitude, high frequency oscillations were observed to occur on the traces following initiation of the first compressive pulse (see Fig. 17). These oscillations were also observed by Kolsky [27] and are thought to result from the effects of radial modes of vibration described by the Pochammer-Chree equations. These modes act, in general, to distort and reduce the amplitude of a propagated pulse.

Damping properties of the aluminum can be observed by comparing the magnitudes of successive reflected pulses. In those shots where the magnitude of the produced stress was less than the observed yield stress, the effects of material damping were concluded to be quite small. In fact, it is quite probable that the effects of material damping (in this case) are of the same order of magnitude as the dispersive effects of radial modes. A quantitative examination of the effects of material damping was not undertaken.

C. Discussion of Possible Error

1. Photo-electric Velocity Measurement

It was necessary to allow the light beams produced by the high-intensity lamps to pass through holes which were 3/8 inch in diameter (silencer holes) in order to produce a sufficient light level at the photo-tube for proper triggering.

As the impacter passes through the barrel, it breaks the initially-established light beam and the triggering pulse is subsequently produced. It is not known, however, if the portion of the light beam that must be broken by the impacting rod is the same for both photo-stations. The worst possible condition that could exist is if one station triggers at a very small reduction in its light level (when the impacter just begins to interrupt the beam) while the other station triggers at a very small light level (when the projectile almost completely blocks the beam). Since the distance over which the velocity is measured is equal to 12 inches, the largest possible error that can be caused by this effect is ±6% of the true velocity.

It was not possible to determine the exact trigger level of each photo-station because dynamic movement of the impacter (10 to 15 fps) is required for triggering to take place. Every effort was made to produce electrically equivalent photo-stations and equal light intensities at both measurement points. Therefore, the actual error resulting from this condition should be quite small.

2. Electrical Noise

In most of the photographic results obtained, it was noticed that the trace indicated a small A.C. voltage preceding the indication of the first compressive pulse (e.g., Fig. 21). It was determined that the frequency of this "noise" was approximately equal to 10kHz for all traces in which it appeared. It was noted that noise at an approximate frequency of 10 kHz also appeared in the traces of the photo-station outputs (see Figs. 12 and 13). It is not certain whether this noise is produced by the light stations or arises from an independent source (such as the motion of the projectile in the barrel). However, its result is to add to the difficulty in interpreting the results of photographed traces. In all cases, an effort was made to determine the contribution of electrical noise and to modify the results in accordance with its observed magnitude.

The contribution of the radial modes of vibration tended to produce oscillations in the pulse crests (see Fig. 17). An attempt was made to average these oscillations in order to determine the true magnitude of the longitudinal strain.

3. Strain Indication

Eastman 910 contact cement was used to fasten the strain gages to the test rod. Indications are that the cement functioned well in this capacity, as the observed pulses rose quite rapidly and produced results similar to those expected in the elastic range of impacter velocities. It was mentioned earlier that strain gage failure occurred in the highest velocity shots. This failure was not associated with the gage itself but with the fastening of lead wires to the strain gage tabs. The lead wires were soldered to the tabs using a very small quantity of solder. However, due to the very high accelerations involved in the impact condition, the inertia forces that are associated with the solder connections become quite large and this effect can manifest itself in the fracturing of the gage tabs.

4. Frequency Response

During the course of the experimentation, it was determined that the frequency response of the measuring equipment is of vital importance. The oscilloscope was observed to limit the frequency response of the strain measurement system. The oscilloscope that was used had an upper frequency response limit of 5kHz (low bandwidth) and an upper frequency response limit of 500 kHz (high bandwidth). In order to more fully describe the implications of frequency response, a photograph of a scope trace obtained at a bandwidth of 500 kHz and a photograph of a scope trace obtained, under comparable impact conditions, at a bandwidth of 5 kHz are shown in Figures 22 and 23, respectively.

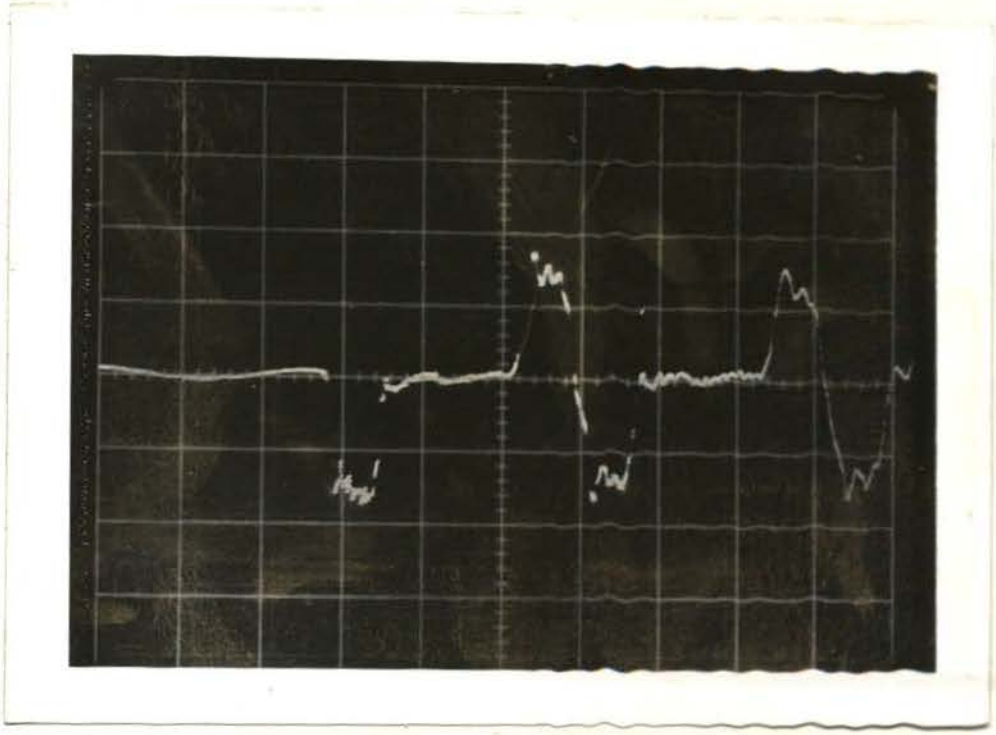

Figure 22. Photograph of stored oscilloscope trace for Shot Number 3. V_o = 46.3 fps, sweep time = 50 μ sec/div, amplification = 5 mv/div, bandwidth = 500 kHz, cal = 0.01584% strain/mv, L = 19 in, L/a = 3 in, and ξ = 7 in.

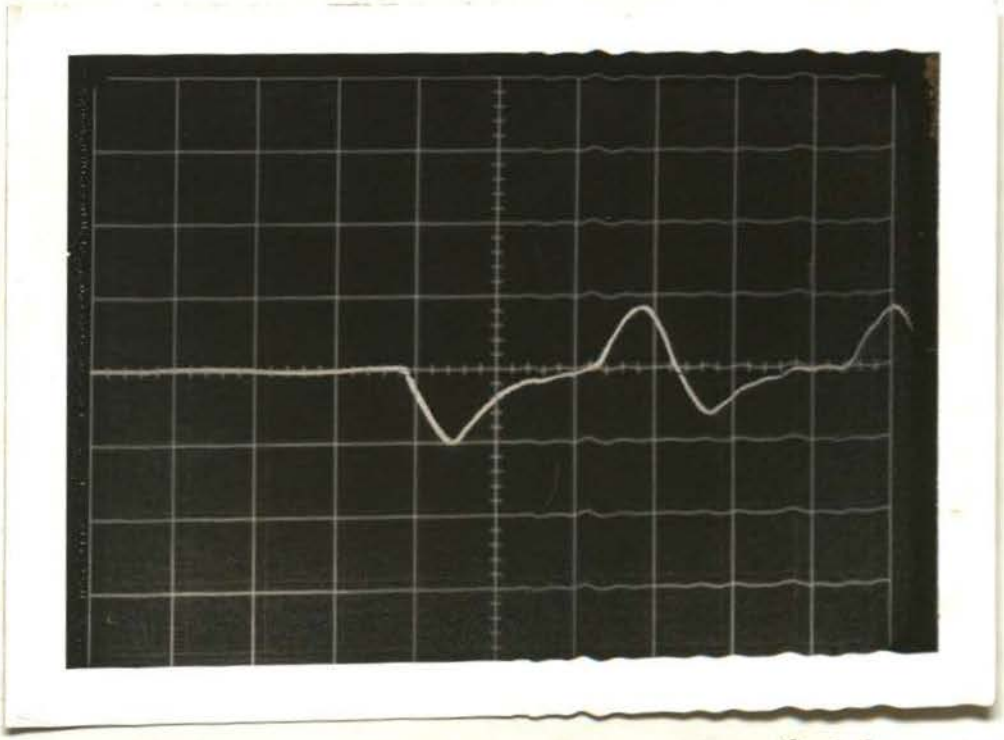

Figure 23. Photograph of stored oscilloscope trace. V_o = 42.3 fps, sweep time = 50 μsec/div, amplification = 5 mv/div, bandwidth = 5 kHz, cal = 0.01584% strain/mv, L = 19 in, L/a = 3 in, and ξ = 7 in.

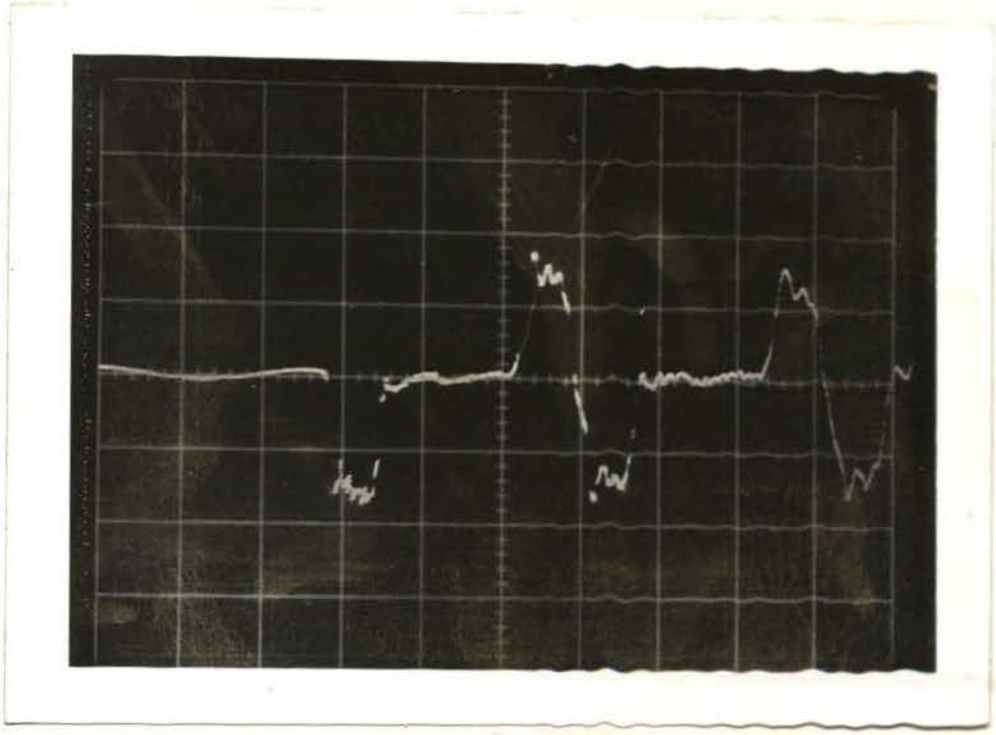

Figure 22. Photograph of stored oscilloscope trace for Shot Number 3. V_o = 46.3 fps, sweep time = 50 μ sec/div, amplification = 5 mv/div, bandwidth = 500 kHz, cal = 0.01584% strain/mv, L = 19 in, L/a = 3 in, and ξ = 7 in.

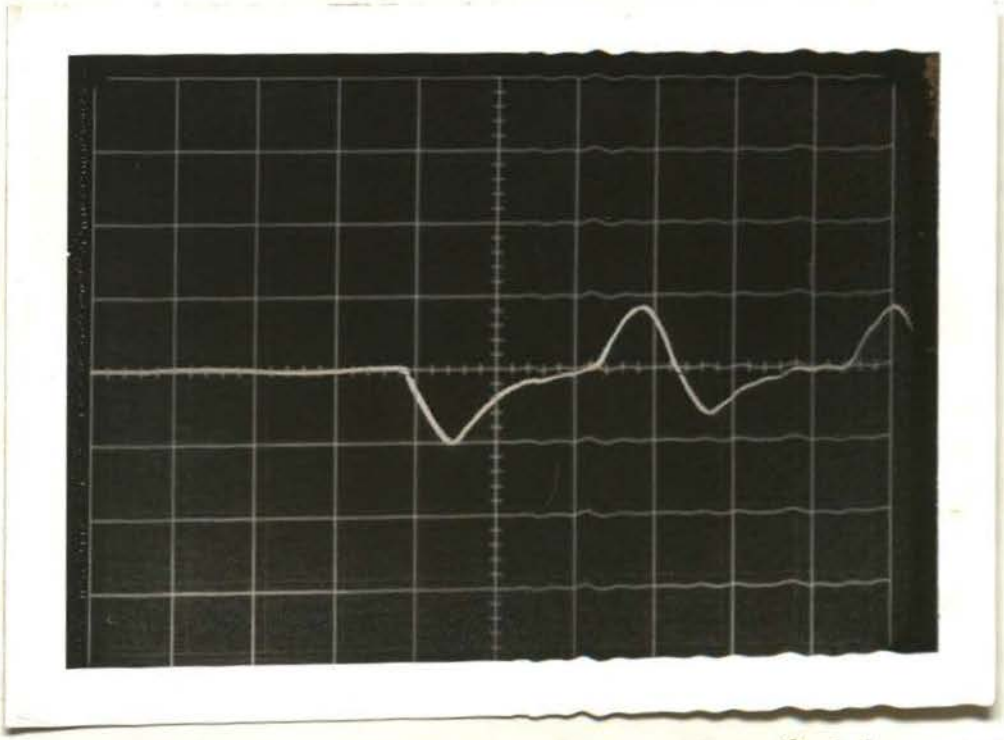

Figure 23. Photograph of stored oscilloscope trace. V_o = 42.3 fps, sweep time = 50 μsec/div, amplification = 5 mv/div, bandwidth = 5 kHz, cal = 0.01584% strain/mv, L = 19 in, L/a = 3 in, and ξ = 7 in.

As can be determined from Figures 22 and 23, the shots were made at comparable impacter velocities and involved identical impacter-test rod geometry. The most noticeable difference in the characteristics of Figures 22 and 23 is the rounding of pulse "corners" that can be observed in Figure 23. Further observation reveals that Figure 23 indicates significantly less pulse magnitude (approximately 50% less) than is shown by Figure 22. This difference is certainly not traceable to the small difference in impacter velocities of the shots.

In general, a pulse consists of a summation of the contributions of a wide spectrum of frequency components. The Fourier series, discussed by Churchill [29] has been used to describe periodic functions in terms of the contributions of their frequency components. The Fourier sine-cosine series describes a periodic function as an infinite summation of contributions from sine and/or cosine functions from a specified minimum to infinity. Physically, the lowest frequency of the series is determined by the frequency of the function that is to be represented. The lowest frequency terms of the series are normally observed to make the largest contribution to the basic shape of the function with the higher frequency terms contributing to a refinement of the basic shape. The number of series terms that is required to accurately describe a function is largely dependent on the shape of that function and is inversely related to the rate of convergence of the series. It is known that a relatively large number of series terms is required to represent waves of the "square" or "rectangular" variety.

The implication of the above discussion is that the strain measuring devices must be sensitive to a relatively wide range of frequencies in order to display the true results with required accuracy. A Fourier analysis of the theoretical wave train corresponding to Figures 22 and 23 shows that the lowest frequency is approximately 6.7 kHz. In the low bandwidth mode, the oscillo-

scope passes frequencies up to 5 kHz without significant attenuation.[1] Physically, this means that all frequencies of the wave train in Figure 23 have been significantly attenuated while the first 74 frequencies (up to 500 kHz) have been passed without significant attenuation for the wave train of Figure 22. Some of the differences between the wave train of Figure 22 and its corresponding theoretical pulse train have probably arisen from frequency response limitations. It is the opinion of the author that the presence of 74 frequencies (without significant attenuation) is sufficient to describe pulse magnitudes to within an accuracy of 1% for the wave trains considered experimentally.

The above discussion implies a "first approximation" to the problem of equipment frequency response. It is suggested that a Fourier analysis be applied to the theoretical pulse train associated with a given impac ter-test rod geometry. Physical evaluation of the Fourier series within the limits of equipment frequency response should then be accomplished. The results of the series evaluation should then be compared to the theoretical wave train in order to determine the expected accuracy of experimental results. This suggested method of Fourier analysis is discussed more thoroughly in Appendix 4.

Unfortunately, many of the published experimental findings in the area of impact studies have not been accompanied by information regarding equipment frequency response limitations. It is possible that some of the discrepancies that have arisen regarding tests with materials result from such frequency response limitations.

---

[1] The attenuation at both of the upper frequency response limits (5 kHz and 500 kHz) is approximately 3 db.

5. Integration Effect of the Strain Gages

This source of error arises from the fact that the strain gages are of finite length (in this case, 0.125 inches). It was determined experimentally that the average velocity of wave propagation in the aluminum was 16,350 ft/sec. Thus, the total time for the wave front to traverse the length of the strain gages is

$$t_g = \frac{(0.125 \text{ in})/(12 \text{ in/ft})}{16{,}350 \text{ ft/sec}} = 0.637 \quad \mu\text{sec}$$

Consider the case where the pulse just arrives at the gage when $t = 0$. If it is assumed that the true strain pulse can be represented by the step function $\varepsilon = \varepsilon_o H(t)$, it follows that

$$\varepsilon_1 = \int_0^t \varepsilon_o \frac{C}{\gamma} dt \qquad (0 \leq t \leq t_g)$$

where γ is the gage length, C is the wave propagation velocity, ε_1 is the indicated strain, and t is time. It can thus be seen that a rectangular pulse (of zero rise time) will have an indicated rise time equal to t_g.

By viewing the photographed oscilloscope traces, it was determined that the rise times of strain pulses were consistently near 5 micro-seconds (the observed initial rise time did not appear to be a function of strain). It is, therefore, possible that the integration effect of the strain gages contributes as much as 0.637/5, or 12.75% of the total observed rise time.

VII. CONCLUSIONS

The experimental results indicate that the simple, one-dimensional theory served quite well to predict wave propagation effects, within the elastic range of loading, for 7075 T651 aluminum rods. The experimental strain-time results are observed to agree within 4% of those calculated using the properties of the aluminum as specified by the manufacturer. This 4% difference was manifest in an experimental, dynamic elastic modulus of 10.0×10^6 psi as opposed to the manufacturer-specified, static elastic modulus of 10.4×10^6 psi (see Figure 20.)

For those tests conducted in the plastic range of loading (e.g., Figure 21), it appeared that the fronts of the experimentally observed strain pulses were of a magnitude approximately equal to the static yield strain of the material. In each of these tests, the "elastic front" was apparently followed by a monotonically increasing plastic strain for the duration of the primary pulse. The duration of the primary pulse was observed to be closely approximated by the value predicted via the elastic theory. It is suspected that this primary pulse was followed by permanent plastic strain, although this condition was not measured quantitatively. The material was observed to sustain stress conditions (predicted by elastic theory) well in excess of the static ultimate strength for pulse durations of 30 micro-seconds. Under the specific conditions of the tests, it was determined that the maximum strain at the strain gage location for impacter velocities producing plastic stresses could be predicted approximately (within 6%) by an extension of the elastic strain-vs-impacter velocity curve for impacter velocities up to 294 fps (see Figure 18).

It was observed that the damping properties of the aluminum were quite

small in the elastic range of loading and it is thought that the effects of material damping can be neglected for design purposes.

From the photographs of oscilloscope traces, it was determined that the minimum strain-rate resulting during experimentation was on the order of 300(in/in)/sec while the maximum strain-rate was approximately 1000(in/in)/sec. However, it was observed that the initial rise time of the pulses was consistently near 5 micro-seconds regardless of the value of the strain. It was, therefore, concluded that the effects of frequency response and "integrating effects" of the strain gages played an important role in the indicated strain-rate. It is the opinion of the author that the strain-rate, as predicted by theory, was nearly infinite but that this fact was obscured by equipment limitations.

Theoretical results, obtained for the longitudinal collision of two Maxwellian rods (see Figures 6 and 7), have indicated that there exists a maximum characteristic length of the material which a dynamically-produced disturbance will effectively traverse. It is thought that this phenomenon can be successfully employed in the design of viscoelastic packaging materials. The theoretical development used for the Maxwellian rods has been applied to Voigt and three-parameter materials (see page 8); however, numerical results have not, as yet, been obtained.

It is the opinion of the author that the air gun launcher technique can successfully be applied to certain of the materials that have demonstrated viscoelastic characteristics.

VIII. RECOMMENDATIONS

The methods and equipment used in this experimentation were observed to produce satisfactory results within the elastic range of loading. Some modifications of the equipment may be necessary, however, when plastic loading is under consideration. During compressive loading, some radial expansion of the material occurs as a result of the Poisson effect. This radial expansion could cause a significant interaction of the lateral surface of the impacter with the interior of the silencer when large, longitudinal strains are produced (as in the plastic range). For Shot Number 12, the plastic strain of the impacting rod was large enough to cause it to become lodged in the silencer. In addition to being an unacceptable inconvenience, this condition very likely caused a significant amount of error in the results. One solution to the problem is to increase the inside diameter of the barrel-silencer to allow for the radial expansion of the rod. Unfortunately, this procedure will eventually produce impacter-test rod alignment problems. A better solution for studies in the plastic range may be to encircle both the impacter and test rod with two, or more, rings of a much softer material (such as teflon).

A determination of impacter and test rod lengths on the basis of a Fourier time analysis is highly advisable in order to insure that the frequency response limitations of the equipment do not significantly alter the true test results.

Perhaps the greatest failing of the experimental method under consideration is that it does not allow for a physical determination of the stress as it does for the strain. This consideration is not vital in the elastic range of loading. However, in the opinion of the author, it becomes quite important in the plastic range of loading. Normally, the stress at the interface of the rods is determined via theoretical considerations involving either the strain-rate independent theory

or the strain-rate dependent theory with the observed value of impacter velocity. It is the opinion of this investigator that an independent means of measuring the stress at the interface of the rods is necessary in order to determine the true validity of any theory of plastic wave propagation.

More efficient shielding of the photo-electric trigger outputs and/or use of shielded strain gage leads should serve to reduce the observed presence of external noise on the scope traces.

As a result of the experimentation it appears that the chamber volume of the air gun launcher is not being used effectively in view of the current barrel length of 48 inches as compared to the silencer length of 36 inches. A substantial increase in the length of the barrel is recommended. It is also recommended that the size of the silencer holes designated for the passage of the light beams be reduced (possibly by a system of lenses) and that the location of photo-station 1 be subsequently moved as close as possible to the muzzle to minimize errors in measurement of the impacter velocity.

IX. BIBLIOGRAPHY

1. von Karman, T., and Duwez, P.: "The Propagation of Plastic Deformation in Solids," J. of Applied Phys. 21:987-994, 1950.

2. Taylor, G. I.: "The Testing of Materials at High Rates of Loading," J. Inst. Civil Engrs. 26:486, 1946.

3. Malvern, L. E.: "The Propagation of Longitudinal Waves of Plastic Deformation in a Bar Exhibiting a Strain-Rate Effect," J. of Applied Mech. 18:203-208, 1951.

4. Davies, E. D. H., and Hunter, S. C.: "The Dynamic Compression Testing of Solids by the Method of the Split Hopkinson Pressure Bar," J. Mech. and Phys. of Solids 11:155-179, 1963.

5. Lindholm, U. S.: "Some Experiments With the Split Hopkinson Pressure Bar," J. Mech. and Phys. of Solids 12:135-142, 1964.

6. Bell, J. F.: "An Experimental Diffraction Grating Study of the Quasi-Static Hypothesis of the Split Hopkinson Bar Experiment," J. Mech. and Phys. of Solids 14:309-327, 1966.

7. Krafft, J. M.: "Elimination of the Transient Strain Fluctuations Which Result From the Longitudinal Impact of Bars," Proc. Soc. Exp. Stress Anal. 12:173-180, 1955.

8. Ripperger, E. A.: "Longitudinal Impact of Two Cylindrical Bars," Proc. Soc. Exp. Stress Anal. 10:209-226, 1952.

9. Bell, J. F.: "Propagation of Plastic Waves in Solids," J. Applied Phys. 30:196-201, 1958.

10. Bell, J. F.: "An Experimental Study of the Unloading Phenomenon in Constant Velocity Impact," J. Mech. and Phys. of Solids 9:1-15, 1961.

11. Oetting, R. B.: "Investigation of the Effect of Low Temperature on the Static and Dynamic Properties of Lucite and a Low Carbon Steel," Ph.D. dissertation, The University of Maryland, 103p. (27 illustrations, 6 tables), 1965.

12. Waser, R. H., Rand, J. L., and Marshall, J. M.: "Stress Wave Propagation in Aluminum," U. S. Naval Ord. Lab, Ballistics Res. Report No. 107, 1964.

13. Broberg, K. B.: "Some Aspects of the Mechanism of Scabbing," Int. Symp. on Stress Wave Propagation in Materials, edited by N. Davids, Interscience , pp. 229-245, 1960.

14. Bland, D. R.: The Theory of Linear Viscoelasticity, Pergamon Press, New York, 1960.

15. Flugge, W.: Viscoelasticity, Blaidsdell Publishing Co., Waltham, Mass., 1967.

16. Lee, E. H., and Kanter, I.: "Wave Propagation in Finite Rods of Viscoelastic Material," J. of Applied Phys. 24:1115-1122, 1953.

17. Morrison, J. A.: "Wave Propagation in Rods of Voigt Material and Viscoelastic Materials With Three-parameter Models," Quart. Applied Math. 14:153-169, 1956.

18. Glauz, R. D., and Lee, E. H.: "Transient Wave Analysis in a Linear Time-Dependent Material," J. of Applied Phys. 25:947-953, 1954.

19. Lee, E. H., and Morrison, J. A.: "A Comparison of the Propagation of Longitudinal Waves in Rods of Viscoelastic Materials," J. Polymer Science 19:93-110, 1956.

20. Berry, D. S., and Hunter, S. C.: "The Propagation of Dynamic Stresses in Viscoelastic Rods," J. Mech. and Phys. Solids 4:72-95, 1956.

21. Norris, D. M., Jr." "Propagation of a Stress Pulse in a Viscoelastic Rod," Experimental Mech. 7:297-301, 1967.

22. Frederick, D., and Chang, T. S.: Continuum Mechanics, Allyn and Bacon, Inc., Boston, Mass., 1965.

23. Kolsky, H.: Stress Waves in Solids, Dover Publications, Inc., New York, 1960.

24. Goldsmith, W.: Impact, Edward Arnold (Publishers), Ltd., London, England, 1960.

25. The Aluminum Company of America: ALCOA Structural Handbook, Pittsburgh, Pa., 1960.

26. Maiden, C. J., and Green, S. J.: "Compressive Strain Rate Tests on Six Selected Materials at Strain Rates from 10^{-3} to 10^{4} Inch Inch/Second," General Motors Defense Research Lab, Santa Barbara, Calif., No. TR65-26, 1965.

27. Kolsky, H., and Douch, L. S.: "Experimental Studies in Plastic Wave Propagation," J. Mech. and Phys. of Solids 10:195-223, 1962.

28. Hull, B. S., and Oetting, R. B.: "Gas Gun Design," U. S. Naval Ord. Lab, White Oak, Maryland, 1963 (unpublished).

29. Churchill, R. V.: Fourier Series and Boundary Value Problems, 2nd edition, McGraw-Hill, New York, 1963.

30. Pipes, L. A.: "The Summation of Fourier Series by Operational Methods," J. of Applied Phys. 21:298-303, 1950.

31. Boresi, A. P.: Elasticity in Engineering Mechanics, Prentice-Hall, Inc. Englewood Cliffs, N. J., 1965.

32. Dove, R. C., and Adams, P. H.: Experimental Stress Analysis and Motion Measurement, Charles E. Merrill Books, Inc., Columbus, Ohio, 1964.

X. VITA

Allen Glenn Behring was born on August 17, 1943, in St. Louis, Missouri. He attended Hazelwood Grade and High School in St. Louis County and was graduated in June, 1961. He enrolled at the University of Missouri - Rolla in September, 1961, and was graduated with the degree of Bachelor of Science in Mechanical Engineering from that same institution in May, 1966.

In 1966, Mr. Behring began a program leading to the degree of Master of Science in Mechanical Engineering at the University of Missouri - Rolla. He was married to the former Miss Elizabeth Wehrenbrecht on June 10, 1967.

He has held the position of student engineer while employed by the Southwestern Bell Telephone Company and has been a graduate teaching assistant at the University of Missouri - Rolla.

Mr. Behring is a member of Sigma Xi, Pi Tau Sigma, Beta Sigma Psi, Theta Tau, and Blue Key.

Mr. Behring is a citizen of the United States of America.

XI. APPENDICES

APPENDIX 1

AIR GUN DESIGN

The air gun launcher used to accelerate the impacter was designed using a modified form of the Pidduck-Kent limiting solution as described by Hull and Oetting [28] . The basic configuration of the air gun is described in Figure 24.

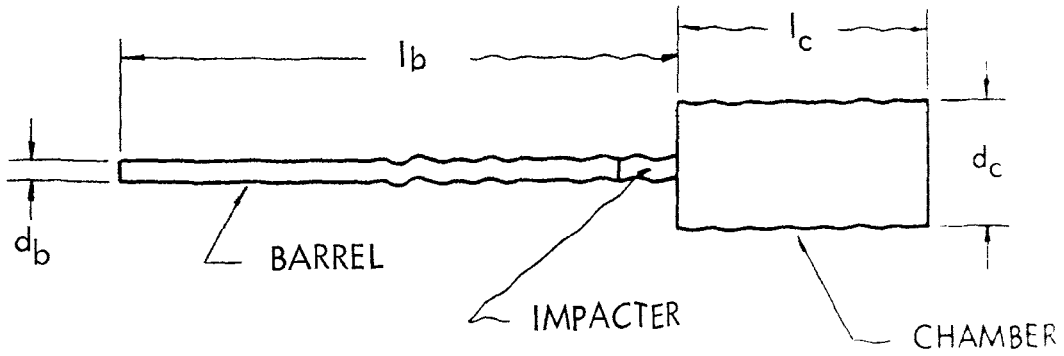

Figure 24. Basic air gun configuration

The impacter velocity, V_o, is given by the equation

$$V_o = \frac{2}{\gamma-1} b \sqrt{a_o} \left[1-\left(\frac{X_b}{Y_b}\right)^{\gamma-1}\right]^{1/2} \tag{1-1}$$

where b is the speed of sound in the propelling gas and γ is the specific heat ratio of propelling gas. The ratio X_b/Y_b is given by the equation

$$\frac{X_b}{Y_b} = \frac{l_c (d_c/d_b)^2}{l_c (d_c/d_b)^2 + l_b} \tag{1-2}$$

and a_o is defined by the equation for the gas mass/missile mass ratio (G M)

$$\frac{G}{M} = \frac{\frac{2\gamma}{\gamma-1} \cdot a_o}{(1-a_o)^{\frac{\gamma}{\gamma-1}}} \left[\frac{(1-a_o)^{\frac{1}{\gamma-1}}}{\frac{\gamma+1}{\gamma-1}} + \frac{1}{\gamma+1} \cdot \sqrt{1-a_o} + \frac{\sin^{-1}\sqrt{a_o}}{\sqrt{a_o}} \right] . \tag{1-3}$$

Equation (1-2) is determinate for a specified air gun geometry. Inasmuch as a_o is contained implicitly in equation (1-3), it is convenient to first solve for the gas mass/missile mass ration (G/M) as a function of $\sqrt{a_o}$ and to display the results in the form of a graph of $\sqrt{a_o}$-vs-(G/M). The parameter $\sqrt{a_o}$ can then be determined for a given chamber pressure and missile mass and used with equation (1-1) to obtain the expected impacter velocity.

For the gun that was used during the second phase of the experimental program (see page 33), the air gun geometry was as follows: $d_b = 0.5$ inches; $l_b = 48$ inches; $d_c = 4$ inches; and $l_c = 12$ inches. It should be noted that l_b denotes the distance from the chamber-breech interface to the nearest pressure-relief hole of the silencer. The Pidduck-Kent equations do not provide for the use of a silencer and it should be noted that the silencer is not shown in Figure 24.

The air gun was constructed entirely from steel. The pressure chamber was constructed from pipe with the front and rear faces welded in place. The barrel-silencer was constructed as a unit from seamless tubing with an original inside diameter of 0.5 inches. The interior of the barrel-silencer was enlarged slightly using a grinding process to permit free passage of the impacting rods. A rough check revealed that the maximum allowable chamber pressure is on the order of 2500 psig with two as a factor of safety. Air pressure was supplied by means of a regulated, high-pressure (2000 psig), bottled source.

It became apparent during the conduct of the first tests that the size and number of the pressure-relief holes were not sufficient to allow uniform motion of the impacter through the velocity-measurement portion of the silencer (experimental results did not agree well with those predicted by theory for the 48 inch barrel). It was observed that as chamber pressure was increased, the experimental velocities became significantly larger than those predicted by the Pidduck-Kent

relations[1] using the above air gun geometry. This phenomenon was attributed to the fact that successively longer portions of the silencer are required to provide the necessary pressure-relief as chamber pressure is increased, thereby increasing the physical barrel length, l_b, to some "effective" value. As can be seen from equations (1-2) and (1-1), this effectively increased barrel length causes an increased impacter velocity. In order to investigate this phenomenon quantitatively, the Pidduck-Kent equations were solved for several different barrel lengths from 48 to 84 inches, allowing the remaining parameters (d_c, l_c, and d_b) to remain at their specified values.

After several step-wise increases in the silencer pressure-relief area, reasonable agreement was obtained between the results yielded by the Pidduck-Kent equations (with $l_b = 72$ inches) and those obtained experimentally (see Figure 25). In general, the slopes of the theoretical and experimental curves of impacter velocity-vs-chamber pressure correspond favorably. This fact was taken as a primary indication that acceleration in the velocity-measurement portion of the silencer was small. By changing the locations of the photo-stations, it was experimentally determined that little change in average impacter velocity was present in the velocity-measurement portion of the silencer for impacter lengths as small as 2 inches with chamber loading pressures up to 200 psig.

The experimental results of Figure 25 can generally be observed to show a smaller impacter velocity for a given chamber pressure than the corresponding theoretical results. It is likely that this phenomenon results, in part, from friction

---

[1] It should be noted that the absolute chamber pressure (psia) is used to calculate G/M in the Pidduck-Kent equations, leading to the prediction of impacter velocities at zero gage pressure. It was observed that much better agreement between theoretical predictions and experimental results could be obtained if gage pressure was substituted in lieu of absolute pressure in the Pidduck-Kent relations. This substitution has been made in the calculation of the theoretical results that are presented in Figure 25.

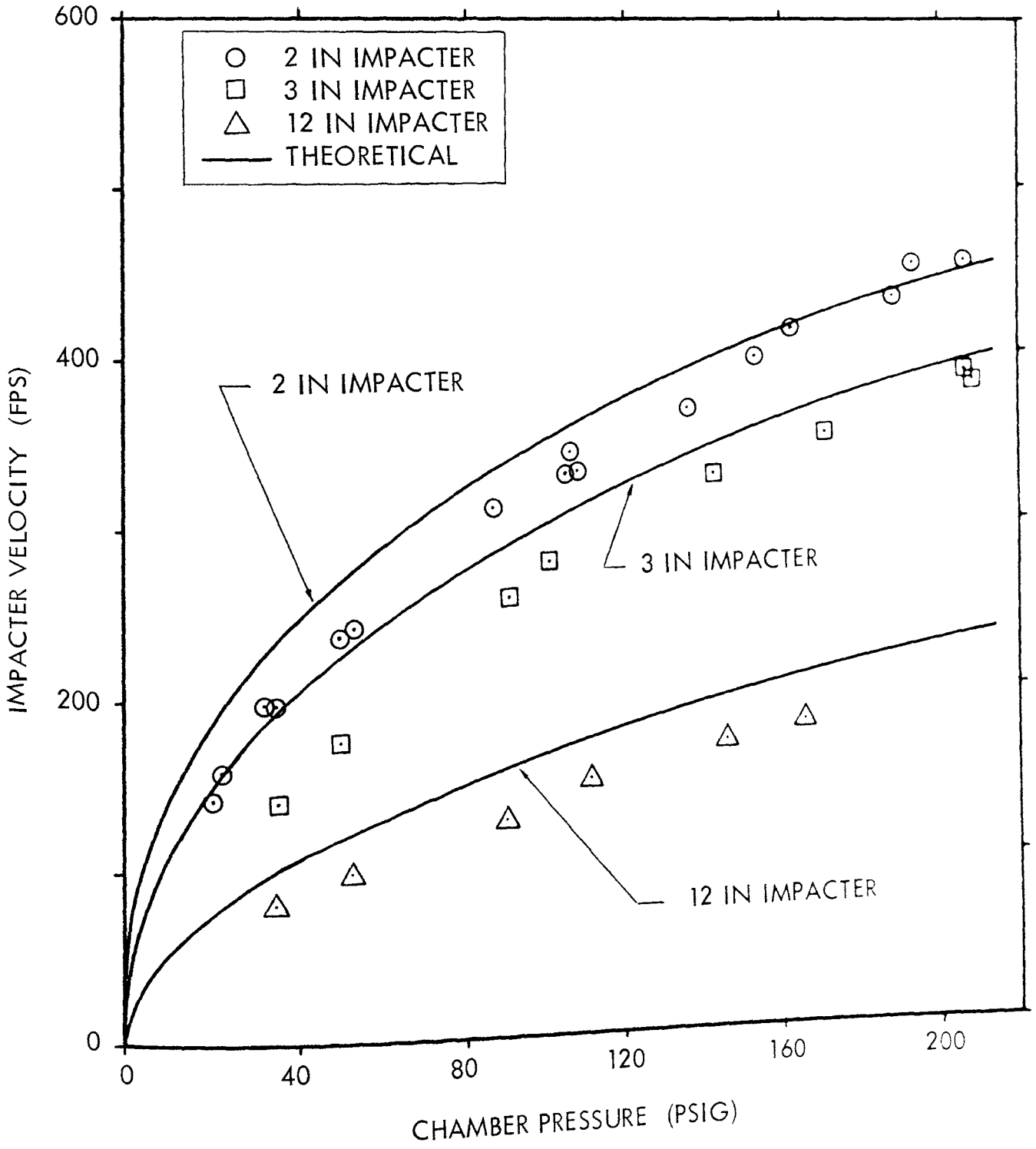

Figure 25. Air gun calibration: theoretical results ($P_{atm} = 0$, $l_b = 72$ in) and experimental results.

between the lateral surface of the impacter and the interior of the barrel-silencer. It is also probable that there is some seepage of the propelling gas along the lateral surface of the impacter as it passes through the barrel.

Equations (1-1), (1-2), and (1-3) were solved with the aid of an IBM model 360 digital computer. The computer program is listed at the end of this appendix. The program first solves equation (1-3) for G/M as a function of $\sqrt{a_o}$ for air ($\gamma = 1.4$) with increments of 0.001 in $\sqrt{a_o}$, beginning at $\sqrt{a_o}$ 0. The corresponding values of G/M and $\sqrt{a_o}$ are stored by the computer and subsequently used in a linear interpolation process to determine $\sqrt{a_o}$ as a function of G/M for use with equation (1-1). The program is constructed to yield results for five barrel lengths and any number of projectile lengths as required. For specific test material parameters, the program will also yield the theoretical elastic wave propagation velocity in the material and the duration of the pulse that is produced by projectiles of the specified lengths. For convenience, an impacter velocity-stress-strain matrix is also calculated using the simple, one-dimensional, elastic theory.

```
C       ME120 152 GAS GUN OPTIMIZATION USING PIDDUCK KENT
C       LIMITING SOLUTION ALLEN G. BEHRING
C       CT=CHAMBER TEMPERATURE (DEGREES RANKINE)
C       XK=SPECIFIC HEAT RATIO OF PROPELLING GAS
C       CD=CHAMBER DIAMETER(IN),CL=CHAMBER LENGTH(IN)
C       R=GAS CONSTANT(FT LBF/LBM R)
C       ROP=PROJECTILE DENSITY(LBM/CU IN),SL=PROJ LENGTH(IN)
C       BD=BARREL DIAMETER(IN),BL=BARREL LENGTH(IN)
        DIMENSION GM(999),AO(999),SQA(999),XBYB(5),UP(5),
       1BL(5),SL(6),ST(5),STX(5)
        READ (1,101) CT,XK,CD,BD,R,CL,ROP,ATM,(BL(K),K=1,5),
       1(SL(L),L=1,6),E,SULT,SYP,SPEC,SINC,VINC
C       PART 1 OF PROGRAM
C       CALCULATION OF G/M VRS. ROOT(AO) FROM PIDDUCK KENT
C       RELATION
        SQA(1)=.001
        A=2.*XK/(XK-1.)
        B=XK/(XK-1.)
        C=1./(XK-1.)
        D=(XK+1.)/(XK-1.)
        F=1./(XK+1.)
        WRITE (3,412) XK
        WRITE (3,413)
C       VARY ROOT(AO) IN SMALL INCREMENTS FROM .001 AND
C       CALCULATE CORRESPONDING VALUES OF (GAS MASS/MISSILE
C       MASS) FROM PIDDUCK KENT RELATION. STORE UNDER INDEX(I)
        DO 42 I=1,999
        AO(I)=SQA(I)**2
        GM(I)=A*(AO(I)/((1.-AO(I))**B))*((1.-AO(I))**C/D+
       1F*(SQRT(1.-AO(I))+ARSIN(SQA(I))/SQA(I)))
        WRITE (3,102) SQA(I),GM(I)
        IF(GM(I)-1000.)42,9,9
   42   SQA(I+1)=SQA(I)+.001
    9   CO=SQRT(32.2*XK*R*CT)
C       VARY PROJECTILE LENGTH STORED UNDER INDEX (L)
        DO 52 L=1,6
        XM=(SL(L)*3.14*BD**2/4.)*ROP
        CV=CL*3.14*CD**2/4.
        WRITE (3,401) CT,XK
        WRITE (3,402) CD,CL
        WRITE (3,403) BD,ATM
        WRITE (3,404) R,ROP
        WRITE (3,406) CO,XM
        WRITE (3,407) CV
        WRITE (3,405) SL(L)
        DO 84 K=1,5
   84   XBYB(K)=(CL*(CD/BD)**2)/(CL*(CD/BD)**2+BL(K))
        N=1
        WRITE (3,410) (BL(K),K=1,5)
        WRITE (3,411)
        CP=ATM
C       PART 2 OF PROGRAM
C       PROJECTILE VELOCITY IS NOW CALCULATED FOR SPECIFIED
C       GUN DESIGN PARAMETERS AT VARIOUS VALUES OF CHAMBER
```

```
C       PRESSURE
C       VARY CHAMBER PRESSURE INDEX (J)
        DO 51 J=1,201
        CPG=CP-ATM
        GX=(CP/(12.*R*CT))*CV
        AM=GX/XM
C       LINEAR INTERPOLATION IS USED TO CALCULATE ROOT(AM) F
C       SPECIFIED (GAS MASS/MISSILE MASS).VALUES FOR
C       INTERPOLATION HAVE BEEN STORED UNDER INDEX(I)
        DO 50 I=N,999
        IF(GM(I)-AM) 50,5,6
     5  SQX=SQA(I)
        GO TO 7
     6  M=I-1
        SQX=SQA(M)+(AM-GM(M))*((SQA(M+1)-SQA(M))/(GM(M+1)-
       1GM(M)))
        GO TO 7
    50  CONTINUE
C       VALUES OF (GAS MASS/MISSILE MASS) FOR SPECIFIED
C       CHAMBER PRESSURE AND CORRESPONDING VALUES OF ROOT(AM)
C       ARE INDICATED IN UP VRS. CP PRINT OUT. G/M AND ROOT
C       (AM) MUST CORRESPOND FAVORABLY WITH THOSE YIELDED BY
C       PIDDUCK KENT RELATION
     7  DO 69 K=1,5
        XBYB(K)=(CL*(CD/BD)**2)/(CL*(CD/BD)**2+BL(K))
    69  UP(K)=(2./(XK-1.))*CO*SQX*(1.-(XBYB(K))**(XK-1.))**.5
        WRITE (3,103) CP,CPG,AM,SQX,(UP(K),K=1,5)
        N=M
    51  CP=CP+10.
C       THIRD PART OF PROGRAM
C       VW=VELOCITY OF WAVE PROPAGATION IN TEST MATERIAL(FPS)
C       ST=THEORETICAL STRESS IN TEST MATERIAL(PSI)
C       STX=THEORETICAL STRAIN IN TEST MATERIAL (%)
C       E=MODULUS OF ELASTICITY OF TEST MATERIAL (PSI)
C       DUR=DURATION OF PULSE PRODUCED BY PROJECTILE
C       (MICRO SECONDS)
C       XLP=LENGTHOF PULSE PRODUCED BY PROJECTILE (IN)
C       SULT=ULTIMATE STRESS OF TEST MATERIAL,STATIC LOAD(PSI)
C       SYP= YIELD STRESS OF TEST MATERIAL,STATIC LOAD(PSI)
C       MAX VELOCITY REFERS TO FINAL VELOCITIES CALCULATED
C       AT TERMINAL CHAMBER PRESSURE FOR BARREL LENGTHS AND
C       SINGLE PROJECTILE LENGTH.
        WRITE (3,427)
        WRITE (3,414)
        WRITE (3,415) ROP
        WRITE (3,416) E
        WRITE (3,418) SULT
        WRITE (3,419) SYP
        WRITE (3,420) SL(L)
        VW=SQRT(386.*E/ROP)/12.
        WRITE (3,417) VW
        DUR=(SL(L)/(VW*6.0))*1000000.
        WRITE (3,422) DUR
        XLP=2.*SL(L)
```

```
      WRITE (3,421) XLP
      DO 68 K=1,5
      ST(K)=ROP*VW*UP(K)/64.4*12.
   68 STX(K)=UP(K)/(2.*VW)*100.
      WRITE (3,423) (BL(K),K=1,5)
      WRITE (3,424) CPG,(UP(K),K=1,5)
      WRITE (3,425) (ST(K),K=1,5)
      WRITE (3,426) (STX(K),K=1,5)
   52 CONTINUE
C     FOURTH PART OF PROGRAM
C     PROGRAM WILL INCREMENT STRESS FROM ZERO TO MAXIMUM
C     SPECIFIED BY INPUT IN INCREMENTS SPECIFIED AND
C     CALCULATE REQUIRED VELOCITY PLUS RESULTANT STRAIN. FOR
C     CONVENIENCE,A VELOCITY-STRESS-STRAIN PRINT OUT IS ALSO
C     GIVEN
C     SPEC=DESIRED MAXIMUM STRESS(PSI)
C     SINC=DESIRED INCREMENTS OF STRESS(PSI)
C     VINC=DESIRED INCREMENTS OF PROJECTILE VELOCITY
C     DUE TO COMPUTER LIMITATIONS,VARIABLES INVOLVING
C     PROJECTILE VELOCITY,STRESS,AND STRAIN HAVE BEEN
C     RE-NAMED.
C     STR=STRESS(PSI)=ATR (MEANING ONLY)
C     STRX=STRAIN(%)=ATRX (MEANING ONLY)
C     UPX=PROJECTILE VELOCITY(FPS)=APX (MEANING ONLY)
      WRITE (3,428)
      WRITE (3,414)
      WRITE (3,415) ROP
      WRITE (3,416) E
      WRITE (3,418) SULT
      WRITE (3,419) SYP
      WRITE (3,417) VW
      WRITE (3,429)
      STR=0.
      APX=0.
      DO 72 M=1,1000
      IF(STR-SPEC)10,10,73
   10 UPX=STR*64.4/(ROP*VW*12.)
      STRX=UPX*100./(2.*VW)
      ATR=ROP*VW*APX/64.4*12.
      ATRX=APX/(2.*VW)*100.
      WRITE (3,430) STR,UPX,STRX,APX,ATR,ATRX
      STR=STR+SINC
   72 APX=APX+VINC
   73 STOP
  101 FORMAT (6F12.2)
  102 FORMAT (2F12.4)
  103 FORMAT (F9.1,3X,F9.1,3X,7F12.4)
  401 FORMAT (2X,'CHAMBER TEMP(R)=',F10.4,6X,'SP HEAT',
     1' RATIO=',F5.2)
  402 FORMAT (2X,'CHAMBER DIA(IN)=',F5.2,11X,'CHAMBER',
     1' LENGTH(IN)=',F5.2)
  403 FORMAT (2X,'BARREL DIA(IN)=',F5.2,12X,'ATM PRESS',
     1'(PSIA)=',F5.2)
  404 FORMAT (2X,'GAS CONSTANT=',F6.2,13X,'PROJECTILE',
```

```
     1' DENSITY=',F7.4)
405  FORMAT (2X,'PROJECTILE LENGTH(IN)=',F5.2)
406  FORMAT (2X,'VEL OF SOUND(FT/SEC)=',F9.4,2X,'PROJ
     1' MASS=',F7.4)
407  FORMAT (2X,'CHAMBER VOLUME=',F10.3)
410  FORMAT (2X,'BARREL LENGTH(IN)=',25X,5F12.2)
411  FORMAT (3X,'CP(PSIA)',4X,'CP(PSIG)',8X,'G/M',7X,
     1'ROOT(AO)',20X,'PROJECTILE VELOCITY (FPS)')
412  FORMAT (2X,'SPECIFIC HEAT RATIO=',F5.2)
413  FORMAT (4X,'ROOT(AO)',6X,'G/M')
414  FORMAT (2X,'TEST MATERIAL IS 7075 T651 ALUMINUM')
415  FORMAT (2X,'TEST MATERIAL DENSITY(LBM/CU IN)=',F7.4)
416  FORMAT (2X,'MODULUS OF ELASTICITY OF TEST MATL(PSI)
     1F12.3)
417  FORMAT (2X,'VELOCITY OF WAVE PROPAGATION IN TEST
     1' MATL=',F9.2)
418  FORMAT (2X,'ULTIMATE STRESS OF TEST MATL(PSI)=',F
419  FORMAT (2X,'YIELD POINT STRESS OF TEST MATL(PSI)=
     1F9.2)
420  FORMAT (2X,'PROJECTILE LENGTH(IN)=',F5.2)
421  FORMAT (2X,'PULSE LENGTH(IN)=',F5.2)
422  FORMAT (2X,'DURATION OF PULSE(MICRO SEC)=',F9.4)
423  FORMAT (2X,'BARREL LENGTH(IN)=',15X,5F14.2)
424  FORMAT (2X,'MAX CP(PSIG)=',F7.2,2X,'MAX VEL(FPS)=
     15F14.4)
425  FORMAT (2X,'MAX EXPECTED STRESS(PSI)=',10X,5F14.4)
426  FORMAT (2X,'MAX EXPECTED STRAIN(%)=',12X,5F14.4,/////)
427  FORMAT (2X,'MAX VELOCITY REFERS TO THAT CALCULATED
     1' AT TERMINAL CP FOR BARREL LENGTHS AND PROJ LENGTHS')
428  FORMAT (2X,'STRESS-VELOCITY-STRAIN SPECTRUM FOR
429  FORMAT (3X,'STRESS(PSI)',2X,'PROJ VEL(FPS)',4X,
     1'STRAIN(%)',11X,'PROJ VEL(FPS)',2X,'STRESS(PSI)',4X,
     2'STRAIN(%)')
430  FORMAT (2X,F12.1,2X,F12.4,2X,F12.7,10X,F12.1,2X,F12.4,
     12X,F12.7)
      END
```

APPENDIX 2

COMPUTER PROGRAM FOR THE SOLUTION OF EQUATIONS (36) AND (37)

The computer program is written to yield the stress and strain distributions with (x/L) resulting from the longitudinal impact of two Maxwellian rods. Stress and strain are indicated as multipliers of the corresponding stress and strain that would be realized in the elastic case. The stress and strain multipliers are calculated from $x/L = 0$ to $x/L = 1.0$ in increments of 0.005 for each of eleven values of normalized time, T.

The output of the program is listed as a stress multiplication matrix and a strain multiplication matrix. The columns of the matrices represent the stress or strain distribution at a given value of normalized time. The data are also presented in the form of computer punch cards which have a corresponding matrix representation. These punch cards can subsequently be used as input data for a plotter program in order to obtain a graphical representation of the results.

Using the IBM model 360 digital computer, approximately one minute of computer time is required for the evaluation of each ten series terms. If the highest mode number of the series is chosen to be 150, 14.1 minutes of computer time is required and the storage allocation requirement is 128,288 bytes.

Further information regarding the construction of the program and its input data requirements can be found in a listing of the program, beginning on the next page.

```
C      ME 120 152 AL BEHRING ONE DIMENSIONAL VISCOELASTIC
C      STRESS AND STRAIN WAVE PROPAGATION IN A CONSTANT-AREA,
C      FINITE ROD. A MAXWELL MODEL IS USED TO DESCRIBE THE
C      STRESS-STRAIN RELATIONSHIP. THE SOLUTION INVOLVES THE
C      CORRESPONDENCE PRINCIPLE AND FOURIER SERIES.
C
C      DEFINITION OF VARRIABLES FOLLOWS
C      E=MODULUS OF ELASTICITY(SPRING IN MAXWELL MODEL)
C      ETA=COEFFICIENT OF VISCOUS DAMPING(DASHPOT IN MAXWELL
C      MODEL)
C      WO=RATIO OF ELASTIC ELEMENT TO VISCOUS ELEMENT (E/ETA)
C      RO=DENSITY (MASS/VOLUME)
C      CO=ELASTIC WAVE PROPAGATION VELOCITY=SQRT(E/RO)
C      X=LAGRANGEAN REFERENCE COORDINATE
C      L=LENGTH OF ROD IN UNSTRAINED STATE
C      XN=NORMALIZED REFERENCE COORDINATE (X/L)
C      T=TIME
C      TAU=CHARACTERISTIC TIME (CO*T/L)
C      TAUO=RELAXATION PARAMETER (WO*L/CO)
C      AS=STRESS MULTIPLICATION FACTOR
C      ES=ELASTIC VALUE OF STRESS (E*VO/(2.*CO))
C      TRUE STRESS = AS*ES
C      BS=STRAIN MULTIPLICATION FACTOR
C      EST=ELASTIC VALUE OF STRAIN (VO/(2.*CO))
C      TRUE STRAIN=BS*EST
C      A=RATIO OF (IMPACTER LENGTH+TEST BAR LENGTH) TO
C      IMPACTER LENGTH, AN INTEGER
C
C      DEFINITION OF INDICES FOLLOWS
C      M=NUMBER OF HIGHEST MODE OF SERIES
C      N=SERIES MODE NUMBER
C      K=NORMALIZED REFERENCE COORDINATE INDEX
C      NT=CHARACTERISTIC TIME INDEX
C      ALL OTHER INDICES DUMMY
C
C      SERIES SET-UP FOLLOWS
       COMMON DEAF(150),CAT(201,150),DELT(150),DELS(150),
      1DOG(150),CHOP(150),CHOPP(10),TAU(12),FROG(11),S(11),
      2AS(11),SX(11),BS(11)
       READ (1,102) TAUO,A,M
       XPI=3.1415926536
       RN=1.
       DO 84 N=1,M
       DEAF(N)=RN*XPI
       XN=0.
       DO 83 K=1,201
       CAT(K,N)=SIN(DEAF(N)*XN)
   83  XN=XN+.005
       DELT(N)=TAUO/(2.*DEAF(N))
       DELS(N)=DELT(N)**2
       DOG(N)=RN*SQRT(ABS(1.-DELS(N)))
   84  RN=RN+1.
       NA=2.*A
       DO 46 N=1,NA
```

```
   46 CHOPP(N)=SIN(DEAF(N)/A)
      N=1
      DO 57 NX=1,M
      IF(N-M)55,55,58
   55 DO 56 ND=1,NA
      CHOP(N)=CHOPP(ND)
   56 N=N+1
   57 CONTINUE
   58 CONTINUE
      TAU(1)=0.
      DO 41 NT=1,11
      FROG(NT)=EXP(TAUO*TAU(NT)/2.)
   41 TAU(NT+1)=TAU(NT)+.1
      XM=M
      WRITE (2,356) TAUO,XM
C     CALCULATION OF STRESS MATRIX FOLLOWS
      WRITE (3,399)
      WRITE (3,427) A
      WRITE (3,428) M
      WRITE (3,400) TAUO
      WRITE (3,421) (TAU(NT),NT=1,11)
      WRITE (3,411)
      XN=0.
      DO 51 K=1,201
      DO 52 NT=1,11
      XS=0.
      S(NT)=0.
      RN=1.
      DO 65 N=1,M
      IF(1.-DELS(N))3,2,1
    3 XS=(1./DOG(N))*CHOP(N)*CAT(K,N)*SINH(XPI*DOG(N)*
     1TAU(NT))
      GO TO 65
    2 XS=(XPI*TAU(NT)*CHOP(N)*CAT(K,N))
      GO TO 65
    1 XS=CHOP(N)*CAT(K,N)*SIN(XPI*DOG(N)*TAU(NT))/DOG(N)
   65 S(NT)=S(NT)+XS
      AS(NT)=-4.*S(NT)/(XPI*FROG(NT))
   52 CONTINUE
      WRITE (3,450) XN,(AS(NT),NT=1,11)
      WRITE (2,388) (AS(NT),NT=2,11)
   51 XN=XN+.005
      WRITE (3,101)
C     CALCULATION OF STRAIN MATRIX FOLLOWS
      WRITE (3,469)
      WRITE (3,427) A
      WRITE (3,428) M
      WRITE (3,400) TAUO
      WRITE (3,421) (TAU(NT),NT=1,11)
      WRITE (3,412)
      XN=0.
      DO 31 K=1,201
      DO 32 NT=1,11
      XS=0.
```

```
      XSS=0.
      S(NT)=0.
      SX(NT)=0.
      RN=1.
      DO 36 N=1,M
      IF(1.-DELS(N))6,5,4
    6 XS=CHOP(N)*CAT(K,N)*(((1.-2.*DELS(N))/DOG(N))*
     1SINH(XPI*DOG(N)*TAU(NT))-(2.*DELT(N)/RN)*COSH(XPI*
     2DOG(N)*TAU(NT)))
      XSS=(1./(RN**2))*CHOP(N)*CAT(K,N)
      GO TO 35
    5 XS=(-2.*DELT(N)/RN)*CHOP(N)*CAT(K,N)
      XXS=(1./(RN**2))*CHOP(N)*CAT(K,N)
      GO TO 35
    4 XS=CHOP(N)*CAT(K,N)*(((1.-2.*DELS(N))/DOG(N))*SIN(XPI*
     1DOG(N)*TAU(NT))-(2.*DELT(N)/RN)*COS(XPI*DOG(N)*
     2TAU(NT)))
      XSS=(1./(RN**2))*CHOP(N)*CAT(K,N)
   35 S(NT)=S(NT)+XS
      RN=RN+1.
   36 SX(NT)=SX(NT)+XSS
      BS(NT)=(-4./XPI)*(S(NT)/FROG(NT)+(TAUO/XPI)*SX(NT))
   32 CONTINUE
      WRITE (3,450) XN,(BS(NT),NT=1,11)
      WRITE (2,388) (BS(NT),NT=2,11)
   31 XN=XN+.005
      WRITE (3,413)
  389 FORMAT (4F18.15)
  102 FORMAT (2F12.6,I5)
  399 FORMAT (2X,'STRESS MATRIX FOLLOWS',////)
  400 FORMAT (2X,'RELAXATION PARAMETER=',F7.3,///)
  413 FORMAT (2X,'CONCLUSION OF STRAIN MATRIX')
  421 FORMAT (2X,'TIME',11F10.2)
  411 FORMAT (2X,'XN',40X,'STRESS MULTIPLICATION FACTOR')
  428 FORMAT (2X,I5,'TERMS OF THE SERIES ARE USED FOR',
     1' EVALUATION')
  450 FORMAT (F6.3,11F10.4)
  388 FORMAT (10F7.4)
  101 FORMAT (2X,'CONCLUSION OF STRESS MATRIX',//////)
  427 FORMAT (2X,'A=',F6.2)
  469 FORMAT (2X,'STRAIN MATRIX FOLLOWS',////)
  412 FORMAT (2X,'XN',40X,'STRAIN MULTIPLICATION FACTOR')
  356 FORMAT (2F6.3)
      CALL EXIT
      END
```

APPENDIX 3

SOME IMPLICATIONS OF THE MALVERN EQUATION

Malvern [3] has suggested that the stress-strain relation for a metal loaded in the plastic range is

$$\frac{d}{dt}\left[E\varepsilon-\sigma\right] = g(\sigma,\varepsilon) \quad .$$

One of the simplest forms of this equation, as suggested by Malvern, postulates that $g(\sigma,\varepsilon)$ is a linear function of the rate of departure of the true stress ( ) from the value given by the static tension test at a specified value of strain ( ). In equation form this simplification yields

$$\frac{d}{dt}\left[E\varepsilon-\sigma\right] = K\left[\sigma-f(\varepsilon)\right] \qquad (3\text{-}1)$$

where K is a constant and the physical significance of the variables is described by Figure 26.

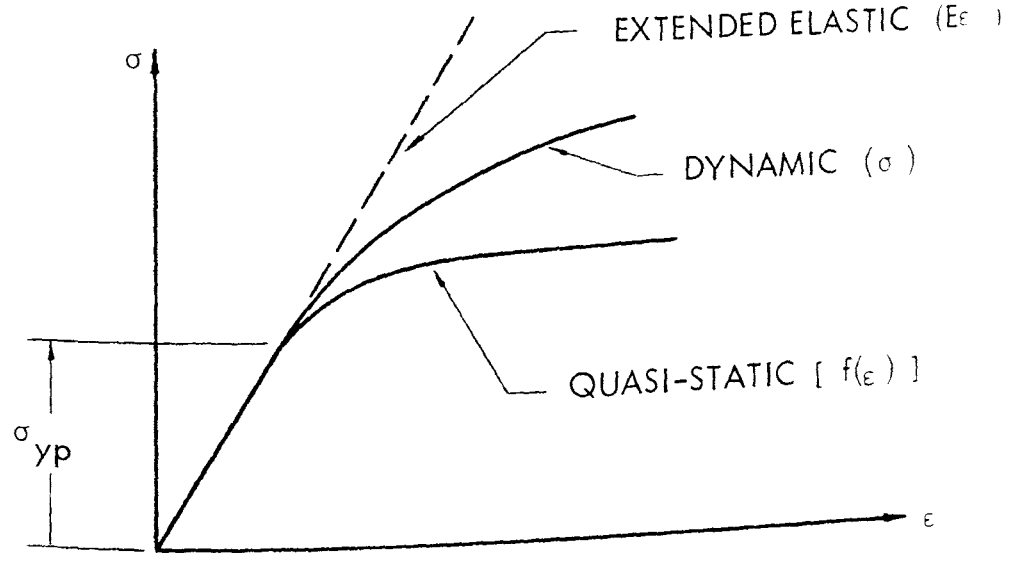

Figure 26. Stress-strain diagram proposed by Malvern

Taking the Laplace transform of equation (3-1), the result is

$$Es\bar{\varepsilon} - E\varepsilon(o) - S\bar{\sigma} + \sigma(o) = K\bar{\sigma} - K\mathcal{L}\left[f(\varepsilon)\right] \tag{3-2}$$

where the bar notation denotes a transformed variable. If it is assumed that plastic loading is applied at $t = 0^+$, then $E\varepsilon(o) = \sigma(o)$ and equation (3-2) becomes

$$\bar{\sigma}\left[K+s\right] = Es\bar{\varepsilon} + K\mathcal{L}\left[f(\varepsilon)\right]$$

or, after suitable re-arrangement,

$$\bar{\sigma} = \frac{Es\bar{\varepsilon}}{K+s} + \frac{K}{K+s}\mathcal{L}\left[f(\varepsilon)\right] \quad . \tag{3-3}$$

Assuming that the strain is specified by the step function $\varepsilon = \varepsilon_o H(t)$ where $H(t)$ is Heaviside's step function, equation (3-3) becomes

$$\bar{\sigma} = \frac{E\varepsilon_o}{K+s} + \frac{K}{K+s}\mathcal{L}\{f[\varepsilon_o H(t)]\} \quad . \tag{3-4}$$

Employing the convolution integral

$$\mathcal{L}^{-1}\left[q(s)r(s)\right] = \int_0^t Q(t-\tau)R(\tau)d\tau$$

to find the inverse of equation (3-4), the result is

$$\sigma = \{E\varepsilon_o e^{-Kt} + f(\varepsilon_o)\left[1-e^{-Kt}\right]\}H(t) \quad . \tag{3-5}$$

From equation (3-5) it can be seen that at $t = 0^+$ the stress is that value predicted by an extension of the elastic curve ($E\varepsilon_o$) and that as t becomes very large, the stress approaches the value predicted by the static test, $f(\varepsilon_o)$. Equation (3-5) describes the "relaxation" phenomenon associated with the Malvern theory.

The relaxation phenomenon described by the Malvern equation is similar to that shown by a Maxwell material. Suitable rearrangement of equation (28) results in

$$\frac{d}{dt}\left[E\varepsilon-\sigma\right] = W_o\left[\sigma-o\right] \quad . \qquad (3\text{-}6)$$

It can be seen that equation (3-1) reduces to equation (3-6) if $f(\varepsilon) = 0$. For a Maxwell material subjected to a step strain, $\varepsilon = \varepsilon_o H(t)$, it can be shown that

$$\sigma = \left[E\varepsilon_o e^{-W_o t}\right] H(t) \quad .$$

Equations (3-5) and (3-7) yield similar results for small values of time such as those associated with pulse propagation. In view of the observed similarity of experimental results obtained in the plastic range of loading (e.g., Figure 21) with the plotted results of the viscoelastic solution (see Figure 7), further investigation into the strain-rate dependent theory is recommended.

APPENDIX 4

SUGGESTED METHOD FOR FOURIER TIME ANALYSIS

If the location of the strain gages (ξ) is chosen such that the initial compressive pulse is measured as closely as possible to the interface of the rods, and such that the strain gages are subjected to the maximum pulse duration ($\frac{2L}{aC}$) for the first and successively reflected pulses, it can be seen from the characteristics diagram of Figure 2 that the strain measurement system will be subjected to the train of pulses indicated in Figure 27.

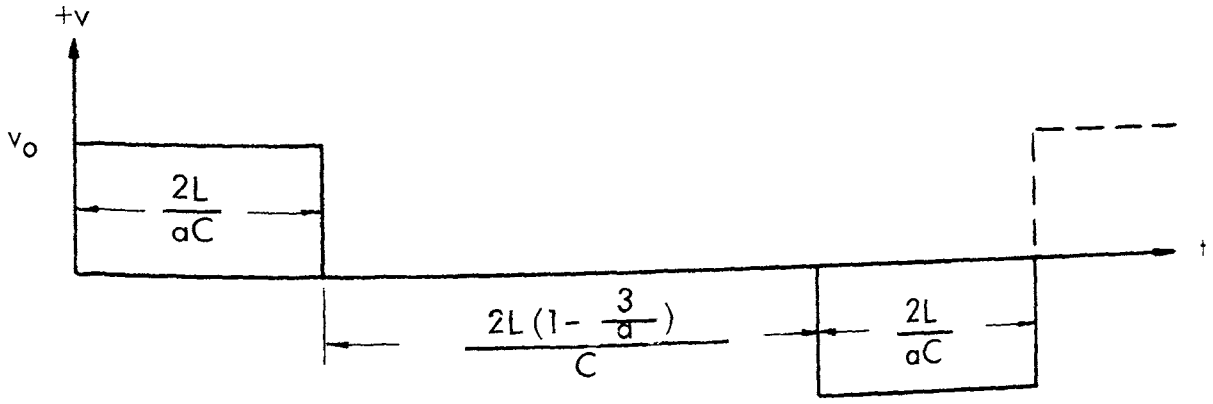

Figure 27. Resultant elastic pulse train

With reference to Figure 27, v represents voltage, t is time, and C is the velocity of elastic wave propagation. The Fourier representation for the pulse train of Figure 27 is

$$v(t) = \frac{2v_o}{\pi} \sum_{n=1}^{\infty} \frac{1}{n} \left[1 - \cos(n\pi)\cos[n\pi e/(d+e)] \right] \sin(2\pi f_n t) \qquad (4\text{-}1)$$

where $d = 2L/aC$, $e = [\,2L\,(1 - \frac{3}{a})\,]/C$, and $f_n = n/(2d+e)$.

From equation (4-1) it can be seen that the lowest frequency present (f_1) is

$$f_1 = 1/(2d+e) \text{ cps} \quad .$$

As an approximation, it is suggested that the upper frequency response limit of the strain measuring system (f_m) should be used as the highest frequency of (4-1), then

$$m \cong f_m/f_1$$

where m is the largest integer that is present in f_m/f_1.

Then, for the impacter-test bar combination under consideration, the "limited" series representation is

$$v(t) = (2v_o/\pi) \sum_{n=1}^{m} (1/n) \left[1 - \cos(n\pi)\cos[n\pi e/(d+e)] \right] \sin(2\pi f_n t) \quad . \qquad (4-2)$$

Numerical evaluation of equation (4-2) and subsequent comparison with the results indicated by Figure 27 should serve as a "first approximation" of the error to be expected as a result of frequency response limitations. A more exact approximation of the expected results can be derived by using the attenuation characteristics of the strain measuring equipment to modify the constants in (4-1).

It should be noted that this theory has been developed using the properties of the test material under elastic loading conditions. If, for a particular impacter-test rod combination, it is determined that the error due to frequency response limitations is acceptable for the elastic case, this acceptability should also prevail for the plastic case.